

OCTOBER 2014

Ph.D in Physics Engineering

MİKAIL ASLAN

**UNIVERSITY OF GAZİANTEP
GRADUATE SCHOOL OF
NATURAL & APPLIED SCIENCES**

**ELECTRONIC STRUCTURE OF LIGAND-PASSIVATED METAL
NANOCLUSTERS**

**Ph.D THESIS
IN
PHYSICS ENGINEERING**

**BY
MİKAIL ASLAN
OCTOBER 2014**

Electronic Structure of Ligand-Passivated Metal Nanoclusters

Ph.D.

In

Physics Engineering

University of Gaziantep

Supervisors

Assoc. Prof. Dr. Ali SEBETCİ

Prof. Dr. Zihni ÖZTÜRK

by

Mikail ASLAN

October 2014

© 2014 [Mikail ASLAN]

REPUBLIC OF TURKEY
UNIVERSITY OF GAZIANTEP
GRADUATE SCHOOL OF NATURAL & APPLIED SCIENCES
PHYSICS ENGINEERING DEPARTMENT

Name of the thesis: Electronic Structure of Ligand-Passivated Metal Nanoclusters

Name of the student: Mikail ASLAN

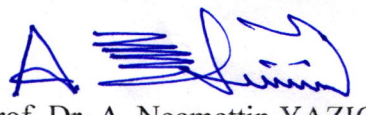
Exam date: 16.10.2014

Approval of the Graduate School of Natural and Applied Sciences


Prof. Dr. Metin BEDİR

Director

I certify that this thesis satisfies all the requirements as a thesis for the degree of
Doctor of Philosophy.

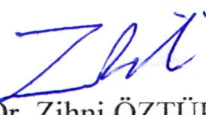

Prof. Dr. A. Necmettin YAZICI

Head of Department

This is to certify that we have read this thesis and that in our consensus/majority
opinion it is fully adequate, in scope and quality, as a thesis for the degree of Doctor
of Philosophy.

Assoc. Prof. Dr. Ali SEBETCİ


Co-Supervisor


Prof. Dr. Zihni ÖZTÜRK

Supervisor

Examining Committee Members

Prof. Dr. Zihni ÖZTÜRK

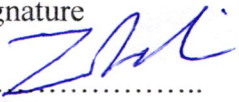
Prof. Dr. Hayriye TÜTÜNCÜLER

Assist. Prof. Dr. Mustafa ŞANVER

Prof. Dr. A. Necmettin YAZICI

Assist. Prof. Dr. Abdulaziz KAYA


Signature







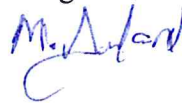




I hereby declare that all information in this document has been obtained and presented in accordance with academic rules and ethical conduct. I also declare that, as required by these rules and conduct, I have fully cited and referenced all material and results that are not original to this work.

Mikail ASLAN

Signature

A handwritten signature in blue ink, appearing to read 'Mikail Aslan', with a stylized flourish at the end.

ABSTRACT

ELECTRONIC STRUCTURE OF LIGAND-PASSIVATED METAL NANOCLUSTERS

ASLAN, Mikail

Ph.D. in Physics Engineering

Supervisors:

Assoc. Prof. Dr. Ali SEBETCİ and Prof. Dr. Zihni ÖZTÜRK

October 2014, 112 pages

The geometric, electronic, and magnetic properties of neutral and ionic ligand-passivated metal nanoclusters have been studied. The adsorption of a number of organic molecules and metal oxides on Pt, Co, Pd, and nanoalloys is investigated by means of density functional theory calculations. Various interaction patterns between the ligands and the metal clusters are constructed and screened with extensive structure searches for the low-lying isomers of the ligand-protected complexes. The optimal adsorption sites are identified and the corresponding electronic and magnetic states are analyzed.

Keywords: Nanoparticles, Metal Clusters, Modeling and Simulation in Materials Science and Engineering, Density Functional Theory, Ligands

ÖZET

LİGANDLARLA PASİFLEŞTİRİLMİŞ METAL NANOTOPAKLARIN ELEKTRONİK YAPILARI

ASLAN, Mikail

Doktora Tezi, Fizik Müh. Bölümü

Tez Yöneticileri:

Doç. Dr. Ali SEBETCİ ve Prof. Dr. Zihni ÖZTÜRK

Ekim 2014, 121 sayfa

Nötr ve iyonik ligandlar ile pasifize edilmiş metal nanotopakların geometrik, elektronik ve manyetik özellikleri çalışıldı. Yoğunluk Foksiyonel Teorisi kullanılarak bir takım organik moleküller ya da metal oksitlerin Pt, Co, Pd, ve bu elementlerden oluşan nano alaşımlar üzerindeki adsorpsiyon etkileri incelenmiştir. Ligandlar ile korunan metal nanotopakların en düşük izomerleri kapsamlı bir tarama ile araştırıldı. En kuvvetli adsorpsiyon için atomların geometrik konumları tespit edildi ve geometrik konumları belirlenen yapıların elektronik ve manyetik durumları analiz edildi.

Anahtar kelimeler: Nanoparçacıklar, Metal Nanotopaklar, Materyal Modelleme ve Simülasyon, Yoğunluk Foksiyonel Teorisi, Ligandlar.

To My Parents

ACKNOWLEDGEMENTS

I would like to express my respect and regards to my supervisor, Prof. Dr. Zihni ÖZTÜRK, my co-supervisor Assoc. Prof. Dr. Ali SEBETCİ and my dear friend Mr. Ahmet KURTOĞLU for their guidance, advice, encouragement and suggestions during the preparation of this thesis.

My special thanks are reserved for my parents for their encouragement, understanding, patience and great help.

This study was supported by The Scientific and Technological Research Council of Turkey (TUBITAK)

TABLE OF CONTENTS

ABSTRACT	v
ÖZET.....	vi
ACKNOWLEDGEMENTS.....	viii
LIST OF TABLES	xi
LIST OF FIGURES	xii
LIST OF ABBREVIATIONS / SYMBOLS.....	xiv
INTRODUCTION.....	1
1.1 Nanoscience	1
1.2 Clusters	2
1.2.1 Metal Clusters.....	2
1.3 Computational Simulation.....	6
DENSITY FUNCTIONAL THEORY.....	7
2.1 Introduction.....	7
2.2 The Schrödinger Equation.....	9
2.3 The Variational Principle.....	12
2.4 The Hartree-Fock Method	12
2.5 Avoiding the Solution of the Schrödinger Equation.....	15
2.6 The Hohenberg and Kohn Theorems	17
2.7 The Energy Functional.....	18
2.8 The Exchange Correlation Functionals.....	22
THE INFLUENCE OF UNSATURATED HYDROCARBON LIGANDS ON THE STABILIZATION OF PLATINUM TETRAMER.....	28
3.1 Introduction.....	28
3.2 Computational Details.....	30
3.3 Results and Discussion	31
3.3.1 Lowest Energy Structure.....	31
3.3.2 Energetics and Stability.....	36
3.3.3 Electronic Properties	41
3.3.4 DFT Chemical Reactivity Descriptors	43

3.4 Conclusion	45
THE INTERACTION OF C₂H WITH BIMETALLIC COBALT-PLATINUM CLUSTERS.....	47
4.1 Introduction	47
4.2 Computational Details	49
4.3 Result and Discussion	49
4.3.1 [Co _m Pt _n C ₂ H] ⁻¹ (m+n=2).....	49
4.3.2 [Co _m Pt _n C ₂ H] ⁻¹ (m+n=3).....	50
4.3.3 [Co _m Pt _n C ₂ H] ⁻¹ (m+n=4).....	53
4.3.4 [Co _m Pt _n C ₂ H] ⁻¹ (m+n=5).....	56
4.3.5 Energy and Electronic Structure.....	61
4.3.6 Magnetic Properties.....	67
4.4 Conclusion.....	68
THE INFLUENCE OF Li_xO LIGANDS ON THE STRUCTURE OF PALLADIUM COBALT CLUSTERS	69
5.1 Introduction	69
5.2 Computational Details	71
5.3 Results and Discussion.....	71
5.3.1 Lowest Energy Structures of Pd _n Co _m LiO (2≤n+m≤4).....	71
5.3.2 Lowest Energy Structures of Pd _n Co _m Li ₂ O (2≤n+m≤4).....	77
5.3.3 Stability and Electronic Properties	82
5.4 Conclusion.....	83
LIST OF REFERENCES	87
VITA.....	111

LIST OF TABLES

Table 2.1 The hierarchy of exchange correlation functionals	27
Table 3.1 Reaction energies with two xc functionals: B3LYP and BW91	38
Table 3.2 The electronic properties of Pt₄(CH)_n (n=1 to 7 and n=12) clusters with B3LYP	39
Table 3.3 The electronic properties of Pt₄(CH)_n (n=1 to 7 and n=12) clusters with xc BPW91	39
Table 3.4 The chemical reactivity descriptors indexes of Pt₄(CH)_n (n=1 to 7 and n=12) clusters in eV.....	43
Table 4.1 The electronic properties of Co_nPt_m-ethynyl clusters with BLYP.....	52
Table 4.2 The dissociation channels of selected anionic Co_nPt_m-ethynyl clusters	66
Table 5.1 The electronic properties of Pd_nCo_mLiO (2≤n+m≤4) structures	76
Table 5.2 The electronic properties of Pd_nCo_mLi₂O (2≤n+m≤4) structures	80

LIST OF FIGURES

	Page
Figure 2.1 The relationship between the real many body system (left side) and the non-interacting system of Kohn Sham density functional theory (right side)	21
Figure 3.1 The lowest energy structures and some isomers of Pt ₄ (CH) _n (n=1 to 5) clusters.....	32
Figure 3.2 The lowest energy structures and some isomers of Pt ₄ (CH) ₆ and Pt ₄ (CH) ₇ clusters.....	35
Figure 3.3 The low-lying isomers of Pt ₄ (benzene) ₂ clusters.....	36
Figure 3.4 The binding energies per atom for Pt ₄ (CH) _n (n=1 to 7 and n=12) clusters.....	37
Figure 3.5 The second finite difference in energies for Pt ₄ (CH) _n (n =2 to 6) clusters.....	40
Figure 3.6 HOMO and LUMO density plot of Pt ₄ (CH) ₄ and Pt ₄ benzene clusters.	42
Figure 4.1 The optimized structures of some isomers of [Co _m Pt _n C ₂ H] ⁻¹ (2≤m+n≤3)	53
Figure 4.2 The optimized structures of some isomers of [Co _m Pt _n C ₂ H] ⁻¹ (m+n=4)	56
Figure 4.3 The optimized structures of some isomers of [Co _m Pt _n C ₂ H] ⁻¹ (m+n=5)	59
Figure 4.4 The BE of [Co _n Pt _m C ₂ H] ⁻¹ for 2≤n+m≤5	61
Figure 4.5 The second finite energies and C ₂ H adsorption energies of [Co _n Pt _m C ₂ H] ⁻¹	63
Figure 4.6 The HOMO-LUMO gaps and VDEs of [Co _n Pt _m C ₂ H] ⁻¹	66
Figure 4.7 Total magnetic spin moments of the ground state, bare Co _n Pt _m and Co _n Pt _m -ethynly clusters (2≤n+m≤5)	67

Figure 5.1 The optimized structure of Pd_nCo_mLiO (2≤m+n≤4).....	71
Figure 5.2 The HOMO and LUMO density plots of Pd_nCo_mLiO (2≤m+n≤4).....	73
Figure 5.3 The BE per atom of Pd_nCo_mLiO (2≤m+n≤4).....	75
Figure 5.4 The optimized structure of Pd_nCo_mLi₂O (2≤m+n≤4)	77
Figure 5.5 The HOMO-LUMO density plots of Pd_nCo_mLi₂O (2≤m+n≤4)	78
Figure 5.6 The BE per atom of Pd_nCo_mLi₂O (2≤m+n≤4)	81

LIST OF ABBREVIATIONS / SYMBOLS

Abbreviations:

BE	B inding E nergy
DFT	D ensity F unctional T heory
EA	E lectron A ffinity
ECP	E ffective C ore P otential
FE	F ermi E nergy
GGA	G eneralized G radient A pproximation
HF	H artree- F ock
HK	H ohenberg- K ohn
HLG	H OMO- L UMO G ap
HOMO	H ighest O ccupied M olecular O rbital
LDA	L ocal D ensity A pproximations
LSDA	S pin-polarized L ocal D ensity A pproximation
LUMO	L owest U noccupied M olecular O rbital
MAE	M ean A bsolute E rror
MC	M etal C luster
MM	M agnetic M oment
MRE	M ean R elative E rror
OER	O xygen E volution R eaction
ORR	O xygen R eduction R eaction
QMC	Q uantum M onte C arlo
SPR	S urface P lasmon R esonance
VDE	V ertical D etachment E nergy
XC	E xchange C orrelation

Symbols:

\hat{H}	Hamiltonian operator
λ_k	k^{th} state of electronic wave function
E_k	Numerical value of the energy state defined by Ψ_k
E_{tot}	Total energy of the system
E_0	The lowest energy
ξ	The spin orbital function
ε	The ground state orbital energies
v_x	The non local exchange potential
$\tilde{h}(r, r')$	The coupling constant averaged exchange-correlation hole
$\varepsilon_{xc}^{\text{hom}}[\rho]$	The energy density of a homogenous electron gas per particle of the density ρ
ρ_α, ρ_β	Electronic density for spin up and spin down respectively
τ	The kinetic energy density
λ	Coupling constant
D	The second finite different energy
μ	Chemical potential
η	Chemical hardness
w	Electrophilicity index

CHAPTER 1

INTRODUCTION

1.1 Nanoscience

For the past few decades, many scientists and engineers who work on material science have been willing to do research on materials that are sized 100 nm or smaller scale to find amazing inventions or implement their discoveries to new applications. Small nanosized particles show unique properties that are different from extended bulk states or from atomic states, which is due to the fundamental reasons: the high surface / volume ratio and the quantum size confinement effect [1]. In order to produce electronic devices very smaller size, quantum concept becomes more important than the conventional understanding of them. For example, the lithographic techniques that are a kind of fabricating of structures in nanometer scale may not be even applicable for these structures. In addition, self-assembly is one of the reliable techniques for the production of regular structures but it is very sensitive to fluctuations. Due to the these problems, the quantum size confinement effect should be taken into consideration so as to comprehend deeply the behavior of nano-devices in microscopic world and to control the nano-structure precisely when building it [2].

Naturally, physical systems are inclined to find their most stable states after doing some process like thermal annealing which is a kind of process for altering material or changing in its properties such as electronegativity and ductility by heating. The most decisive state is the lowest total energy that the structure in a physical system possesses when compared to all other possible structures. Finding the lowest total energy that the structure owns by theoretical way can provide to determine the properties of the systems. Although determining the structure of a complex system is

challenging work and may cost a lot for computational time, theoretical studies in the determination of the most stable state play important roles. This represents the candidate structures manually relying on human intuition [2].

1.2 Clusters

Clusters, intermediate structures between single atoms and molecules and bulk matter, may range from 2 atoms to tens of thousands. Metal clusters have been gaining importance extensively in last few decades due to their novel properties [3]. One of the main differences between clusters and bulk material is the surface area / volume ratio. While this ratio is less significant for macroscopic systems, it is really important for small clusters since the ratio is significantly large. Thus, the physical properties of the clusters like electronegativity are intrinsically different from those of bulk material. For instance, the tiny clusters of metals may show the characters of insulators or semiconductor with remarkable electronic properties [4]. Moreover, the properties such as ionization potential, electron affinity may have odd-even oscillations with different sizes which means that clusters may not be only some cut outs of solid materials [5]. Clusters may have exciting shapes because of the large number of surface atoms with unsaturated coordination. The geometries and electronic structures of the metal cluster have been deduced in terms of models such as jellium model or nuclear liquid drop model [3].

Due to the development of nano-science and nano technology, the study of the electronic properties of nanoclusters has attained considerable significance. Computer simulations play an important role in the comprehension of the evolution of the structures, physical and chemical properties of clusters. Understanding the evaluation of the properties of the clusters as they grow is one of the fundamental questions of the cluster science [4].

1.2.1 Metal Clusters

Metal clusters (MCs), in particular, play an important role in catalysis, medical science, and nanostructured electronic devices. For the medical science field, to

defeat some diseases or treatment of the diseases such as, filariasis, malaria, brain fever and dengue, which results in the existence of mosquitoes, plant obtained by the synthesis of metal nanoparticles may be prior to control the population of mosquitoes so as to reduce the effect of such kind of diseases via appropriate control methods [6]. For instance, Selvaraj and co-workers used mesocarp layer extract of *Cocos nucifera* and managed to synthesize silver clusters due to their biocompatibility, low toxicity, green approach and environmental friendly nature and antimicrobial properties that they show by treating silver nitrate solution with aqueous extract of *C. nucifera* coir at 60 Celsius [7,8]. They checked the realibility of their method by analyzing the excitation of surface plasmon resonance (SPR) using UV-vis spectrophometer at 433 nm [9]. For the nanostructured electronic devices, MCs has possible application in the microelectronics and sensor technology subfields [9,10]. For example, Nicola Cioffi and co-workers produced gold/surfactant core/shell colloidal nanoparticles with a controlled morphology and chemical composition using sacrificial anode technique with galvanostatic mode for the surface-modification of gate electrodes implemented in field effect capacitor sensors for NO_x sensing [11]. They preferred Au-MCs based gas sensor due to the novel reactivity properties, increased surface area-volume ratio, high sensing performance level and adjustment of sensor properties [11-13].

Among transition metal clusters, platinum is used as an essential electrode material due to its relatively high catalytic activity and stability. Thus, platinum metal cluster offer a wide range of remarkable properties as a variety of technology Cluster applications. For small MCs, the determination of the ground state structure by experiment is challenging. There exists only a small minority of studies using a wide range of spectroscopic techniques, viz. resonance two-photon ionization, dissociation methods, lasers induced fluorescence and stark spectra [14-20]. Theoretical studies performed by ab initio methods [21-35] and empirical potential methods [36-41] have been reported.

Co clusters are one of the important metal clusters because of their magnetic properties and significance in magnetic storage devices [42-47]. The significance of studying small Co clusters may be summarized as its possible contribution to the solution of the technologically important question of how magnetic characteristic

varies in reduced dimensions [48]. The ground state structure of the metal nanoparticles is generally determined from photoelectron spectroscopy and chemical probe experiments. A study [49] was conducted that 50–800 numbers of atoms of Ni_n and Co_n nanoparticles have icosahedral structures but the structures of small Co_n ($n \leq 50$) mono metal clusters were not well classified. Relatedly, for both pure and ammoniated nanoparticles within the size range of $n = 50\text{--}100$, the Co_n reactions with water and ammonia reveal icosahedral structures [50]. Nevertheless, it was reported that small, monometallic clusters could adopt different type of structures [51]. Yoshida and coworkers [52] accomplished to find the geometry and electronic structures of Co_n anions ($n = 3\text{--}6$) by using photoelectron spectra. The magnetic features of monometallic Co_n particles within the range of $n=20\text{--}300$ were studied by Stern–Gerlach experiments by various groups [42–44,47] and concluded that the magnetic moment per atom for small Co_n particles are considerably larger than the bulk value ($1.7 \mu_B$ [53]).

Pd is one of the essential materials as catalyst in numerous applications as well. Reduction of very active NO by CO happens in the existence of very dispersed Pd clusters supported on alumina [54]. Additionally, ultradispersed supported Pd nanoparticles of up to 2 nm in size behaves highly active catalysts in hydrogenation processes [55] owing to much higher selectivity in the conversion of triple to double bonds than that of bulk Pd [56]. Furthermore, current observation of Pd nanoparticles in terms of ferromagnetism provides the probability of potential use of these particles in magnetic storage materials [57]. Wide-ranging experimental studies have been conducted on Pd particles over many years [58–62]. Early Stern–Gerlach experiments indicated the absence of magnetic moments in Pd nanoparticles among these experimental studies [58,59,62] Photoemission experiments proposed a Ni-like spin distribution in Pd_n nanoparticles at $n=6$ and a nonmagnetic behavior at $n = 15$. Despite the encouraging experimental marks, they could not give satisfactory info on the electronic and geometrical structures of very minute Pd nanoparticles. These properties are required to comprehend the size dependence of chemisorption and catalytic properties of nanosized particles [63].

The case of nanoalloy substances is of great concern in the chemical industry. Such constituents are motivating since one of the metals may adjust the catalytic properties

of the other substances due to structural and electronic effects. It has been reported that in many particles at nanoscale, the low lying geometry is one of the fundamental part that particles are predominantly occupied by one of the constituents and its surface holds most of the second element. Smaller volumes of element might be adequate to get similar effects as those achieved by single element catalysts if the active element is the one that constitutes from the surface [64]. Thus, it is significant to study CoPd nanoalloy particles at the nanoscale. In Fisher-Tropsch reactions [65-67], CoPd nanoparticles displayed better selectivity over pure Co particles. The artificial fabrication of fuels by changing carbon monoxide and hydrogen is appealing many researchers in this area due to the recent huge fluctuations in the prices of hydrocarbons [64].

The study of Co–Pt nanoalloy particles is one of the major aims of the low-temperature polymer electrolyte membrane fuel-cell technology in order to develop and reduce Pt loading as the oxygen-reduction catalyst [68]. Numerous analyses [69-72] such as the series of binary Pt–X alloys (X =Mn, Cr, Co, Ni) supported on carbon [73], have been conducted to solve the role of alloying in the electrocatalytic activity of Pt for the oxygen-reduction reaction. Those analyses revealed that the intrinsic activity of nanoparticles depends on particle size, shape and composition. By decreasing the size of the clusters, their catalytic activities are inclined to upturn due to the bigger surface areas of smaller nanoparticles and the structural sensitivity to some reactions.

Utilizing ligands with functional groups attached to the metal atoms surface lets the formation of functional nano assemblies and binding the clusters to various substrates surfaces. Besides, the ligand environment affects the electronic properties of the clusters. There exists a huge amount of information for small bare or nanoalloy metal nanoparticles but much less theoretical emphasis has been given to the ligation of these clusters with stabilizing molecules. The purpose of most of the computer studies is to determine the relationship between structure and property alteration. The knowledge of the property variation with geometry also allows one to carry out computer experiments to design new stable clusters with desired properties. Thus, this computational study would be a contribution to the understanding of the

influence of ligands on the stabilization of metal clusters to design new stable clusters with desired properties

1.3 Computational Simulation

Computational methods are widely used tools for the fields of chemistry, physics, and material engineering. The increasing speed and availability of computational resources in grouping with newly developed and increasingly accurate models provides scientists to solve and rationalize chemical phenomenon. Additionally, computer simulations allow us to investigate probabilities to check whether the exciting properties of clusters are preserved in different environments. For instance, whether the high magnetic moments of gas-phase clusters will be retained when they are deposited on a substrate. It also allows one to check whether highly stable clusters can be assembled to form solids. This type of approach can lead us to the development of novel cluster based materials.

Another point is that the experiments on clusters especially on gas-phase clusters yield little information about their structures. In this regards, simulations complement the experiments by providing structural input. From the application point of view, the interaction between the cluster and the substrate matrix is of paramount importance. The properties of such systems are governed by many body electron ion interactions.

In the present study, we have used a computing system of four 6-core AMD Opteron Processors 8435 800MHz with 512KB cache, 128 GB RAM, 2 TB HDD, and Ubuntu 12 operating system. The system is constructed at Zirve University by the start-up funds granted to Dr. Sebetci.

CHAPTER 2

DENSITY FUNCTIONAL THEORY

2.1 Introduction

For the quantum mechanical simulation of clusters, molecular, periodic and solid systems in the scope of physics, material science, chemistry and multiple branches of engineering, the density functional theory (DFT) has been the dominant method over the past 30 years. DFT is the prevailing implementation of the computations for the quantum state of atoms, molecules, crystals, surfaces and their interactions, and for the ab-initio molecular dynamics.

The introduction of the DFT began after the foundation of quantum mechanics. In 1927, in order to determine approximate wavefunctions and energies for atoms and ions, Hartree developed a function, which is now called Hartree function. A few years later, Fock and Slater, the students of Hartree, proposed a self consistent function in regard to Pauli Exclusion Principle and multi-electron wavefunction in the form of Slater-determinant (the determinant of one particle orbitals) respectively so as to cope with the total ignorance of the antisymmetric properties of electrons. Although Hartree-Fock (HF) Method was not prevalent until 1950s due to the complexity of calculations of the HF model, the method is a good approach for the approximation to the systems.

In the same year that Hartree derived the Hartree function, by approximating the distribution of electrons in an atom, Thomas and Fermi suggested a statistical model to calculate the energy of atoms. In this model, the kinetic energy of an atom is expressed by the functional of electron density and adds two terms of electron-electron and nuclear-electron interactions in order to compute the atomic energy. In the early stage of this model, it did not include the exchange energy of the atom that

results from Pauli exclusion principle, which is identified in the HF Theory. In 1928, Dirac enlarged the Hartree function by adding an exchange energy functional part.

It is accepted that the Thomas-Fermi model is a significant first step of the DFT but its uses are very restricted presently due to the largest source of error that originates from the statement of the kinetic energy functional term that is only an approximation. This approximation leads to inaccuracy in the exchange energy and this is due to the whole disregard of electron correlation. Despite this, it is known as an antecedent of the DFT [74].

In 1964, Hohenberg and Kohn (HK) wrote an important article that provides the basis of DFT. In this paper, they used electron density functional that includes merely 3 variables instead of the complicated many electron wavefunction that includes $3N$ variables, where N is the numbers of electrons and each electron has 3 spatial coordinates. Thus, the huge amount of variables become out of the concern by using electron density functional that has only 3 variables. According to their first theorem, the ground state energy merely depends on the electron density. In addition, HK proposed the second theorem that the ground state energy can be found via optimizing the energy of the system in terms of electron density.

HK Theorem postulates the relations between electron density functional and system properties. However, it does not precisely describe what the relations between them are. Kohn-Sham (KS) approach is the most commonly used method instead of optimizing the energy of the system that is implemented at the HK Theorem. Only one year later than their significant article published in 1964, KS solved the multi electron issue by simplifying it into non-interaction electron problem inside an effective potential involving the external potential and the influence on the Coulomb for the exchange and correlation interactions between electrons in the article they wrote. It is a challenging work to deal with the correlation and exchange energy in the scope of the KS-DFT. Up to now, to find out the exchange and correlation energy, there are not still an exact method. Nevertheless, the Local Density Approximation (LDA), the simplest approximation, is related to the uniform electron gas model to obtain exchange energy that exact value can be obtained from Thomas-Fermi model and to obtain the correlation energy from fits to the uniform electron

gas. In an effective potential, wavefunction can be effortlessly exemplified by a Slater determinant of orbitals and also the kinetic energy functional of this system is totally known while the total energy functional still has unknown exchange correlation (xc) part [74].

By using the LDA, the results are excellent with experimental data when comparing to other methods related to the solution of many body problem in quantum mechanics. However, DFT was still inaccurate till 1990s in quantum chemistry field. Now, DFT is widely used method to determine electronic structures of the systems in many areas after refining better approximation methods to model xc interactions.

2.2 The Schrödinger Equation

Most of the quantum chemical approaches are based on the approximate solution of the time-independent Schrödinger equation that is given as the following:

$$H\Psi_k(\vec{x}_1, \vec{x}_2, \dots, \vec{x}_A, \vec{R}_1, \vec{R}_2, \dots, \vec{R}_B) = E_k \Psi_k(\vec{x}_1, \vec{x}_2, \dots, \vec{x}_A, \vec{R}_1, \vec{R}_2, \dots, \vec{R}_B) \quad (2.1)$$

Here, H is a differential Hamiltonian operator of a molecular system with a number of N electrons and M is the number of nuclei where H denotes the total energy:

$$H = -\frac{1}{2} \left[\sum_{k=1}^N \nabla_k^2 + \frac{1}{M_q} \sum_{q=1}^M \nabla_q^2 \right] - \sum_{k=1}^N \sum_{q=1}^M \frac{Z_q}{r_{kq}} + \sum_{k=1}^N \sum_{l>k}^N \frac{1}{r_{kl}} + \sum_{q=1}^M \sum_{m>q}^M \frac{Z_q Z_m}{R_{qm}} \quad (2.2)$$

In the equations, k and l are for N electrons while q and m are for the M nuclei. The first two expressions in H depict the kinetic energy of electrons and nuclei where M_q is the mass of nucleus q . The rest three expressions describe the potential energy part of the Hamiltonian that shows electrostatic interaction between nuclei and electrons, electrons and electrons, and nucleus and nucleus, respectively. R_{ab} (and correspondingly r_{ab}) is the distance between the particles a and b . The wave function $\Psi_k(\vec{x}_1, \vec{x}_2, \dots, \vec{x}_N, \vec{R}_1, \vec{R}_2, \dots, \vec{R}_M)$ describes the electronic wave function of the k 'th state of the system. The electronic wave function is a function of $3N$ spatial coordinates \vec{r}_k

and the N spin coordinates \vec{s}_k , shown as the expression \vec{x}_k and the $3M$ spatial coordinates of the nuclei \vec{R}_l as well. Ψ_k covers all possible information of the quantum state. Lastly, E_k is the numerical value of the energy of the state defined by Ψ_k .

The Schrödinger equation can be simplified if we assume nuclei do not move. Even for the hydrogen atom having single proton in its nucleus, the mass of the nucleus is roughly 1800 times more than that of the electron. In short, the movement of the nucleus is much slower than the movement of the electron so that we can accept that the electron moves in the vicinity of the stationary nucleus. This is known as Born-Oppenheimer approximation. In this approximation, the potential energy term due to the repulsions between nuclei. The potential energy becomes only a constant. Thus, the Hamiltonian equation can be simplified as

$$H_{elec} = -\frac{1}{2} \sum_{k=1}^N \nabla_k^2 - \sum_{k=1}^N \sum_{q=1}^M \frac{Z_q}{r_{kq}} + \sum_{k=1}^N \sum_{l>k}^N \frac{1}{r_{kl}} = T + V_{Ne} + V_{ee} \quad (2.3)$$

The solution of the Schrödinger equation with Hamiltonian operator described in the equation 2.3 is the electronic wave function and the electronic energy E_{elec} varies only with the electron coordinates while the nuclear coordinates do not explicitly appear in the electronic wave function. On the other hand, the total energy E_{tot} has two terms, which are electronic energy E_{elec} and the constant nuclear repulsion term E_{nuc}

$$E_{nuc} = \sum_{q=1}^M \sum_{m>q}^M \frac{Z_q Z_m}{R_{qm}}, i.e.,$$

$$H_{elec} \Psi = E_{elec} \Psi \text{ for the electron particle} \quad (2.4)$$

and

$$E_{tot} = E_{elec} + E_{nuc} \quad (2.5)$$

As the electronic wave function is not an observable quantity, taking square of the electronic wave function can only do the physical explanation in that

$$|\Psi(\vec{x}_1, \vec{x}_2, \dots, \vec{x}_N)|^2 d\vec{x}_1 d\vec{x}_2 \dots d\vec{x}_N \quad (2.6)$$

shows the probability that all electrons are found at the same time in the volume element. There must be no difference in the probability on the condition that any two electrons' coordinate are interchanged, viz.,

$$|\Psi(\vec{x}_1, \vec{x}_2, \dots, \vec{x}_k, \vec{x}_l, \dots, \vec{x}_N)|^2 = |\Psi(\vec{x}_1, \vec{x}_2, \dots, \vec{x}_l, \vec{x}_k, \dots, \vec{x}_N)|^2 \quad (2.7)$$

The second wave function formed by the interchange is the same as the first one for bosonic particle having integer spin while for Fermions having half-integral spin, the interchange causes the sign change between two electronic wave functions. Electrons have half spin so that they are Fermions. The wave function must change its sign in the case of the interchange:

$$\Psi(\vec{x}_1, \vec{x}_2, \dots, \vec{x}_k, \vec{x}_l, \dots, \vec{x}_N) = -\Psi(\vec{x}_1, \vec{x}_2, \dots, \vec{x}_l, \vec{x}_k, \dots, \vec{x}_N) \quad (2.8)$$

This is called antisymmetry principle. The result of this principle is the generalization of Pauli exclusion principle that is two electrons cannot occupy the same state. The probability of finding N number of electrons anywhere in space must be exactly unity,

$$\int \int \Psi(\vec{x}_1, \vec{x}_2, \dots, \vec{x}_N) d\vec{x}_1 d\vec{x}_2 \dots d\vec{x}_N = 1 \quad (2.9)$$

A wave function is said to be normalized if it satisfies the equation 2.9.

2.3 The Variational Principle

The average electronic total energy is the expectation value of H operator, i.e.;

$$E[\Psi] = \int \Psi^* \hat{H} \Psi d\bar{x} \equiv \langle \Psi | \hat{H} | \Psi \rangle \quad (2.10)$$

The expression $E[\Psi]$ refers that the total energy is a functional of the wave function. The variational theorem states that the energy is higher than the ground state energy E_0 if not the wave function Ψ matches to ground state wave function Ψ_0 :

$$E_{trial}[\Psi] \geq E_0 = \langle \Psi_0 | \hat{H} | \Psi_0 \rangle \quad (2.11)$$

The method in regard to the variation theorem to determine the lowest energy and its wave function is to optimize the functional $E[\Psi]$ by searching through all suitable A -electron wave functions. If the electron wave function gives the lowest energy, then, it will be Ψ_0 and the energy will be E_0 . This can be shortly expressed by

$$E_0 = \min_{\Psi \rightarrow N} E[\Psi] = \min_{\Psi \rightarrow N} \langle \Psi | \hat{T} + V_{Ne} + V_{ee} | \Psi \rangle \quad (2.12)$$

Here, $\Psi \rightarrow N$ shows that Ψ is an allowed N -electron wave function. The variational principle can be applied as to subsets of all possible functions as well. The aim of the use of these subsets is to optimize the equation given above within some algebraic schemes. The calculation will be the best approximation to the real electronic wave function using those particular subsets.

2.4 The Hartree-Fock Method

The HF Method is the milestone of nearly all wave function based quantum mechanical methods. Comprehension of the logic behind this approximation will be better help for the analysis of the density functional theory [75].

As mentioned before, it is not possible to solve the equation 2.12 by examining through all acceptable N -electron electronic wave functions so a suitable subset is needed to be described. The subset should offer a physically sensible approximation to the exact wave function. HF theory includes an ansatz for the structure of electronic wave functions: it is an antisymmetric product of functions $\zeta_k(\vec{x}_k)$ each of which depends on the coordinates of a single electron, that is;

$$\Psi_{HF} \cong \phi = \frac{1}{\sqrt{N!}} \begin{vmatrix} \zeta_1(\vec{x}_1) & \zeta_2(\vec{x}_1) & \dots & \zeta_N(\vec{x}_1) \\ \zeta_1(\vec{x}_2) & \zeta_2(\vec{x}_2) & \dots & \zeta_N(\vec{x}_2) \\ \cdot & \cdot & & \cdot \\ \cdot & \cdot & & \cdot \\ \zeta_1(\vec{x}_N) & \zeta_2(\vec{x}_N) & \dots & \zeta_N(\vec{x}_N) \end{vmatrix} \quad (2.13)$$

or using a convenient short-hand notation:

$$\phi = \frac{1}{\sqrt{N!}} \det\{ \zeta_1(\vec{x}_1) \quad \zeta_2(\vec{x}_2) \dots \zeta_N(\vec{x}_N) \} \quad (2.14)$$

ϕ is referred as slater determinant. The functions $\zeta_k(\vec{x}_k)$ are spin orbitals, which consists of one of the two spin functions $\alpha(s)$ or $\beta(s)$ and a spatial orbital $\theta_k(\vec{r})$.

$$\zeta(\vec{x}) = \phi(\vec{r})\sigma(\vec{s}), \quad \sigma = \alpha, \beta \quad (2.15)$$

The spin functions are the orthonormal property, that is, $\langle \alpha | \alpha \rangle = \langle \beta | \beta \rangle = 1$ and $\langle \alpha | \beta \rangle = \langle \beta | \alpha \rangle = 0$.

Substitution of the equation 2.14 for electronic wave function into the equation 2.3 produces the following expression for the HF energy:

$$E_{HF} = \langle \phi | \hat{H} | \phi \rangle = \sum_i^N (i | \hat{h} | i) + \frac{1}{2} \sum_i^N \sum_j^N (ii | jj) - (ij | ji) \quad (2.16)$$

$$(i | \hat{h} | i) = \int \zeta_i^*(\vec{x}_1) \left\{ -\frac{1}{2} \nabla^2 - \sum_q^M \frac{Z_q}{r_{1q}} \right\} \zeta_i(\vec{x}_1) d\vec{x}_1 \quad (2.17)$$

describes the one electron term, which is kinetic energies of the electrons and the interactions between electrons and nucleus respectively.

$$(ii | ij) = \iint |\zeta_i(\vec{x}_1)|^2 \frac{1}{r_{12}} |\zeta_j(\vec{x}_2)|^2 d\vec{x}_1 d\vec{x}_2 \quad (2.18)$$

$$(ij | ji) = \iint \zeta_i(\vec{x}_1) \zeta_j^*(\vec{x}_1) \frac{1}{r_{12}} \zeta_j(\vec{x}_2) \zeta_i^*(\vec{x}_2) d\vec{x}_1 d\vec{x}_2 \quad (2.19)$$

are the two electrons terms, which are called coulomb and exchange integrals, respectively. They describe the electron interaction for two electrons. E_{HF} is a functional of the spin orbitals, $E_{HF} = E[\{\zeta_i\}]$. By using variation theorem on the equation 2.16 for the choice of the orbitals, we can find the best orbitals that minimize E_{HF} energy with the restriction that the orbitals are orthonormal. Thus, HF equation can be written as

$$\left\{ -\frac{1}{2} \nabla^2 - \sum_q^M \frac{Z_q}{r_{iq}} + \int \frac{\rho(\vec{x}_2)}{r_{12}} d\vec{x}_2 \right\} \zeta_i(\vec{x}_1) + \int v_x(\vec{x}_1, \vec{x}_2) \zeta_i(\vec{x}_2) d\vec{x}_2 = \varepsilon_i \zeta_i(\vec{x}_1) \quad (2.20)$$

Here, ε_i are the orbital energies, the third term is exchange energy and v_x , the non local exchange potential, is such that

$$\int v_x(\vec{x}_1, \vec{x}_2) \zeta_i(\vec{x}_2) d\vec{x}_2 = - \sum_j^N \int \frac{\zeta_j(\vec{x}_1) \zeta_j^*(\vec{x}_2)}{r_{12}} \zeta_i(\vec{x}_2) d\vec{x}_2 \quad (2.21)$$

The HF equations represent the influence of the mean field potential consisting of the non-interacting electrons under the Coulomb potential and a non-local exchange potential.

Although from this starting point, correlated methods (better approximations) for the wave function and the ground state energy can be obtained, such improvements computationally costs very high and the scales are so quickly with the number of the electrons treated [76]. Moreover, to obtain accurate solutions, a large basis set that means very flexible description of spatial variation of the electronic wave function should be used. For molecular calculations, many correlated methods were developed such as, MP2, MP3, MP4, CISD, CCSD, CCSD(T) [77]. The calculations carried out by CCSD(T) are accurate enough for predicting the chemical properties of systems, such as reaction rates, stability, etc. On the other hand, despite rapid advances in computer technology, the application of these methods to realistic models of systems of interest is not feasible due to their prohibitively high computational expenses [78].

In condensed matter science, the discussion above refers that the direct solution of the Schrödinger equation is not currently possible. For the development and use of DFT, this is a major motivation since it can be possible to solve ground state energy without solving the Schrödinger equation and determining the $3N$ dimensional wave function find ground state energy, we may not need to solve Schrödinger equation exactly.

2.5 Avoiding the Solution of the Schrödinger Equation

It is not necessary to know $3N$ dimensional wave function to calculate the total energy. Knowledge of the two-particle probability density, i.e., the probability of finding an electron at \vec{x}_1 and an electron \vec{x}_2 density of electrons is adequate.

The second order density matrix for the analysis of the energy expression is defined as

$$P_2(\vec{x}'_1, \vec{x}'_2; \vec{x}_1, \vec{x}_2) = \frac{N(N-1)}{2} \int \Psi^*(\vec{x}'_1, \vec{x}'_2, \dots, \vec{x}'_N) \Psi(\vec{x}_1, \vec{x}_2, \dots, \vec{x}_N) d\vec{x}_3 d\vec{x}_4 \dots d\vec{x}_N \quad (2.22)$$

The diagonal elements of P_2 , often referred to as the two-particle density matrix, are

$$P_2(\vec{x}_1, \vec{x}_2) = P_2(\vec{x}_1, \vec{x}_2; \vec{x}_1, \vec{x}_2) \quad (2.23)$$

This equation is the required two-electron probability function and entirely defines all two-particle operators. The first order density matrix can be written in terms of P_2 as:

$$P_1(\vec{x}'_1, \vec{x}_2) = \frac{2}{N-1} \int P_2(\vec{x}'_1, \vec{x}_2; \vec{x}_1, \vec{x}_2) d\vec{x}_2 \quad (2.24)$$

The total energy is defined in terms of P_1 and P_2 :

$$E = \text{tr} \begin{pmatrix} \hat{H} & \hat{P} \end{pmatrix} = \int \left[\left(-\frac{1}{2} \nabla_1^2 - \sum_q \frac{Z_q}{r_{1q}} \right) P_1(\vec{x}'_1) \right]_{x_1=x'_1} d\vec{x}_1 + \int \frac{1}{r_{12}} P_2(\vec{x}_1, \vec{x}_2) d\vec{x}_1 d\vec{x}_2 \quad (2.25)$$

Hence, the total energy can be computed by the diagonal elements of the P_1 and P_2 . This makes the calculation simpler since the solution of the Schrödinger equation for the wave function is not required and the problem in a space of $3N$ coordinates has been reduced to a problem in a 6 dimensional space. Shortly, it is enough to find the first and second order density matrixes rather than solving the Schrödinger equation exactly in order to determine the energy.

Methods related to the direct optimization of $E(P_1, P_2)$ have the particular problem of ensuring that the density matrices are constructible from an antisymmetric Ψ . Imposing this constraint is an unsolved issue [79,80]. Thus, without calculating many body wave function, to calculate the total energy, the equation 2.25 is does not lead to a reliable method for computing the total energy.

2.6 The Hohenberg and Kohn Theorems

Hohenberg and Kohn proved the following two theorems in 1964 [81]. The first theorem states:

The electron density determines the external potential to within an additive constant.

According to this statement, the electron density individually determines the Hamiltonian operator in the equation 2.3. The Hamiltonian is specified by the external potential and the total number of electrons, N , which can be computed from the density simply by integration over all space. Hence, in fact, the operator can be individually defined by the given charge density so the electronic wave functions Ψ of all states and all properties of the systems can be determined.

They did an explicit proof of the given theorem that became general to contain systems with degenerate states in proof given by Levy [82]. The theoretical spectroscopist E. B. Wilson came up with a very straightforward proof of this theorem in a conference in 1965 at which it was being presented. Wilson's comment is that the electron density uniquely describes the charges and the positions of the nuclei and thus trivially determines the Hamiltonian. The proof based on the fact that, the electron density possesses a cusp at the nucleus:

$$Z_\alpha = \frac{-1}{2\bar{\rho}(0)} \left[\frac{\partial \bar{\rho}(r_\alpha)}{\partial r_\alpha} \right]_{r_\alpha=0} \quad (2.26)$$

where, $\bar{\rho}(\vec{r})$ is the spherical average of the charge density, ρ such that one can uniquely determine Hamiltonian by examining charge density carefully. The Wilson's observation causes to start the interest for the interaction between electrons and nucleus although Levy proof is more general. Shortly, the first theorem states that the energy is a functional of the density.

The second theorem forms a variational principle:

For any positive definite trial density, ρ_t , such that $\int \rho_t(\vec{r}) d\vec{r} = N$ then $E[\rho_t] \geq E_0$

The second theorem's proof is very clear since it is known from the first theorem that a unique trial Hamiltonian, H is found by the trial density. Hence, the trial wave function, Ψ_{trial} ; $E[\rho_t] = \langle \Psi_{trial} | \hat{H} | \Psi_{trial} \rangle \geq E_0$ obeys the variational theorem for the Schrodinger equation (see the equation 2.15). By the second theorem, DFT is restricted to the studies for finding ground state.

These two theorems lead to the following fundamental statement of DFT:

$$\delta \left[E[\rho] - \mu \left(\int \rho(\vec{r}) d\vec{r} - N \right) \right] = 0 \quad (2.27)$$

The minimum of some functional $E[\rho]$ corresponds the ground state energy and density provided that the density contains the correct number of electrons. The Lagrange multiplier of this limitation is the electronic chemical potential (μ).

The equation 2.27 indicates that there is an universal functional, independent of the external potential, which can be used to find the ground state density and energy by minimizing this functional if its form is known.

2.7 The Energy Functional

It can be concluded from the equation 2.3 that the energy functional consists of three terms, which are the electronic kinetic energy, the attraction between the electrons and nuclei (external potential), and the electron-electron interactions so the energy functional can be written as:

$$E[\rho] = T[\rho] + V_{ext}[\rho] + V_{ee}[\rho] \quad (2.28)$$

The external potential is trivial:

$$V_{ext}[\rho] = \int \hat{V}_{ext} \rho(\vec{r}) d\vec{r} \quad (2.29)$$

The remaining two terms are unknown. Direct minimization of the energy would be achievable on the condition that good approximations to those functionals could be found. There are a lot research on this possibility [83].

Kohn and Sham proposed the following method to approximate the kinetic energy and electron-electron functionals [84]. They presented fictitious system of N number of non-interacting electrons to be described by a single determinant wave function in N number of orbitals. The electron density and kinetic energy are identified from the orbitals in this system:

$$T_s[\rho] = -\frac{1}{2} \sum_i^N \langle \zeta_i | \nabla^2 | \zeta_i \rangle \quad (2.30)$$

The kinetic energy here $T_s[\rho]$ is the energy of non-interacting electrons in the system rather than the true kinetic energy $T[\rho]$. That produces the ground state density:

$$\rho(\vec{r}) = \sum_i^N |\zeta_i|^2 \quad (2.31)$$

A set of orbitals forming explicitly the density confirms that it can be constructed from an asymmetric wave function.

A significant component of the electron-electron interaction, which is the classical Coulomb interaction, can be written in terms of the density:

$$V_H[\rho] = \frac{1}{2} \int \frac{\rho(\vec{r}_1) \rho(\vec{r}_2)}{r_{12}} d\vec{r}_1 d\vec{r}_2 \quad (2.32)$$

The energy functional may be modified as:

$$E[\rho] = T_s[\rho] + V_{ext}[\rho] + V_H[\rho] + E_{xc}[\rho] \quad (2.33)$$

Here, the last term is the exchange-correlation functional, which can be expressed as:

$$E_{xc}[\rho] = (T[\rho] - T_s[\rho]) + (V_{ee}[\rho] - V_H[\rho]) \quad (2.34)$$

The exchange correlation functional is basically the total of the error made in using a non-interacting kinetic energy and treating the electron-electron interaction classically. After writing the functional explicitly in terms of the density, and applying the variational theorem, we determine the orbitals which minimize the energy, satisfy the following set of equations with respect to the density:

$$\left[-\frac{1}{2}\nabla^2 + v_{ext}(r) + \int \frac{\rho(r')}{|r-r'|} dr' + v_{xc}(r) \right] \zeta_i(r) = \varepsilon_i \zeta_i(r) \quad (2.35)$$

Here, $v_{xc}(r)$, local multiplicative potential, is the functional derivative of the exchange correlation energy.

$$v_{xc}(r) = \frac{\delta E_{xc}[\rho]}{\delta \rho} \quad (2.36)$$

The behavior of non-interacting electrons in an effective local potential is described by this set of non-linear equations called the Kohn-Sham equations. The orbitals produce the exact ground state density and energy by using the equation 2.31 and 2.35 respectively when the exchange functional is provided.

These Kohn-Sham equations and the HF equations, see the equation 2.20, have similar structure except that the non-local exchange potential of the HF equations is replaced by the local exchange-correlation potential, v_{xc} . At this point, one should note that exchange-correlation potential here includes an element of the kinetic energy and is not the summation of the exchange and correlation energies as they are known in HF and correlated wave function theories [77].

The Kohn-Sham methodology establishes an exact correspondence of the density and ground state energy of a system comprising of non-interacting Fermions and the real many body system described by the Schrödinger equation. A cartoon that describe this relationship simply is given in Figure 2.1.

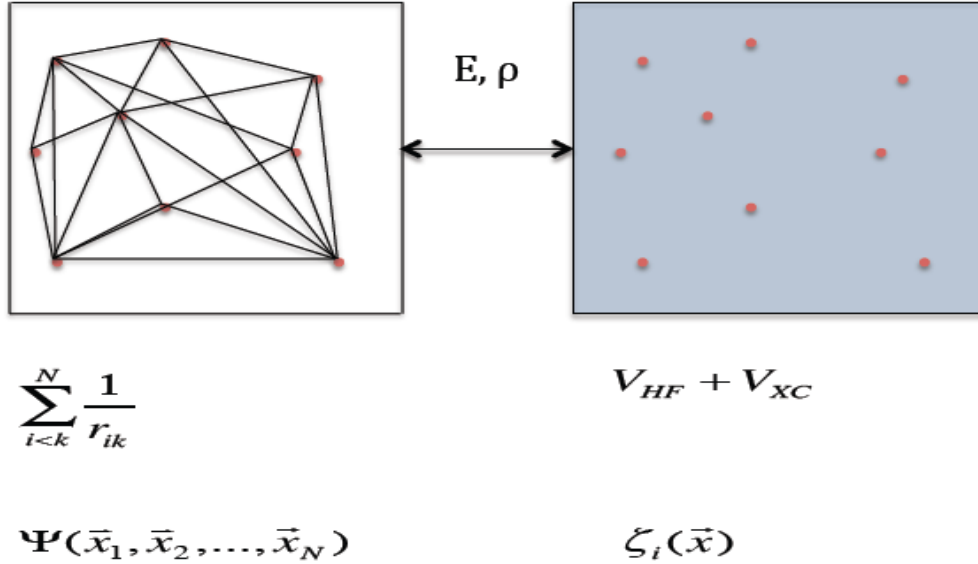


Figure 2.1 The relationship between the real many body system (left side) and the non-interacting system of Kohn Sham density functional theory (right side) [77]

Only if the exact functional is known, the correspondence of the charge density and energy of the many-body and the non-interacting system can be exact. KS-DFT is an empirical methodology in the sense that we do not know the exact functional. Since the functional is universal namely independent of the materials that are studied in principle, we could solve the Schrödinger equation exactly and find the energy functional and its associated potential for any particular system. However, this costs greater struggle than a direct solution of the energy. Nonetheless, the capability of determining precise properties of the universal functional in a number of systems provides exceptional to the functional to be developed and utilized in a wide-rang of materials. This property is generally associated with an ab initio theory so that the approximations to density functional theory are often referred to as ab initio or first principle methods.

The computational cost of solving the KS equation scales normally as N^3 due to the requirement of the orthogonality of N orbitals but in current practice is reducing to N^1 through the exploitation of the locality of the orbitals [77].

In order to calculate local and global minima of the structures, DFT represents a useful and highly accurate option instead of the wave function methods mentioned before. The effectiveness of the DFT, in practice, depends on the approximation used for the exchange correlation energy.

2.8 The Exchange Correlation Functionals

There are some exchange correlational functionals, which can be classified as two main categories that are empirical and non-empirical functionals. The empirical functionals can be derived from the experimental results for particular materials while the non-empirical functionals are obtained from the results of first-principles calculations. In this thesis, the non-empirical functionals will be reviewed.

The exchange correlational energy consists of two parts as mentioned before. One of the parts is that the exchange expression originates from the Pauli principle, which refers that two identical electrons cannot occupy the same quantum state simultaneously. The correlation expression comes from the motion of the electrons, which we accept independent of each other. The other part is that the exchange energy term is precisely known from the HF method [85] whereas the correlation expression is identified merely in parameterized forms, and can be determined by using the Quantum Monte Carlo (QMC) method with some limiting cases [77].

2.8.1 The Local Density Functional

The most regularly used exchange-correlation functionals are known to be Local Density Approximation (LDA) and Spin-polarized Local Density Approximation (LSDA) [84]. The LDA exchange-correlation energy is defined as:

$$E_{xc}^{LDA} = \int \rho(\vec{r}) \epsilon_{xc}^{LDA}[\rho] d\vec{r} \quad (2.37)$$

Here, $\epsilon_{xc}^{LDA}[\rho]$ is the exchange correlation energy per electron. In this approach, $\epsilon_{xc}^{LDA}[\rho]$ is accepted as a functional of the local density and is identified as:

$$\epsilon_{xc}^{LDA}[\rho] = \epsilon_{xc}^{\text{hom}} \quad (2.38)$$

where, $\epsilon_{xc}^{LDA}[\rho]$ states the energy density of a homogenous electron gas per particle of the density ρ . Hence, in this method, the exchange-correlation potential and the exchange correlation energy are substituted by the related terminologies for the homogenous electron gas. The homogenous electron gas is a system of a uniform density in its ground state. Thus, this density describes it. For this reason, LDA exchange correlational function is a good choice where the density of the system changes gradually.

The exchange energy of the homogenous electron gas can be determined analytically whereas the correlation energy is obtained with quantum mechanical calculations. The form of the exchange energy density modified by Dirac [86] is shown as:

$$\epsilon_x[\rho] = -\frac{3}{4} \left(\frac{3}{\pi}\right)^{1/3} \rho^{1/3} \quad (2.39)$$

Perdew and Zunger derived the most known approximation for the correlation [87]. They used the output of quantum mechanical calculation of Ceperley and Alder [88].

LDA was preferred for those systems having quite smooth density such as bulk materials. However, there exist some weaknesses for this approximation such as over estimated dielectric constants, errors in binding energies up to 30 %, inadequate calculations for magnetic properties and the shorter lattice constants than the experiment values.

2.8.2 The Generalized Gradient Approximation

In order to allow for the influence on the inhomogeneity in charge density of the physical system, LDA needs to be modified the dependency of the density gradient $\nabla\rho$. Functionals including the gradient of the density and holding the some rules and

negativity constraints conditions are known as Generalized Gradient Approximation (GGA), which can be generically written as:

$$E_{xc}^{GGA}[\rho_\alpha, \rho_\beta] = \int f(\rho_\alpha, \rho_\beta, \nabla\rho_\alpha, \nabla\rho_\beta) d\vec{r} \quad (2.40)$$

Where, ρ_α, ρ_β are electronic density for spin up and spin down respectively

As usual, it is accepted that E_{xc}^{GGA} has two parts, which are exchange and correlation

$$E_{xc}^{GGA} = E_x^{GGA} + E_c^{GGA} \quad (2.41)$$

and the approximations of the functional are generally made separately for both of them.

Perdew and Wang (PW91) exchange correlation functional includes no experimental parameter. This functional is obtained from the constant gas approximations with exact constraints in 1991 [89-91]. Perdew, Burke, and Ernzerhof, PBE exchange correlation functional did a correction on PW91 [92]. Lee, Yang and Parr (LYP) is another popular functional for the correlation [93]. It is not based upon uniform electron gas and obtained the correlation energy as an explicit functional of the density and its gradient. The LYP functional contains one empirical parameter. This correlation functional is usually associated with Becke's exchange functional and is known as BLYP.

Importantly, GGA does not offer a complete non-local functional. The only advantage of GGA is that it contains the local variation of the densities. Furthermore, for both the energy and potentials, GGA in its original form does not produce the simultaneous asymptotic behavior. In currently developed functionals, a cut-off procedure on density is implemented to obtain satisfactory results. Nonetheless, GGA has improvements over LDA in many systems in condensed matter physics and chemistry with the exception in the long-range weakly bound systems such as van der Waals interactions.

2.8.3 The Meta-GGA Functionals

Recently, for exchange correlation functionals, a rather elegant formalism, which depends on the semi-local information in the Laplacian of the spin density or of the local kinetic energy density, has been developed [94-96]. This kind of functionals is generally referred to as meta-GGA functionals.

The general form of such functionals can be written as:

$$E_{xc}^{GGA} = \int \rho(\vec{r}) \varepsilon_{xc}(\rho, |\nabla\rho|, \nabla^2\rho, \tau) d\vec{r} \quad (2.42)$$

τ is the kinetic energy density:

$$\tau = \frac{1}{2} \sum_i |\nabla \zeta_i|^2 \quad (2.43)$$

The performance of these functionals will be discussed in the following sections.

2.8.4 The Hybrid Functionals

The non-interacting density functional system and the fully interacting many body system have an “exact” connection between each other by means of the integration of the work done in gradually turning on the electron-electron interactions. According to this adiabatic connection approach [97], the “exact” functional can be formally written as:

$$E_{xc}[\rho] = \frac{1}{2} \iint \int_{\lambda=0}^1 [\langle \rho(\vec{r})\rho(\vec{r}') \rangle_{\rho,\lambda} - \rho(\vec{r})\delta(\vec{r} - \vec{r}')] \frac{\lambda e^2}{|\vec{r} - \vec{r}'|} d\vec{r} d\vec{r}' d\lambda \quad (2.44)$$

where the expectation value $\langle \rho(\vec{r})\rho(\vec{r}') \rangle_{\rho,\lambda}$ is the density-density correlation function, which is calculated at density $\rho(\vec{r})$ for a system described by the effective potential:

$$V_{eff} = V_{en} + \frac{1}{2} \sum_{i \neq j} \frac{\lambda e^2}{|\vec{r}_i - \vec{r}_j|} \quad (2.45)$$

Hence, on the condition that the variation of the density-density correlation function with the coupling constant (λ) is known, the exact energy could be determined. By replacing the pair correlation function with that for the homogeneous electron gas, the LDA is recovered.

With the adiabatic integration approach, a different approximation for the exchange-correlation functional is proposed. The non-interacting system corresponds identically to the HF ansatz at $\lambda=0$ whereas the LDA and GGA exchange correlation functions are formed to be perfect approximations for the fully interacting homogenous electron gas, i.e. a system with $\lambda=1$. Thus, it makes sense to approximate the integral over the coupling constant as a weighted sum of the end points, i.e. we may set:

$$E_{xc} \approx aE_{Fock} + bE_{xc}^{GGA} \quad (2.46)$$

Coefficients a and b to be computed by reference to a system for which the exact result is known. Becke used this method by defining a new functional with coefficients obtained by a fit to the observed energies such as atomization energies, proton affinities, ionization potentials and total atomic energies for several small molecules [98]. The resultant energy functional is as following:

$$E_{xc} = E_{xc}^{LDA} + 0.2(E_x^{Fock} - E_x^{LDA}) + 0.72\Delta E_x^{B88} + 0.81\Delta E_c^{PW91} \quad (2.47)$$

Where, ΔE_x^{B88} and ΔE_c^{PW91} are extensively used GGA corrections [99] to the LDA exchange and correlation energy respectively. This kind of hybrid functionals are now very commonly applied in chemical applications, The accuracy of the calculations, such as binding energies, geometries and frequencies is better than the best GGA functionals especially for organic chemistry.

2.8.5 The Performance of the Exchange Correlation Functionals

There is a natural hierarchy among the exchange correlational types. The studies for the corrections are going on the underlying functional form and the description of ground state properties is improving. The most remarkable recent advance is the non-local nature of the exchange potential that is presented in one form or another. A current hierarchy is given in Table 2.1.

Table 2.1 The hierarchy of exchange correlation functionals [77]

Dependencies	Family
Exact exchange, $ \nabla\rho $, ρ	Hybrid
$\nabla^2\rho$, τ	Meta-GGA
$ \nabla\rho $	GGA
ρ	LDA

Kurth and coworkers and Adamo and coworkers have recently been studied the performance of some selected functionals in calculations for a number of molecular and material properties [96,100]. The details can be found in the references.

CHAPTER 3

THE INFLUENCE OF UNSATURATED HYDROCARBON LIGANDS ON THE STABILIZATION OF PLATINUM TETRAMER

3.1 Introduction

Metal clusters (MCs) play an important role in catalysis, medical science and nanostructured electronic devices [6,101-103]. Using ligands with functional groups attached to the surface metal atoms allows for the construction of functional nanoassemblies and binding the clusters to surfaces of various substrates. Moreover, the ligand environment could significantly affect the electronic properties of the metal surfaces and the clusters themselves [104].

Colloidal MCs are cardinal for comprehension of catalytic process by formulating model catalytic systems. Using industrial catalysts supported small MCs with large variations in size and shape generally leads to face with the problems related to control the distribution of the active sites of different reaction products on the catalyst surfaces [105,106]. For this reason, in the last few decades, the study of colloidal metal particles in solution, in the nanoscale regime, with tailored properties have been carried out as the high surface volume ratio of MCs for obtaining high amounts of active sites per metal mass and most catalytic reaction changed according to the surface characteristics for given metals are important keys to take under control catalytic reaction by controlling over the nanoparticle size and shape. Thus, colloidal of metal particles of technological application due to the stabilization of metallic particles efficiently in solution have recently attracted more attention to the systems related to the synthesis of colloidal metallic particles starting from single atoms, ions, or small clusters in the model catalytic systems [107-113]. To keep the growing units from coalescence into thermodynamic equilibrium phase, the ligands could significantly affect the growing units [114-117].

Pt metal clusters are one of the ingredients of colloidal suspensions in the field of catalysis [118]. Approximately 1 nanometer sized Pt particles on chlorinated for industrial catalysts were introduced in the 1960s [119]. Lewis and co-workers contributed for the addition of Pt particles in catalytic hydrosilylation reactions [120]. After them, Colloidal metal nano particles started to use many homogenous catalytic reactions in solution, from hydrogen peroxide decomposition to cross coupling and supported metal nanoparticles on substrate-heterogeneous catalytic reactions [120,121]. Barcaro and Fortunelli studied Pt metalorganic complexes via changing the number of metal atoms and the quantity of organic ligands. They studied small $Pt_n(\text{ligand})_m$ ($n=1$ to $n=3$) clusters since very minute metallic clusters usually containing no more than 10 atoms, coated by solvent molecules can be produced by the metal vapor deposition technique but when producing these small metallic clusters, this technique has problem due to the low thermal stability of the solvates, which even if kept at low temperatures, decompose slowly with the formation of insoluble aggregates [122]. They tried to find possible solution for the stabilization of solvents by using ligands, which are used for inhibiting the coalescence of aggregates [110]. Mittendorfer and coworkers investigated the adsorption of the unsaturated hydrocarbons on Pt and Pd surfaces with the help of ab initio calculations [123]. Zaera and Langmuir studied species CH_3 , CH_2 and CH on Pt surfaces experimentally. They showed both kinetic and spectroscopic evidence for the construction of adsorbed methyl (CH_3) and methylene (CH_2) moieties on Pt surfaces and additional kinetic data, which imply that methylidyne (CH) groups also form on the same substrate [124]. Wang and Andrews studied three Pt- C_2H_2 reaction product isomers experimentally and theoretically. They formed the vinylidene $PtCCH_2$, reacting laser-ablated Pt atoms with C_2H_2 upon co-condensation in excess argon and neon [125]. Granatier and coworkers investigated the interaction between the Pt atoms and benzene molecules using a symmetric Pt-Bz half-sandwich complex with various level of wave function theory including several functionals of the Density Functional Theory [126]. Majumdar and coworkers examined the interaction $(\text{benzene})_n$ ($n=1,2,3$) with Pt and Pt_2 using a variety of the computational techniques. They found physisorbed structures and energetically lower chemisorbed species [127].

In this part of our study we have investigated $Pt_4(CH)_n$ ($1 \leq n \leq 7$) and $Pt_4(\text{benzene})_2$

clusters within the framework of DFT. There is a number of studies available for Pt-hydrocarbon complexes, however less theoretical emphasis has been given to the platinum atoms with unsaturated hydrocarbons including equal number of hydrogen and carbon atoms. Due to the interesting catalytic properties and strong chemical structure of Pt tetrahedron, we studied Pt tetrahedron molecules with very reactive CH units to see the stability and reactivity of these structures by increasing the number of CH ligands. To understand the influence of the unsaturated hydrocarbon ligands on the stabilization of pure Pt tetramer, the geometric, energetic, electronic properties, vibrational frequency and global reactivity indexes were studied by using density functional theory within spin polarized generalized gradient approximation and hybrid exchange correlation functionals. Locally stable isomers are distinguished from transition states by vibrational frequency analysis. We present the obtained results and discuss the influence of the unsaturated hydrocarbon ligands on the stabilization of the Pt tetramer in the following sections.

3.2 Computational Details

NWChem 6.0 package [128] has been used to perform geometry optimizations, and to find the total energies, the vibrational frequencies, and the highest occupied and the lowest unoccupied molecular-orbital (HOMO–LUMO) gaps by DFT calculations. CRENL [129] basis set and relativistic effective core potential (ECP) have been chosen for Pt where the outer most 18-electrons ($5s^2 5p^6 5d^9 6s^1$) are treated as valence to reduce the number of electrons explicitly considered in the calculations. For C and H atoms the split valence 6-31G* basis set has been employed. The reliability of the CRENL basis set and ECP were determined by comparing atomic excitation energies with accurate all-electron calculations where maximum errors were found to be less than 0.12 eV for Pt [129]. The default convergence criteria of the code have been employed during the calculations which are 1×10^{-6} Hartree for energy and 5×10^{-4} Hartree / a_0 for energy gradient. The hybrid B3LYP [93,98,130] exchange-correlation functional is chosen for the transition metal cluster with hydrocarbon ligands studied in the present work. In addition, the ground state geometrical structures obtained by B3LYP hybrid functional that have been re-optimized by BPW91 [92] GGA and SVWN5 [131] LDA functionals as

well. The geometry optimizations without any symmetry constraints in various electronic spin multiplicities were carried out.

3.3 Results and Discussion

3.3.1 Lowest Energy Structure

The most stable structures of $\text{Pt}_4(\text{CH})_n$ ($1 \leq n \leq 7$) hydrocarbon Pt tetramers are presented in Figure 3.1 and Figure 3.2. It can be seen in these figures that CH is adsorbed on the Pt tetramer in a molecular form with carbon instead of hydrogen bonding to platinum for each case studied in the present work. The lowest energy structure of Pt_4 is an equilateral triangular pyramid (distorted tetrahedron), which has C_{3v} point group symmetry in the triplet magnetic state [132,133]. Addition of CH ligands to the Pt tetrahedron do not change the tetrahedral configuration of the metal cluster up to the species $\text{Pt}_4(\text{CH})_4$ although Pt-Pt bond distances change in the lowest energy configurations. For the higher sizes, tetrahedral character of the Pt tetramer is lost except the size $n=6$. This exception is reasonable since benzene is a stable aromatic hydrocarbon, which can bind to the Pt tetramer strongly due to its delocalized electrons without affecting the structure of the metal cluster so much. The re-examination of the most stable structures obtained by using B3LYP with LDA (SVWN5) and GGA (BPW91) exchange-correlation functionals do not alter the geometric structures and bond lengths significantly.

The first CH molecule absorbed on Pt tetramer on a hollow site forming Pt_4 methylidyne (see Figure 3.1a) reduces the point group symmetry to C_s . The magnetic ground state of Pt_4 methylidyne is doublet. The magnetic multiplicities of all the ground state structures obtained in the present study are always the lowest multiplicities, namely singlet for the systems having even number of electrons and doublet for the ones having odd number of electrons. The hollow site absorption and four coordination of carbon indicate that sp^3 hybridization in CH radical is energetically favorable in the reaction with Pt tetramer. Pt-Pt bond distances of the optimized structure of Pt_4 methylidyne (2.6 Å) slightly differ from that of pure Pt_4 (2.7 Å).

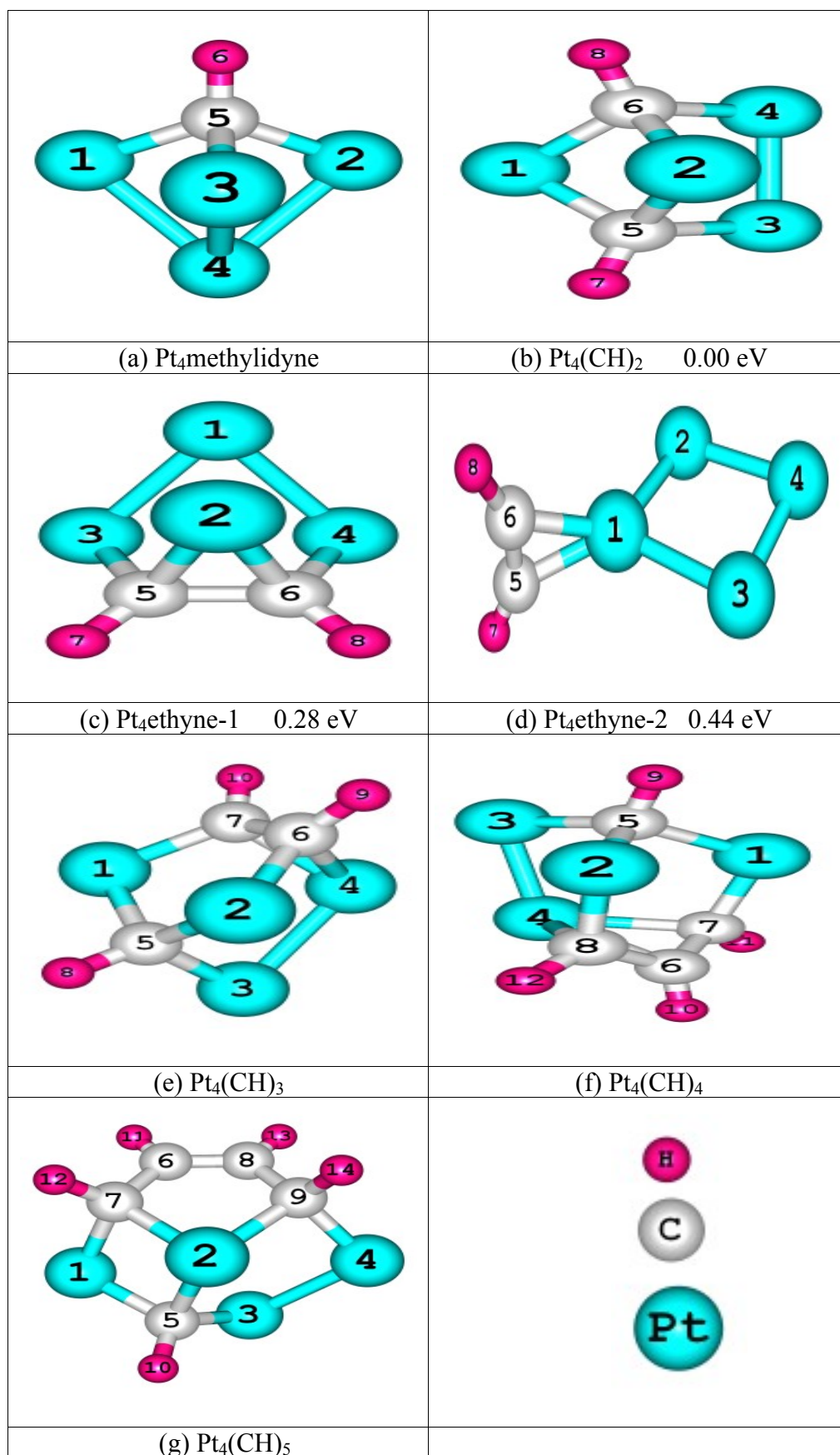


Figure 3.1 The lowest energy structures and some isomers of Pt₄(CH)_n (n=1 to 5) clusters.

The absorption of CH results in a small decrease in the Pt-Pt distances and therefore the three-coordinated Pt atom gets close to the plane formed by the other three Pt atoms. The Pt-C bond length is 1.9 Å whereas the C-H bond distance is 1.1 Å. The second CH ligand prefers to be adsorbed again on another hollow site (see Figure 3.1b), which means that the system has a tendency to optimize the metal-carbon interaction at the expense of the carbon-carbon interaction. The point group symmetry of the lowest energy structure of Pt₄(CH)₂ is C_{2v}. The adsorption of the second CH molecule leads to a stretch in the Pt-Pt bond lengths where the average Pt-Pt bond distance becomes 2.9 Å. As a second isomer of Pt₄(CH)₂, Pt₄ethyne (see Figure 3.1c) has C_s symmetry and its energy is 0.28 eV higher than that of the structure in Figure 3.1b. In this structure, there are two different bond lengths between Pt and C atoms: 2.1 Å and 1.9 Å whereas the C-C bond distance is 1.4 Å. The third isomer of Pt₄(CH)₂, which is the second low-lying isomer of Pt₄ethyne, is given in the Figure 3.1d having C_s symmetry. The binding energy of this structure is 0.44 eV higher than that of the lowest energy one. The Pt-Pt distances are 2.5 Å, while Pt-C bond distance is 2.0 Å in this structure. In summary, the chemical bond formation of two C atoms on Pt tetramer is not energetically favorable when the number of CH ligands is 2.

After the size 2, as the number of CH ligands on the Pt tetramer is increased, the new coming CH radicals prefer to form C bonds rather than to form Pt bonds only since sharing some valence electrons between carbon atoms becomes favorable over constructing new metal-carbon interactions. Thus, the third CH molecule is adsorbed on a Pt-C bridge site by constructing a C-C bond of 1.4 Å (see Figure 3.1e). Pt-Pt distances are between 2.6 Å and 3.2 Å in this structure. As the two Pt atoms get closer to each other the others are separated. Similarly, the fourth CH goes near to the two C atoms instead of binding to the single C (see Figure 3.1f). This structure of Pt₄(CH)₄ has C_s symmetry. The average C-C bond distance is 1.4 Å, which is similar to that of the previous case. There is no significant change in the part of the structure where the single C is bonded to the three Pt atoms and to the H. The average Pt-C bond distance is 2.0 Å. After the adsorption of the fifth CH molecule, the range of the Pt-Pt distances is 2.6 Å – 3.2 Å, which is similar to the previous size. In the lowest energy structure of Pt₄(CH)₅, four C atoms and a Pt atom construct a ring. Two of the C atoms in the ring are doubly bounded to each other (1.3 Å). Single C-C

bond distances are 1.5 Å. The lowest energy structure of $\text{Pt}_4(\text{CH})_6$ is a Pt_4 benzene (see Figure 3.2a) having C_s symmetry where the ring of 6 C atoms adsorbed on a triangular surface of the Pt tetramer. The Pt-C bond lengths in this structure are approximately 2.2 Å. The second isomer of Pt_4 benzene shown in Figure 3.2b has higher energy (0.06 eV) than the first one. In this second structure, which has C_{2v} symmetry, the benzene ring is adsorbed on the bridge site of Pt tetrahedron where the average Pt-Pt distance is 2.6 Å. This result can be interpreted as the following: the π orbitals of the benzene ring have more overlap with the valence orbitals of the Pt tetramer when the ring is adsorbed on the surface of the cluster. The third isomer (see Figure 3.2c) is in the form of $\text{Pt}_4(\text{H})_2$ benzyne whose binding energy is 0.08 eV higher relative to the lowest energy structure of Pt_4 benzene. In this case, two of the six H atoms bind to Pt atoms instead of C atoms. When the seventh CH radical is added, we have a benzene ring and one CH molecule adsorbed on a hollow site in $\text{Pt}_4(\text{CH})_7$. The average Pt-C bond distances do not change significantly. In the other lowest energy structure of $\text{Pt}_4(\text{CH})_7$ (see Figure 3.2f), the benzene is isolated from Pt_4CH structure and its energy is 1.28 eV higher than the first one. When we investigate $\text{Pt}_4(\text{benzene})_2$ structures, we identified the lowest energy structure as two benzene molecules adsorbed on different bridge sites of Pt tetramer (see Figure 3.3a). The average Pt-Pt bond distance in this structure is 2.6 Å. The C-C (1.4 Å) and Pt-C bond distances (2.2 Å) are similar with those of the smaller sizes. A second isomer of $\text{Pt}_4(\text{benzene})_2$ is given in Figure 3.3b, which has higher energy (0.50 eV) than the first isomer where one of the benzene rings is adsorbed on a bridge site while the other is adsorbed on a top side. In the third configuration (Figure 3.3c), we put second benzene molecule parallel to the previous one and relax the structure. The second benzene remains isolated at the end of the geometry optimization, however the total binding energy of this configuration is 1.80 eV higher than the first isomer. Pt_4 biphenyl is identified as a fourth isomer (Figure 3.3d) where an H_2 molecule separated from the rest of the structure.

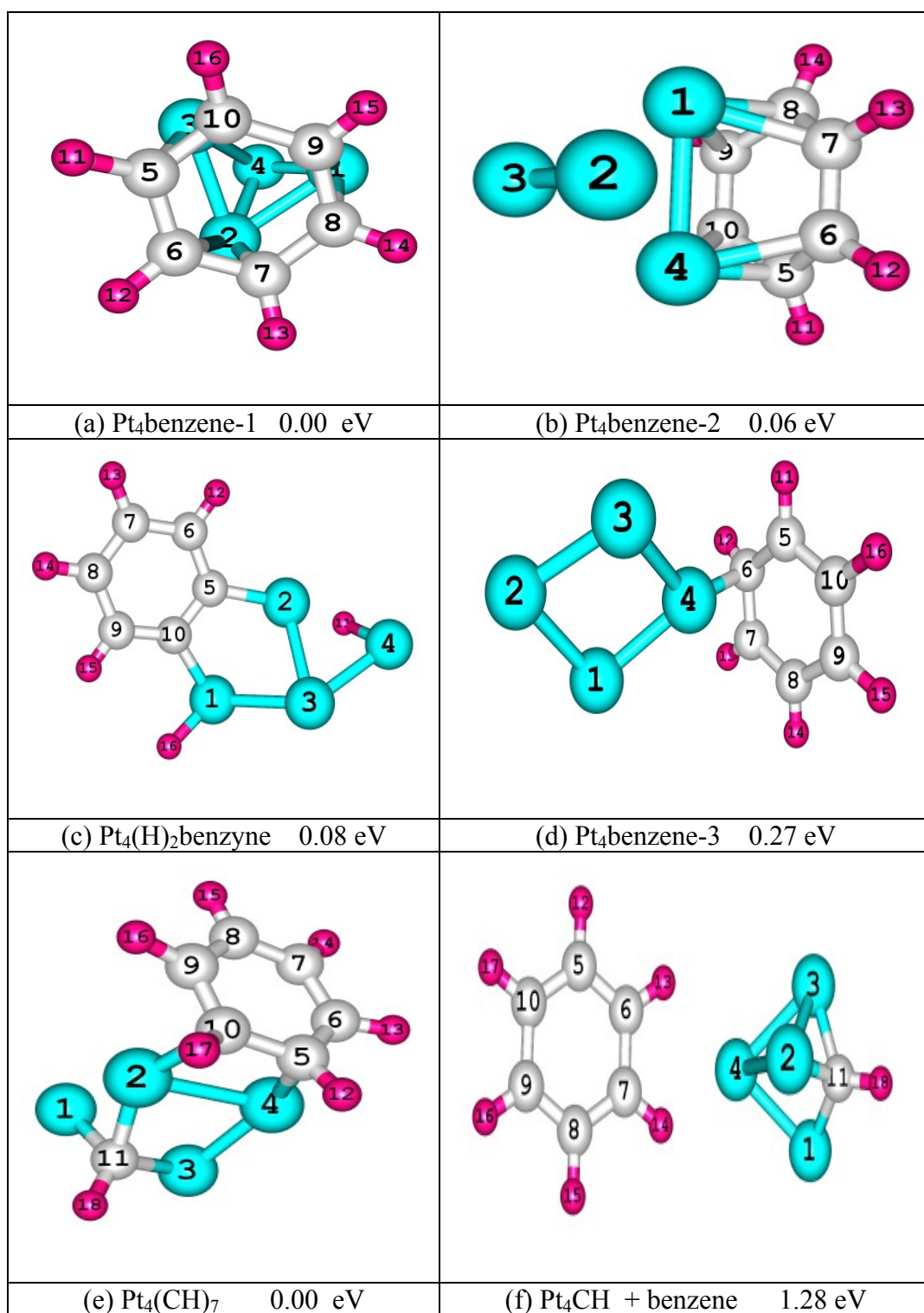


Figure 3.2 The lowest energy structures and some isomers of Pt₄(CH)₆ and Pt₄(CH)₇ clusters

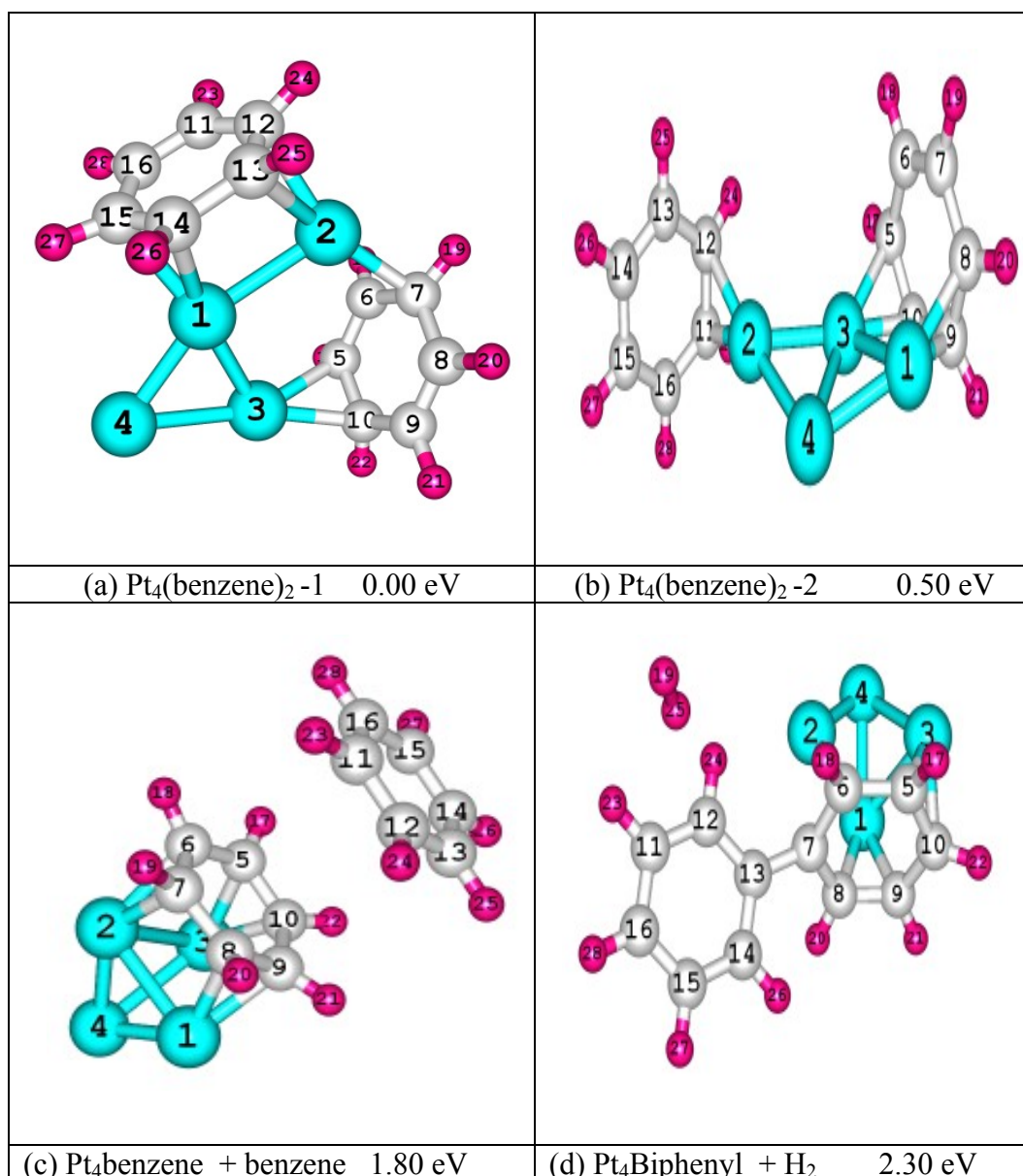


Figure 3.3 The low-lying isomers of $Pt_4(benzene)_2$ clusters

3.3.2 Energetics and Stability

In order to predict the relative stabilities of the $Pt_4(CH)_n$ ($1 \leq n \leq 7$ and $n=12$) structures, the binding energy per atom and the second finite difference in energies are calculated and plotted in Figure 3.4 and Figure 3.5 respectively.

The binding energy per atom (BE/n) has been obtained in the following way:

$$BE/n = (nE[C] + nE[H] + 4E[Pt] - E[Pt_4(CH)_n]) / n \text{ from } n = 1 \text{ to } n = 11 \quad (3.1)$$

where $E[*]$ is the total energy of the neutral Carbon, Hydrogen, Platinum atoms and the metalorganic cluster, respectively. It is clear that the binding energies per atom of the species continuously increase with the increase of the number of CH molecules (see Figure 3.4), which indicates that the species can constantly gain energy during the growth process as the gained energy rate slows down. The binding energy per atom of the pure platinum tetramer is 2.4 eV/atom. After the absorption of the first CH molecule, the binding energy increased rapidly to 3.7 eV/atom.

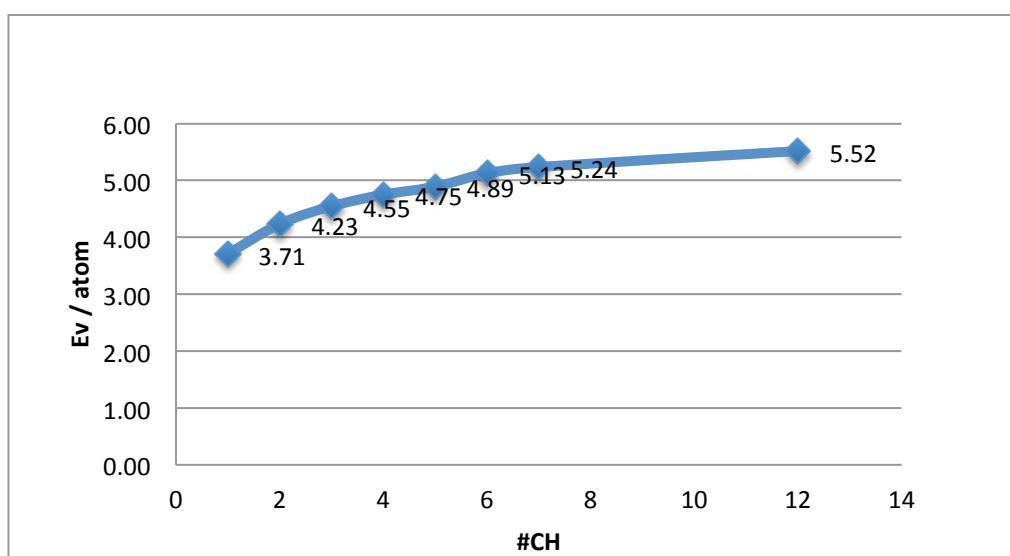


Figure 3.4 The binding energies per atom for $Pt_4(CH)_n$ ($n=1$ to 7 and $n=12$) clusters

To further illustrate the stability of the species and their size dependent behaviors, we have considered the second finite difference in energies that is a sensitive quantity frequently used as a measure of the relative stability of the complexes and is often compared directly with the relative abundances determined in mass spectroscopy experiments. Moreover, clusters are especially abundant magic number sizes in mass spectra as they are most stable ones. The second finite different energies (D_n) can be calculated as

$$D_n = E_{n+1} + E_{n-1} - 2E_n \quad (3.2)$$

where E_n is the total energy of the cluster $Pt_4(CH)_n$. The second finite difference (D) in energies versus cluster size plot is given in Figure 3.5.

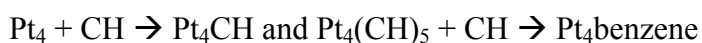
Table 3.1 Reaction energies with two xc functionals: B3LYP and BPW91

Reaction	ΔE (eV) B3LYP	ΔE (eV) BPW91
Pt ₄ + CH → Pt ₄ methylidyne	-7.12	-7.51
Pt ₄ CH + CH → Pt ₄ (CH) ₂	-6.11	-6.54
Pt ₄ (CH) ₂ + CH → Pt ₄ (CH) ₃	-6.06	-6.30
Pt ₄ (CH) ₃ + CH → Pt ₄ (CH) ₄	-6.02	-6.36
Pt ₄ (CH) ₄ + CH → Pt ₄ (CH) ₅	-5.92	-6.78
Pt ₄ (CH) ₅ + CH → Pt ₄ benzene	-8.11	-7.71
Pt ₄ benzene + CH → Pt ₄ (CH) ₇	-6.68	-6.76

Due to the definition of the second finite difference in energies, we examined these energies for Pt₄(CH)_n clusters from n = 2 to n = 6. The peak at the size of Pt₄benzene indicates that this species is the most stable one in the present study. Pt₄(CH)₅ can be considered as the least stable structure as it corresponds to a dip in the plot. Commonly, the more stable the species, the lower reactivity of the species to absorb CH. Thus, Pt₄benzene is expected to be more abundant in mass spectra when compared to the other sizes.



reaction energies calculated by B3LYP and BPW91 xc-functionals are given in Table 3.1. For each n, the reaction is exothermic. The most favorable reactions are



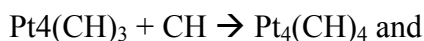
since the reaction energy for them are the least values in Table 3.1 for both of the xc-functionals. On the other hand the least favorable reactions are

Table 3.2 The electronic properties of Pt₄(CH)_n (n=1 to 7 and n=12) clusters with B3LYP

Cluster	Electron Affinity (eV)	I.P (eV)	B.E per atom (eV/atom)	HOMO-LUMO gap (eV)	Lowest and highest vibrational frequencies (cm ⁻¹)
Pt ₄ methylidyne	1.52	6.72	3.71	1.43	60-2208
Pt ₄ (CH) ₂	1.82	7.01	4.23	2.01	45-3017
Pt ₄ ethyne	2.10	6.26	4.20	1.46	15-3100
Pt ₄ (CH) ₃	0.00	6.41	4.55	2.34	57-3098
Pt ₄ (CH) ₄	0.78	9.38	4.75	2.41	59-3174
Pt ₄ (CH) ₅	1.82	6.14	4.89	2.20	37-3185
Pt ₄ benzene	2.09	5.99	5.13	2.28	66-3213
Pt ₄ (CH) ₇	2.14	6.40	5.24	1.96	32-3087
Pt ₄ (benzene) ₂	1.50	6.06	5.52	1.93	60-2208

Table 3.3 The electronic properties of Pt₄(CH)_n (n=1 to 7 and n=12) clusters with xc BPW91

Cluster	Electron Affinity (eV)	I.E (eV)	B.E per atom (eV/atom)	HOMO-LUMO gap (eV)	Lowest and highest vibrational frequencies (cm ⁻¹)
Pt ₄ methylidyne	1.59	6.77	6.21	0.58	46-2943
Pt ₄ (CH) ₂	1.86	6.90	5.92	0.75	43-2950
Pt ₄ ethyne	2.00	6.43	5.86	0.48	57-3051
Pt ₄ (CH) ₃	1.69	6.38	5.72	1.19	50-3026
Pt ₄ (CH) ₄	0.90	6.83	5.59	1.14	29-3121
Pt ₄ (CH) ₅	1.82	6.87	5.53	1.47	63-3069
Pt ₄ benzene	2.02	6.10	5.55	0.05	72-3137
Pt ₄ (CH) ₇	2.12	6.38	5.50	0.83	29-3149
Pt ₄ (benzene) ₂	1.53	6.07	5.37	0.43	46-2943



The reaction energies calculated by employing BPW91 xc-functional is slightly different from those of B3LYP. In general BPW91 gives less reaction energies than B3LYP. For instance, the reaction energies of



are -6.54 eV and -6.11 eV by BPW91 and B3LYP, respectively. Interestingly this general trend has an exception at Pt_4 benzene species. BPW91 reaction energy (-7.71 eV) of Pt_4 benzene is higher than B3LYP reaction energy (-8.81 eV). We can interpret this result as an indication of the observation that while B3LYP functional is more appropriate for organic molecules, BPW91 functional is more suitable for metallic clusters. Nevertheless, it can be said that the choice of the xc-functional does not affect the trend for the favorable reactions in the present study.

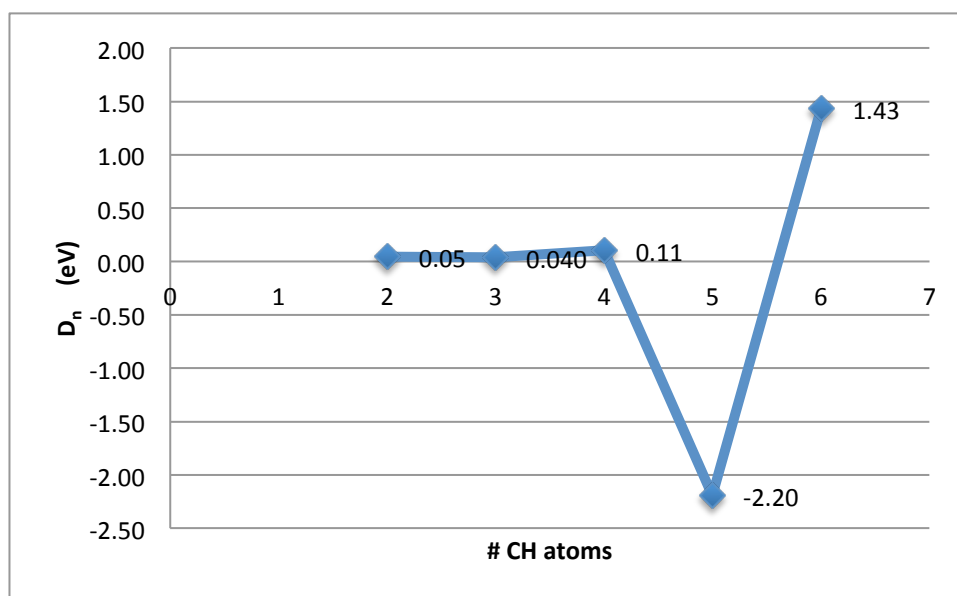


Figure 3.5 The second finite difference in energies for $\text{Pt}_4(\text{CH})_n$ ($n=2$ to 6) clusters

3.3.3 Electronic Properties

Vertical ionization potentials (IP) and electron affinities (EA) are calculated as the total energy difference of neutral, anionic and cationic species in the following way:

$$\text{IP}[\text{Pt}_4(\text{CH})_n] = E[\text{Pt}_4(\text{CH})_n^+] - E[\text{Pt}_4(\text{CH})_n] \quad (3.5)$$

$$\text{EA}[\text{Pt}_4(\text{CH})_n] = E[\text{Pt}_4(\text{CH})_n] - E[\text{Pt}_4(\text{CH})_n^-] \quad (3.6)$$

Here, $E[\text{Pt}_4(\text{CH})_n]$, $E[\text{Pt}_4(\text{CH})_n^-]$ and $E[\text{Pt}_4(\text{CH})_n^+]$ refer to total energy of the neutral, anionic and cationic clusters respectively. The energy of the highest occupied molecular orbital (HOMO) can be considered as a measure of the tendency of the structure to give an electron, whereas the energy of the lowest unoccupied molecular orbital (LUMO) as a measure of the tendency of the structure to accept an electron. The higher the HOMO energy, the higher is the tendency to give an electron, and the lower the LUMO energy, the higher is the tendency to accept an electron. A large HOMO-LUMO gap (HLG) has been considered as significant requirement for chemical stability [134]. Calculated ionization potentials (IP), electron affinities (EA), HLGs and lowest and highest vibrational frequencies for both of the xc-functionals are given in the Table 3.2 and 3.3. We have also given the 3D plots of the frontier orbitals, HOMO and LUMO for $\text{Pt}_4(\text{CH})_4$ and $\text{Pt}_4\text{benzene}$ in Figure 3.6.

Pure Pt tetramer has 1.60 eV (B3LYP) HLG energy [132,133]. The successive adsorption of CH units on Pt tetramer leads to change the gap energy between 1.41 to 2.41 eV (B3LYP). The two functionals have a qualitative agreement on the electronic properties (see Table 3.2). In general, BPW91 HLGs are about 1.00 eV less than B3LYP gaps. As $\text{Pt}_4\text{methylidyne}$ and Pt_4ethyne have the lower gaps, and $\text{Pt}_4(\text{CH})_3$, $\text{Pt}_4(\text{CH})_4$, and $\text{Pt}_4(\text{CH})_5$ have the higher gaps for both of the functionals, there is an anomaly in the calculated gaps of $\text{Pt}_4\text{benzene}$ due to the reason we mentioned above. The HLG of this system obtained by using BPW91 (0.05 eV) is the lowest value, while the same energy obtained by using B3LYP (2.28 eV) is one of the highest ones. Species having large HLGs can be expected to have less chemical activities, whereas those having small gaps are expected to have more chemical activities. The lowest EAs are obtained for $\text{Pt}_4(\text{CH})_3$ and $\text{Pt}_4(\text{CH})_4$ clusters, while the highest EAs in the present study are obtained for $\text{Pt}_4(\text{CH})_7$, Pt_4ethyne , and

Pt₄benzene with both of the functionals. The Pt₄(CH)₄ and Pt₄(CH)₂ clusters have the highest IPs with both of the functionals. The calculated vibrational frequencies with both of the functionals are again in qualitative agreement with each other and these values can be compared with experimental values and can be assigned to different modes of vibrations in these systems.

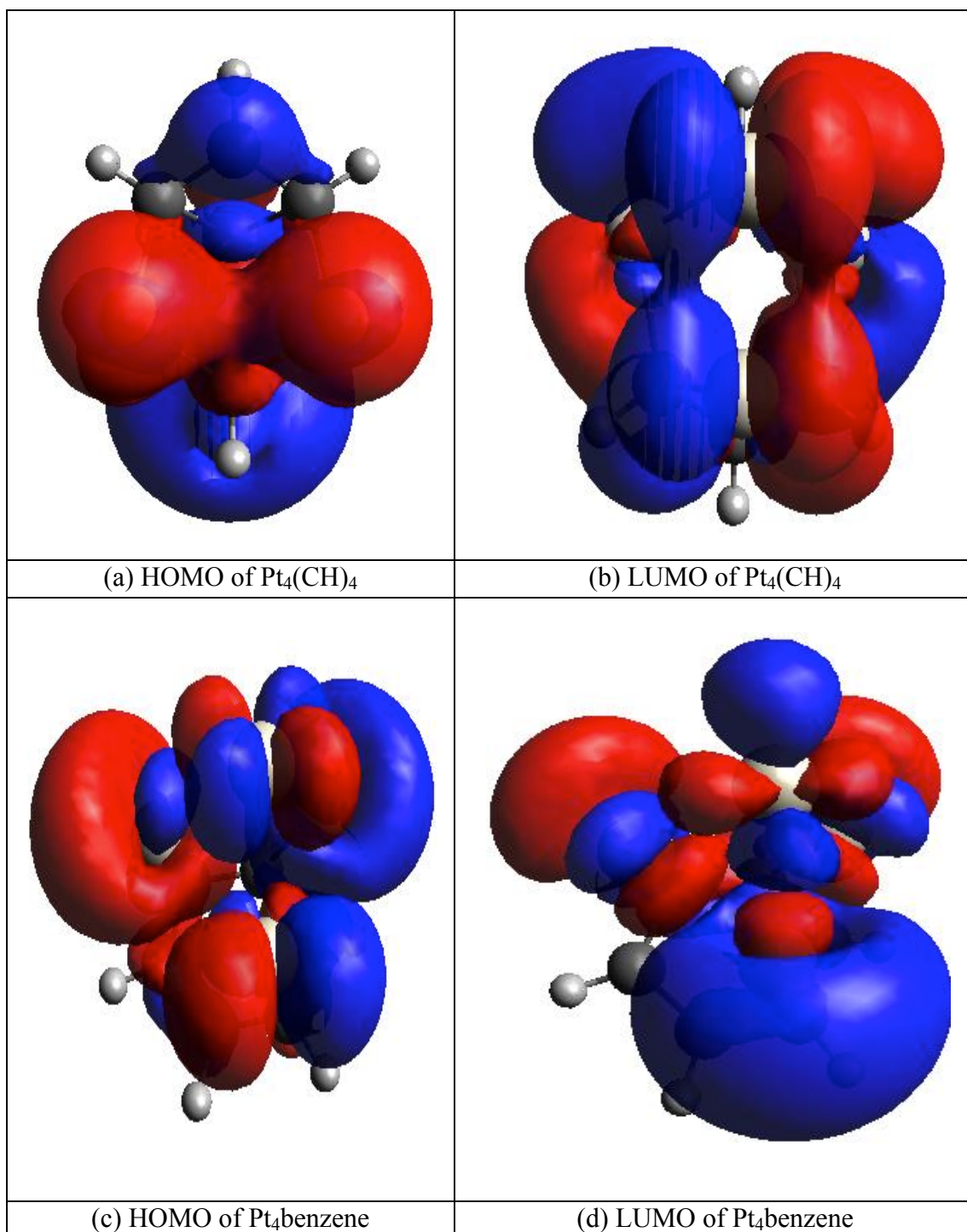


Figure 3.6 HOMO and LUMO density plot of Pt₄(CH)₄ and Pt₄benzene clusters.

3.3.4 DFT Chemical Reactivity Descriptors

In this section, we center our attention on the characterization of the species we have studied in terms of reactivity descriptors such as chemical potential (μ), chemical hardness (η) and electrophilicity index (w). Those quantities are displayed in Table 3.4. We calculated electronic chemical potential and chemical hardness according to the finite difference approximation [135]:

$$\mu = -(1/2)(IP+EA) \quad (3.7)$$

$$\eta = (1/2)(IP-EA) \quad (3.8)$$

μ determines the escaping tendency of electrons from an equilibrium system and η can be defined as a resistance to the charge transfer [136]. The global electrophilicity index is derived from the chemical potential and hardness as the following [135]:

$$w = \mu^2 / 2\eta \quad (3.9)$$

w measures the stabilization in energy as the environment gives systems extra electronic charges.

Table 3.4 The chemical reactivity descriptors indexes of Pt₄(CH)_n (n=1 to 7 and n=12) clusters in eV

Clusters	Chemical Potential (μ)		Chemical Hardness (η)		Electrophilicity Index (w)	
	B3LYP	BPW91	B3LYP	BPW91	B3LYP	BPW91
Pt ₄ methylidyne	-4.12	-4.18	2.60	2.59	3.27	3.37
Pt ₄ (CH) ₂	-4.42	-4.38	2.60	2.52	3.75	3.80
Pt ₄ ethyne	-4.18	-4.22	2.08	2.22	4.21	4.01
Pt ₄ (CH) ₃	-3.21	-4.03	3.21	2.35	1.60	3.46
Pt ₄ (CH) ₄	-5.08	-3.86	4.30	2.96	3.00	2.52
Pt ₄ (CH) ₅	-3.98	-4.34	2.16	2.52	3.66	3.74
Pt ₄ benzene	-4.04	-4.06	1.95	2.04	4.19	4.03
Pt ₄ (CH) ₇	-4.27	-4.25	2.13	2.13	4.29	4.24

Pt ₄ (benzene) ₂	-3.78	-3.80	2.28	2.27	3.14	3.18
--	-------	-------	------	------	------	------

Global indicators constitute good indexes to describe the reactivity and the intrinsic electronic properties of the system, and show the feasibility of the chemical change. It is harder to lose an electron but easier to take another one when μ becomes more negative [136]. It is observed in Table 3.4 that $\text{Pt}_4(\text{CH})_4$ has the lowest chemical potential of -5.08 eV by B3LYP, however the same species has one of the highest chemical potentials (-3.86 eV) by BPW91 indicating an inconsistency of this functional with B3LYP. η generally shows parallel tendency with chemical potential descriptors. Accordingly, $\text{Pt}_4(\text{CH})_4$ is the hardest one for both of the functionals in our calculations. The smallest chemical hardness belongs to Pt_4 benzene with the values of 1.95 eV (B3LYP) and 2.04 eV (BPW91). According to the ω values given in Table 3.4, the $\text{Pt}_4(\text{CH})_7$ is the most susceptible from the external environment for both of the functionals. The electrophilicity index, which can be one of the essential parameter for the selection of a catalyzer, shows oscillating behavior in Table 3.4.

3.4 Conclusion

In this part of the study, we have performed spin-polarized DFT calculations to study the interaction of the $\text{Pt}_4(\text{CH})_n$ ($n= 1$ to 7 and $n=12$) metalorganic complexes by varying the number of CH ligands. The geometric properties, energetics and stability, electronic properties and chemical reactivity indexes have been discussed. From the analyses of the results, the following conclusions can be drawn: First of all, during the growth process with CH on Pt tetramer, atop site adsorption of CH to the species is not energetically favorable. CH is adsorbed on the tetramer in the molecular form with carbon instead of hydrogen bonding to platinum. The first and second adsorptions of CH ligands occur on the hollow sites of the Pt tetramer. After the size 2, as the number of CH ligands on the Pt tetramer is increased, CH radicals start to form C bonds. This trend continues up to the size 6. The lowest energy configuration of $\text{Pt}_4(\text{CH})_6$ becomes a Pt_4 benzene where the ring of 6 C atoms adsorbed on a triangular surface of the Pt tetramer. For $\text{Pt}_4(\text{benzene})_2$ structures, the lowest energy structure is obtained as two benzene molecules adsorbed on different bridge sites of the Pt tetramer. Finally, regarding the relative stability criteria, reaction energies, chemical reactivity descriptor indexes and electronic properties of the studied

clusters, $\text{Pt}_4(\text{CH})_4$ and $\text{Pt}_4\text{benzene}$ metal unsaturated hydrocarbon complexes are found to be the most stable species among the studied sizes.

CHAPTER 4

THE INTERACTION OF C₂H WITH BIMETALLIC COBALT-PLATINUM CLUSTERS

4.1 Introduction

In recent years, a great deal of effort has been devoted to study magnetic CoPt nanoalloy clusters [137-165] due to their potential usage in ultra-high density magnetic storage applications [166]. The characterization of the magnetic anisotropy energy distribution of a diluted assembly of CoPt nanoparticles with a mean diameter of 3 nm by using superconducting quantum interference device magnetometry was reported by Tournus and coworkers. They found experimental evidence of a magnetic anisotropy constant dispersion with a comparison of unselected CoPt clusters and size-selected Co clusters [167]. Tizizios and coworkers reported the synthesis of 3D ferromagnetic CoPt polypod-like nanostructures [150]. On the theoretical side, Sebetci studied small bimetallic CoPt clusters in terms of their structural, energetic, electronic and magnetic properties by using DFT method within the generalized gradient approximation. As a general trend, he found the average binding energies of Co-Pt metallic clusters increase with Pt doping [168]. Another theoretical study conducted by Feng and coworkers [169]. They examined magnetic and electronic properties of CoPt nanoparticles having equal number of Pt and Co atoms.

The ethynyl radical (C₂H) is a significant reactive intermediate in hydrocarbon combustion process [170-172]. It is also a widespread interstellar molecule including a variety of sources [173-177]. In the past decades, C₂H radical has been attracted much attention [178-181]. Ervin et al. determined electron affinity of C₂H as 2.97 eV [182]. Zhou et al. studied C₂H and C₂D radicals by slow electron velocity-map imaging of the related anion [178]. Investigating the interactions between metal and

organic molecules is significant in both heterogeneous and homogeneous catalytic systems. Adsorption of a small molecule or atom may modify the electronic and magnetic properties and stability of the transition metal clusters. Experimental and theoretical works were performed to study the interaction complexes formed between metal atoms and ethynyl radical [183-187]. The linear geometric structure of CrC_2H in the ground and excited states and the vibrational spectrum of CrC_2H at the 11 100 and 13 300 cm^{-1} region were reported by Brugh and coworkers [188]. By combination of resonance-enhanced two-photon ionization, laser induced fluorescence, and photoionization efficiency spectroscopy experiments with DFT calculations, Looock et al. determined the frequencies of different modes of YbC_2H [189]. $\text{FeC}_2\text{H}^{-1}$ and $\text{PdC}_2\text{H}^{-1}$ were studied experimentally [190,191]. Da-Zhi Li and coworkers investigated the interaction of C_2H radical with neutral and anionic small gold clusters [192]. Yuan et al. investigated the small anionic CoC_2H complexes by mass spectrometry, the photoelectron spectra and DFT calculations [193]. However, to the best of our knowledge, there has been no study reported to date on the interaction between C_2H radical and bimetallic clusters. Thus, it is worthy to investigate anionic bimetallic CoPtC_2H nanoalloy complexes systematically in order to understand the mechanism and elucidate more details on the formation of small CoPtC_2H nanoalloy complexes

In the present part of the work, we have investigated the structural, energetic, electronic and magnetic properties of the $[\text{Co}_n\text{Pt}_m\text{C}_2\text{H}]^{-1}$ ($2 \leq n+m \leq 5$) clusters within the framework of DFT and addressed the following important questions: How does C_2H adsorption change the properties of the structure at a given cluster size? How does it change the magnetic properties of bimetallic Co-Pt clusters? What is the influence of cluster size and chemical component on the reactivity of Co-Pt clusters with C_2H adsorption?

Locally stable isomers are distinguished from transition states by vibrational frequency analysis as well. We present the obtained results and discuss the interaction complexes formed between CoPt bimetallic clusters and ethynyl radical in the following sections.

4.2 Computational Details

Computational details of this part are the same with that of the previous chapter. In addition to them, CRENL basis set and ECP is used for Co where the outer most 17-electrons ($3s^23p^63d^74s^2$) are treated as valence to reduce the number of electrons explicitly considered in the calculations. BLYP functional has been employed in the calculations.

4.3 Result and Discussion

The optimized geometries of the low-lying isomers of anionic $[\text{Co}_m\text{Pt}_n\text{C}_2\text{H}]^{-1}$ ($2 \leq m+n \leq 5$) clusters obtained in this study are given in Figure 4.1, Figure 4.2 and Figure 4.3 for the structures with $2 \leq m+n \leq 3$, $m+n=4$, and $m+n=5$, respectively. We have considered many spin multiplicities and various initial configurations. In addition, Table 4.1 represents spin moments, binding energies per atom, HLGs, vertical detachment energies (VDE) and highest and lowest vibrational frequencies of the studied clusters.

4.3.1 $[\text{Co}_m\text{Pt}_n\text{C}_2\text{H}]^{-1}$ ($m+n=2$)

Some of the low-lying isomers of anionic Co_mPt_n -ethynyl ($m+n=2$) clusters are displayed in Figure 4.1. The C-C bond distance of the free ethynyl radical is calculated as 1.25 Å. The obtained results show that when the radical is adsorbed on an atop side, this bond length is not changed so much.

The ground state geometry of $[\text{Co}_2\text{C}_2\text{H}]^{-1}$ system has been identified as a linear structure with C_s symmetry. When C_2H radical approaches to Co dimer, the C atom at the end of the radical binds to the Co atom. In this structure the Co-C bond distance is 1.92 Å, the Co-Co bond distance is 2.38 Å and the magnetic state is the quintet state ($4 \mu_B$ spin moment). The Co-Co bond distance of pure diatomic cobalt particle is given between 1.99 Å and 2.13 Å in the literature. These calculated values of bond lengths are in good agreement with the previous theoretical calculations of the Co-Co bond length as 2.43 Å and the Co-C bond length as 1.95 Å [193]. The BE

per atom and VDE of this structure are calculated as 4.46 eV and 1.25 eV (see Table 4.1). The magnetic moment of 1C is 6 μ_B while 1A and 1B are 4 μ_B and 1B has a relative energy of 0.91 eV with respect to the lowest energy structure 1A. The third isomer 1C having C_s symmetry is, see Figure 4.1, 1.27 eV higher in energy than the ground state configuration. The structure 1D is energetically the most unfavorable structure with 8 μ_B spin moment.

The ground state configuration of $[\text{CoPtC}_2\text{H}]^{-1}$ is a linear structure with C_s group symmetry. The C_2H is adsorbed onto the Co atom rather than the Pt atom where the C-Pt bond distance is 2.28 Å. The elongation between Co-Pt distance upon ethynyl radical absorption is by 0.04 Å while the Co-Pt bond length in pure bimetallic CoPt nanoalloy is 2.24 Å. The second low-lying minima of $[\text{CoPtC}_2\text{H}]^{-1}$ is also a linear structure, which has 0.59 eV higher energy than the lowest one. The magnetic moments of 2A and 2B are 3 and 1 μ_B respectively and the third isomer 2C has 3 μ_B , which has 0.78 eV higher energy than the ground state. The ground state configuration of the anionic Pt dimer-ethynyl cluster with C_s symmetry is nonlinear planer structure in the triplet magnetic state. The angle between Pt-Pt-C atoms is 160°. The Pt-Pt distance in the pure Pt dimer is 2.21 Å. The adsorption of ethynyl radical leads to a stretch in the Pt-Pt bond length where the Pt-Pt bond distance becomes 2.46 Å. In addition, bridge site adsorptions have higher energy than atop site adsorption, which continues for the trend that atop site adsorption has lower energy than bridge site adsorption. The elongation for Pt-Pt and C-C distance is by 0.24 Å and 0.05 Å respectively in bridge site adsorption whereas there is no significant change for the typical Pt-C distance in both adsorption types.

4.3.2 $[\text{Co}_m\text{Pt}_n\text{C}_2\text{H}]^{-1}$ ($m+n=3$)

The VDE of the particles for $m+n=3$ ranges from 4.29 to 5.06 eV (see Table 4.1). The doping of the Pt atom in these structures leads to increase in VDE. Furthermore, the C-C bond distance in ethynyl radical in the lowest ground state isomers is between 1.24 and 1.44 Å where the $\text{C}\equiv\text{C}$ bond of acetylene (1.20 Å) [194] and the $\text{C}=\text{C}$ bond of ethene (1.33 Å) [195].

Different research groups calculated the lowest energy structure of bare cobalt trimer and reported a triangular structure and a linear structure [196-200]. Yoshida and coworkers reported Co-Co distances of the anionic bare Co trimer in the linear structure between 2.25-2.50 Å in their experimental and theoretical calculations [201]. The lowest energy structure (4A) of the anionic Co₃-ethynyl nanoparticle is a planar Y-like structure with a BE of 4.29 eV and it has high point group symmetry, C_{2v} with 7 μ_B spin moment. The average Co-Co bond distance in this ground state structure, which has a perfect isosceles triangular Co₃ unit, is 2.4 Å. Furthermore, the addition of one Co atom to the [Co₂C₂H]⁻ leads to increase in VDE where the VDE in the structure 4A is 1.52 eV that is consistent with the results in Ref [193] (see Table 4.1). The second isomer 4B and the third isomer 4C have approximately the same relative energies with respect to the ground state energy although they are in different magnetic states. The fourth isomer 4D is constructed by the bridge side binding of the terminal C atom of the ethynyl radical, which is in the octet magnetic state. The Co-C bond lengths are 2.04 and 1.96 Å in this structure.

As one of the Co atoms is replaced by a Pt atom, the lowest energy structure of anionic Co₂Pt-ethynyl nanoparticles becomes the structure of a triangular bimetallic unit including a Pt atom at the apex and two Co atoms at the base with average Co-Pt bond length of 2.44 Å. While the distances between Co and Pt atoms are stretched slightly as the amounts of 0.06 and 0.11 Å, the separation between Co atoms is shrunk as much as 0.15 Å after the adsorption of ethynyl radical. Its BE is 4.71 eV/atom where the quintet magnetic state is the same with the bare Co₂Pt cluster. In the second isomer 5B where ethynyl radical binds atop site, the Co-C bond distance is 1.92 Å with a relative energy of 0.49 eV with respect to the lowest energy structure. The third isomer 5C and the fourth isomer 5D have average Co-C bond lengths of 1.91 Å and 1.98 Å, respectively.

As Pt doping increases, the BE of anionic CoPt₂-ethynyl increases to 4.89 eV. For this species (6A), ethynyl radical prefers energetically to bind Pt atom rather than Co atoms, which is different from the bridge side adsorption of the previous case.

Table 4.1 The electronic properties of Co_nPt_m-ethynyl clusters with BLYP

Cluster		Spin moment (μ_B)	BE per atom (eV)	HOMO-LUMO Gap (eV)	VDE (eV)	Lowest and Highest Vibrational Frequencies (cm ⁻¹)
[Co ₂ C ₂ H] ⁻	Present Work	4	4.46	0.33	1.25	55-3360
	Literature				1.53*	
	Exp.				1.50*	
[CoPtC ₂ H] ⁻		3	5.08	0.63	2.53	37 -3369
[Pt ₂ C ₂ H] ⁻		2	5.26	0.28	2.66	43-3384
[Co ₃ C ₂ H] ⁻	Present Work	7	4.29	0.03	1.52	64-3368
	Literature				1.59*	
	Exp.				1.81*	
[Co ₂ PtC ₂ H] ⁻		4	4.71	0.73	1.47	68-3154
[CoPt ₂ C ₂ H] ⁻		3	4.89	0.72	2.26	56-3387
[Pt ₃ C ₂ H] ⁻		0	5.06	1.05	1.64	41- 2968
[Co ₄ C ₂ H] ⁻	Present Work	8	4.09	0.73	1.53	171-3191
	Literature				1.82*	
	Exp.				1.63*	
[Co ₃ PtC ₂ H] ⁻		7	4.41	0.71	1.70	58-3249
[Co ₂ Pt ₂ C ₂ H] ⁻		4	4.70	0.74	1.87	42- 3175
[CoPt ₃ C ₂ H] ⁻		3	4.85	0.45	2.01	39-3216
[Pt ₄ C ₂ H] ⁻		2	4.95	0.16	3.09	28-3055
[Co ₅ C ₂ H] ⁻	Present Work	9	3.94	0.51	1.96	65-3183
	Literature				2.15*	
	Exp.				1.88*	
[Co ₄ PtC ₂ H] ⁻		8	4.24	0.63	2.82	35- 3195
[Co ₃ Pt ₂ C ₂ H] ⁻		7	4.45	0.53	2.22	16-3224
[Co ₂ Pt ₃ C ₂ H] ⁻		6	4.64	0.76	2.63	37 -3390
[CoPt ₄ C ₂ H] ⁻		5	4.76	0.33	2.44	25-3101
[Pt ₅ C ₂ H] ⁻		2	4.79	1.21	2.16	23-2975

* Ref [193]

The C-Pt distance is 1.94 Å and the Pt-Pt distance is 2.81 Å while these bond lengths of 3A is 1.95 and 2.46 Å respectively. The magnetic moments of all three isomers possessing C_s symmetry given in Figure 4.1 for this cluster are $3 \mu_B$, $1 \mu_B$ and $3 \mu_B$ respectively. It can be seen in Figure 4.1 that the second isomer 6B and third isomer 6C have close ground state energies with 6A. In addition, in both of these two isomers 6B and 6C, adsorption of the ethynyl molecule occurs at the bridge instead of the top side adsorption of 6A.

The BE of anionic Pt_3 -ethynyl cluster is calculated as 5.06 eV which is the highest value for $m+n=3$ systems. It can be noted that the doping of Pt atom to the cluster leads to increase in BE value. However, the difference in the BE of $[CoPt_2C_2H]^{-1}$ and $[Pt_3C_2H]^{-1}$ (0.17 eV) is close to that of $[Co_2PtC_2H]^{-1}$ and $[CoPt_2C_2H]^{-1}$ (0.18 eV) while it is smaller than that of $[Co_3C_2H]^{-1}$ and $[Co_2PtC_2H]^{-1}$ (0.42 eV). In this structure, four coordination of Carbon that indicates sp^3 hybridization resulting from delocalized electrons in ethynyl radical was seen for the first time among all nanoparticles we have mentioned so far. This triggers to expand the C-C bond length in C_2H radical importantly. In addition, the second isomer 7B has the same singlet magnetic moment as the case of the isomer 7A (see Figure 4.1) while the magnetic state of the third isomer 7C is triplet.

4.3.3 $[Co_mPt_nC_2H]^{-1}$ ($m+n=4$)

Some of the low-lying isomers of anionic Co_mPt_n -ethynyl clusters are displayed in Figure 4.2. In these structures, the trend of VDE, which ranges from 1.53 eV to 3.09 eV, continues so that doping of Pt to the clusters leads to increase in VDE.

In the lowest energy structure of anionic Co_4 -ethynyl cluster, ethynyl is adsorbed on the bridge site with a total BE of 4.09 eV for the whole system. The ground state structure of bare Co_4 in a previous study by Sebetci [196] was found as an out of plane rhombus while the ground state structure of bare Co_4 by other theoretical calculations in the literature varies. It has been reported to be a planar rhombus structure or an out of plane rhombus structure and a distorted tetrahedral structure.

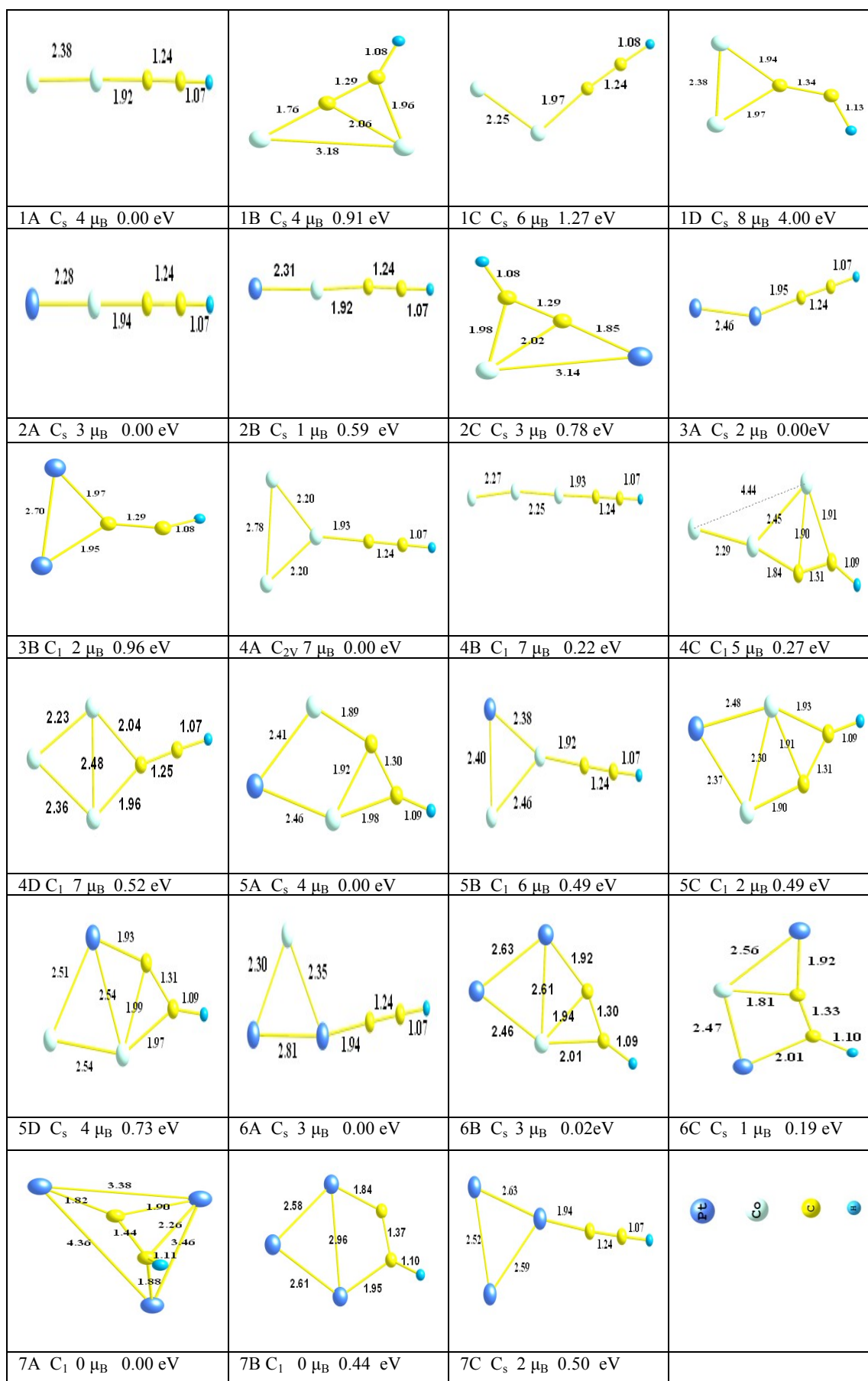


Figure 4.1 The optimized structures of some isomers of $[\text{Co}_m\text{Pt}_n\text{C}_2\text{H}]^{-1}$ ($2 \leq m+n \leq 3$)

The lowest energy structure of $[\text{Co}_4\text{C}_2\text{H}]^-$ obtained by Yuan et al. [193] is consistent with our result. Upon ethynyl adsorption, the magnetic moment of bare Co_4 ($10 \mu_{\text{B}}$) is reduced to $8 \mu_{\text{B}}$ in the structure 8A, which is the same for the second isomer 8B (see Figure 4.2) while the third isomer 8C has $10 \mu_{\text{B}}$ spin moment and a relative energy of 0.44 eV with respect to the lowest energy structure. The energy difference between the first isomer and the second isomer is relatively small.

The Co-Co and Co-Pt edge bond lengths of the bare Co_3Pt in the rhombus structure are 2.25 Å and 2.38 Å, respectively [196]. The adsorption of ethynyl radical leads to expand the Co-Co bond lengths. It can be noted that the doping of one Pt atom to anionic Co_3 -ethynyl nanoparticle causes to weaken the bond between cobalt atoms. In the second isomer of $[\text{Co}_3\text{PtC}_2\text{H}]^-$ (9B), which has 0.71 eV higher energy than the first isomer (9A), the adsorption occurs on the top side of the Pt atom, where the magnetic state is quartet and the average Pt-Co bond length is about 2.50 Å. The third and fourth isomers given in the Figure 4.2 are not energetically favorable due to the big relative energies.

As one of the Co atoms replaced by a Pt atom, the BE and VDE of the lowest energy structure of $[\text{Co}_2\text{Pt}_2\text{C}_2\text{H}]^-$ becomes 4.70 eV and 1.87 eV, respectively. The BE and VDE of this structure is slightly lower and slightly higher than those of anionic CoPt_2 -ethynyl structure, respectively whereas they are lower than those of the anionic Co_2Pt -ethynyl structure (see Table 4.1). The C-C bond distance in the first isomer 10A is 1.30 Å, which is longer than that of the $\text{C}\equiv\text{C}$ bond of acetylene (1.20 Å) [194] and shorter than that of the $\text{C}=\text{C}$ bond of ethene (1.33 Å) [195]. When the spin magnetic moments are considered, it is seen that there is an abrupt decrease from $7 \mu_{\text{B}}$ to $4 \mu_{\text{B}}$ where the transition from $[\text{Co}_3\text{PtC}_2\text{H}]^-$ to $[\text{Co}_2\text{Pt}_2\text{C}_2\text{H}]^-$. The magnetic state of the second isomer 10B with C_s symmetry is $6 \mu_{\text{B}}$ while the third and fourth isomers have $2 \mu_{\text{B}}$ and $8 \mu_{\text{B}}$ magnetic states, respectively.

Compared with the bare CoPt_3 given in the reference [168], the CoPt_3 in the lowest energy structure of $[\text{CoPt}_3\text{C}_2\text{H}]^-$ obtained in the present study is distorted significantly while the CoPt_3 units in the second and the third isomers are perturbed slightly. This indicates that the adsorption gives rise to considerable structural change for the lowest energy structure 11A. Besides obvious lengthening of Pt-C

bond length where two Carbon atoms prefer to bond to the same Pt atom, the Pt-Pt bond distance in this structure is longer than that of the corresponding pure Co-Pt nanoalloy cluster [168]. In addition, the magnetic moment of bare CoPt_3 is $5 \mu_B$ [196] while the magnetic moment of all the isomers of anionic $\text{CoPt}_3\text{C}_2\text{H}$ given in the Figure 4.2 is $3 \mu_B$. The total energies of the second and the third isomers are 0.37 eV and 0.71 eV higher than that of the first one, respectively.

The ground state structure of Pt tetramer is a distorted tetrahedron in triplet magnetic state with Pt-Pt bond distance of 2.60 Å. In the previous section, which is published as the reference [202], the Pt-C and the Pt-Pt distances in $\text{Pt}_4\text{methylidyne}$ were calculated as 1.95 Å and 2.63 Å, respectively and the two different bond lengths of Pt-C in Pt_4ethyne are 2.1 Å and 1.9 Å. In addition, The BEs of $\text{Pt}_4\text{methylidyne}$, Pt_4ethyne , $\text{Pt}_4\text{benzene}$ and $\text{Pt}_4(\text{benzene})_2$ are 3.71 eV, 4.20 eV, 5.13 and 5.52 eV, respectively. On the other hand, due to the adsorption of ethynyl radical, the Pt units in the structure 12A does not preserve its tetrahedral structural type in triplet magnetic state. The Pt-Pt bond lengths in this particle are 2.58 Å, 2.74 Å, and 3.16 Å. The BE of this structure is 4.95 eV as well. As one Co atom replaced by Pt atom, The C-C bond distance in anionic $\text{Pt}_4\text{C}_2\text{H}$ becomes longer than that of the $[\text{CoPt}_3\text{C}_2\text{H}]^-$ structure. The lengthening of the C-C bond distance can be due to losing of some sharing valence electrons between carbon atoms over new Pt-C interactions. In the second isomer possessing 0.31 eV relative energy with respect to the lowest energy structure, the tetrahedral unit of the bare Pt tetramer becomes a nonplanar, rhombus like structure. While the magnetic moments of the first and second isomers are $2 \mu_B$, the third isomers having distorted tetrahedral unit has $4 \mu_B$ magnetic moment, which is not energetically favorable since it has a 1.32 eV relative energy.

4.3.4 $[\text{Co}_m\text{Pt}_n\text{C}_2\text{H}]^-$ ($m+n=5$)

Some of the low-lying isomers of anionic $\text{Co}_m\text{Pt}_n\text{-ethynyl}$ ($m+n=5$) clusters are displayed in Figure 4.3. The BE values of these species vary between 3.94 eV and 4.79 eV. The increase rate of BE from anionic $\text{Co}_5\text{-ethynyl}$ to $\text{Pt}_5\text{-ethynyl}$ clusters is slowing down as seen in Table 4.1.

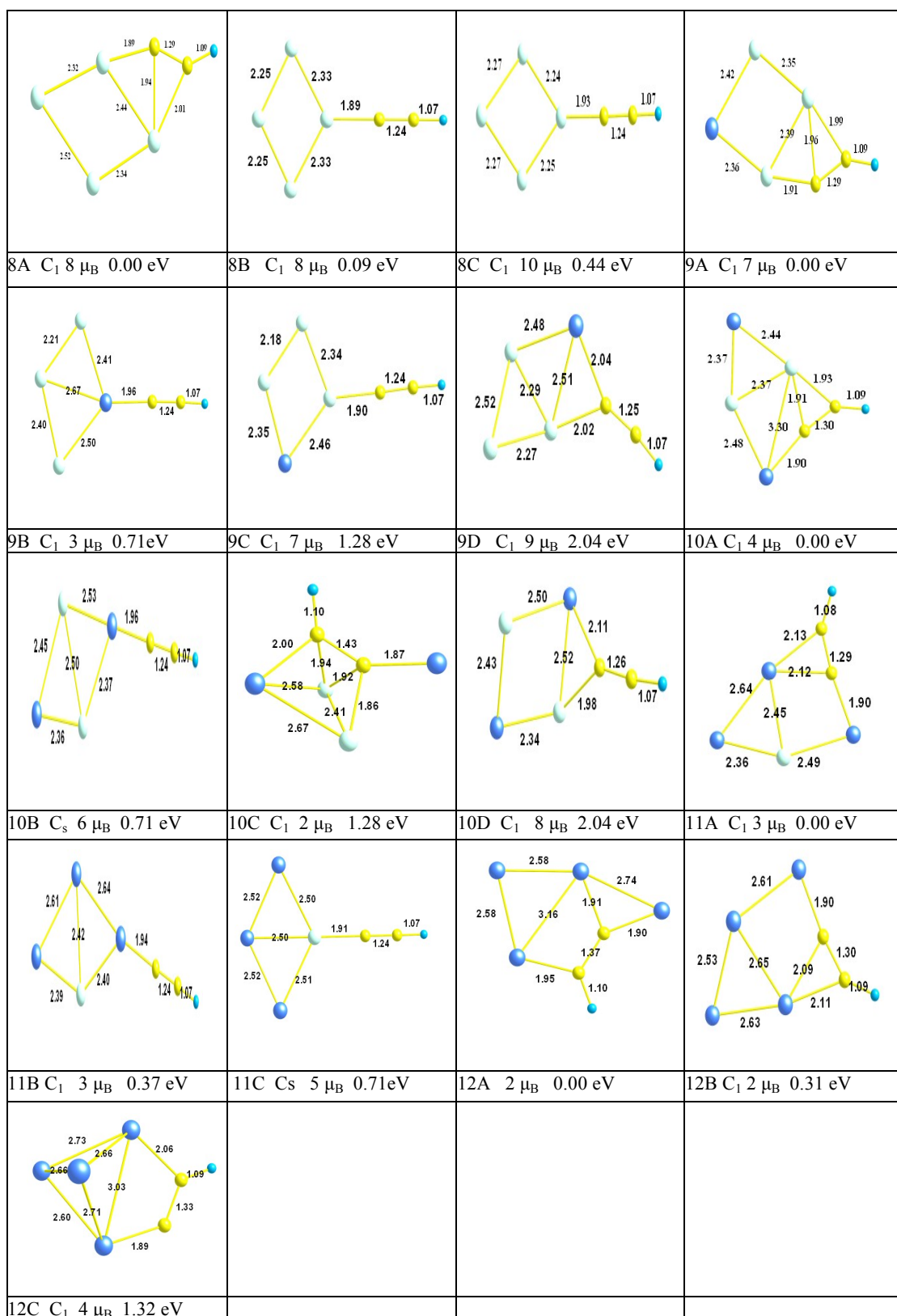


Figure 4.2 The optimized structures of some isomers of $[\text{Co}_m\text{Pt}_n\text{C}_2\text{H}]^{-1}$ ($m+n=4$)

The ground state structure of bare Co_5 in a previous study was calculated as planar W-like structure [196] while it has been reported to be a C_{4v} square pyramid [203], a C_{2v} rhombus pyramid [204] and a D_{3h} trigonal pyramid [199,205,206] in the other literature. The lowest energy structure of $[\text{Co}_5\text{C}_2\text{H}]^-$ obtained in the present work contains nearly planar W-like structure, which is consistent with the result found by Yuan et al. [193] where B3YLP xc functional was used in their optimizations. In the ground state structure of anionic Co_5 -ethynyl cluster, carbon atoms are absorbed on the bridge side with a total BE of 3.94 eV. The calculated VDE (1.96 eV) is close to the experimental value of 1.88 eV (see Table 4.1). In all isomers except for the third one, the magnetic moment is $9 \mu_B$ but the bare Co pentamer and the third isomer have high magnetic moment: $11 \mu_B$. In the lowest energy structures of anionic Co_{2-3} -ethynyl clusters, the ethynyl radical binds only one Co atom where the C-C bond length is 1.24 Å, which is slightly longer than 1.20 Å of the triple C-C bond of the acetylene, whereas much shorter than 1.33 Å of the double C-C bond of the ethene. It can be inferred that ethynyl radical having triple C-C bond is slightly affected by the Co_{2-3} metal clusters. In the lowest energy structures of the anionic Co_{4-5} -ethynyl structures, the C-C bond lengths are calculated as 1.29 Å and 1.30 Å, which are between the $\text{C}\equiv\text{C}$ and $\text{C}=\text{C}$ bond distances. Therefore, the Co_{4-5} nanoparticles have more effect on the $\text{C}\equiv\text{C}$ bond of ethynyl radical than those of Co_{2-3} nanoparticles, which might be valuable for the $\text{C}\equiv\text{C}$ bond activation.

As a Pt atom replaces a single Co atom, the lowest energy morphology does not change very much (see Figure 4.3), where two atoms are slightly out of the plane. The Co-Pt bond lengths of anionic Co_4Pt -ethynyl cluster are 2.41 Å and 2.39 Å while the Co-Co distances are between 2.21 Å and 2.61 Å. The second isomer of the $[\text{Co}_4\text{PtC}_2\text{H}]^-$ is constructed by atop adsorption of C_2H radical to one of the most coordinated Co atoms with a BE of 4.76 eV. In the second isomer, which has capped tetrahedron structure, the magnetic moment is $10 \mu_B$ with a relative energy of 0.69 eV. The third and fourth isomers have similar structure with the first one in nonet magnetic state.

The second, third, and fourth isomers of anionic Co_3Pt_2 -ethynyl clusters have a triangular bipyramidal unit where Co atoms with the average Co-Co bond length of

2.43 Å are on the base of pyramid and Pt atoms with average Pt-Co distance of 2.51 Å are on the apexes of pyramids. In the lowest energy structure of this specie, the metal atoms construct a rectangular pyramid. The second and the third isomers have the same magnetic moment with the first one and their BEs are 0.34 eV and 0.78 eV higher than that of the first isomer.

In the ground state of the anionic Co_2Pt_3 -ethynyl structure with a BE of 4.64 eV, ethynyl radical adsorbed on the Pt side instead of Co in septet magnetic state which is the same with the total spin magnetic moment of the bare Co_2Pt_3 cluster. In all isomers except the second one which has 0.55 eV relative energy with respect to the first isomer, the C_2H radical prefers to be adsorbed on the atop site. The second isomer has 4 μ_{B} magnetic moment with the C-C bond length as 1.36 Å while the magnetic moment of the first isomer having C_s symmetry is 6 μ_{B} which has a C-C bond length of 1.24 Å.

The lowest energy structure (17A) of anionic CoPt_4 -ethynyl cluster is a distorted pyramid where 4 Pt atoms with an average Pt-Pt bond length of 2.85 Å are on the base plane and the Co atom with an average Co-Pt bond length of 2.46 Å is at the apex of the pyramid. The ethynyl radical is adsorbed on the Pt-Pt bridge side in the first isomer. In the second isomer (17B) possessing 5 μ_{B} magnetic moment, the ethynyl radical adsorbed on the Co-Pt bridge side. The third isomer has C_4 point group symmetry where the ligand is adsorbed on Co atop site. The energy of the third isomer is 0.87 eV higher than that of the lowest energy structure.

The BE of Pt pentamer-ethynyl nanoparticle is slightly higher than that of the CoPt_4 nanoparticle (see Table 4.1). Among Pt_{2-5} -ethynyl clusters, the BE per atom of $[\text{Pt}_2\text{C}_2\text{H}]^-$ (5.26 eV) is the highest one. As depicted from Table 4.1, the BEs per atom of the $[\text{Pt}_n\text{C}_2\text{H}]^-$ clusters are decreasing when n varies from 2 to 5. On the other hand, the VDEs given in Table 4.1 indicate an oscillating manner for Pt_{2-5} -ethynyl clusters. The C-C bond length in the lowest energy structure of $[\text{Pt}_5\text{C}_2\text{H}]^-$ is calculated as 1.46 Å, where both of the C atoms are four coordinated.

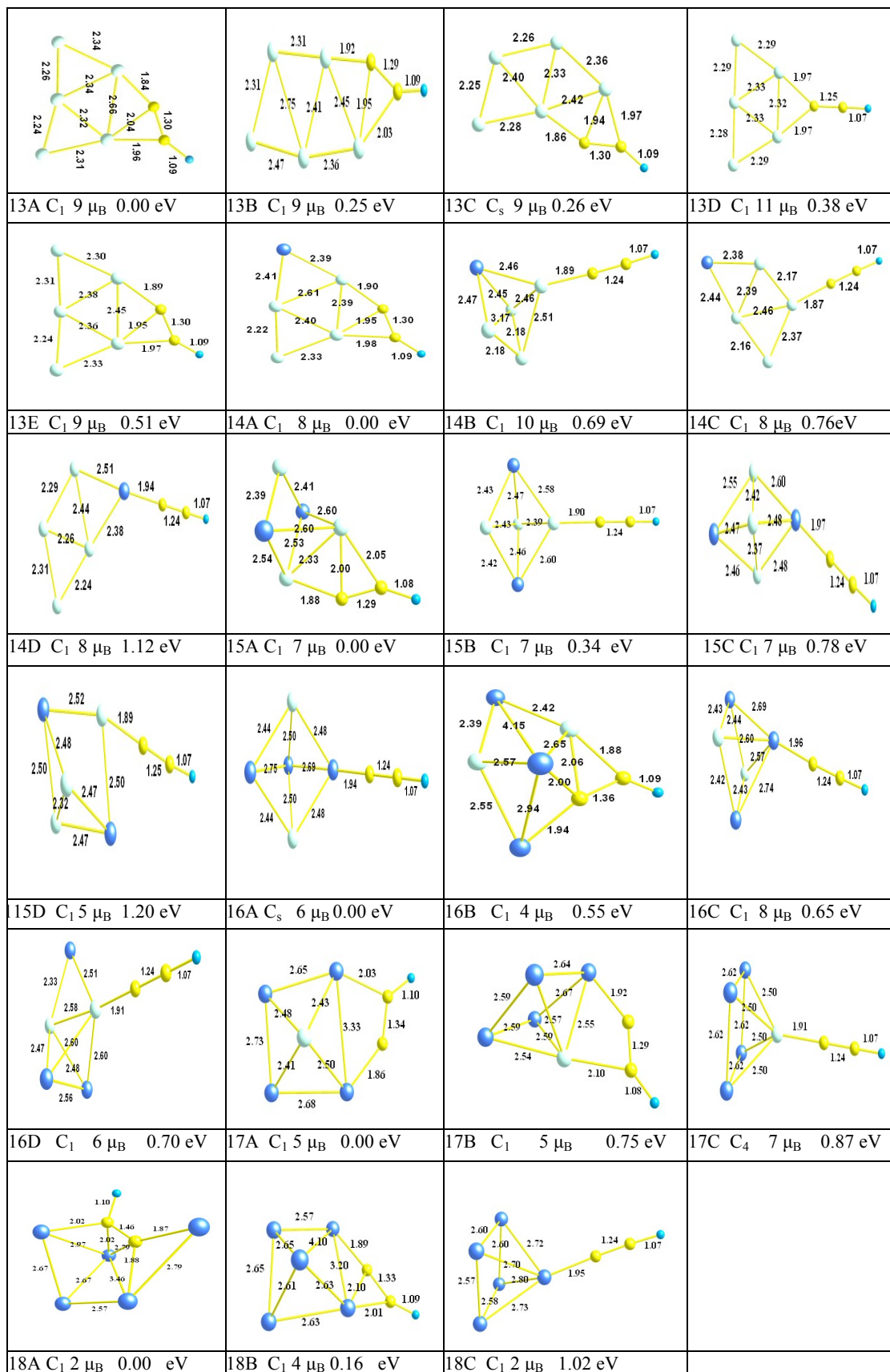


Figure 4.3 The optimized structures of some isomers of $[Co_mPt_nC_2H]^{-1}$ ($m+n=5$)

4.3.5 Energy and Electronic Structure

The BE can generally be defined as a measurement of the clusters' thermodynamic stability. Thus, to predict the relative stabilities of the Co_nPt_m -ethynyl structures, the BEs per atom are tabulated in Table 4.1 and plotted in Figure 4.4. The BE per atom has been obtained in the following way:

$$B.E = \frac{2E[C] + E[H] + nE[Co] + mE[Pt] - E[\text{Co}_n\text{Pt}_m\text{C}_2\text{H}^-]}{n + m + 3} \quad \text{for } 2 \leq n+m \leq 5 \quad (4.1)$$

where $E[*]$ is the total energy of C, H, Pt, and Co atoms and the clusters. The BEs per atom for the lowest energy structures we have studied vary from 3.81 eV to 5.06 eV. From Table 4.1 and Figure 4.4 it can be seen that the highest BE belongs to the anionic Pt_2 -ethynyl structure while the lowest one belongs to the anionic Co_5 -ethynyl specie. It can be noted that the BEs of the species increase with Pt doping to the species having a certain total number of Co and Pt atoms. In other words, provided that the size of the species kept constant, this can be well understood as increasing Pt composition means more bonds involving Pt atoms, that is, the Pt-Pt or Pt-Co and Pt-C bonds, which are stronger than those of the Co-Co and Co-C. However, increasing the size of the cluster leads to decrease the BEs of the clusters gradually. This indicates that the species cannot constantly gain energy during the growth process.

To further illustrate the stability of the species and their size dependent behaviors, we have considered the second finite difference in energies that is a sensitive quantity frequently used as a measure of the relative stability of the complexes and is often compared directly with the relative abundances determined in mass spectroscopy experiments. Moreover, clusters are especially abundant magic number sizes in mass spectra as they are most stable ones. The second finite different energies (D_n) can be calculated as

$$D_{n,m} = E_{n+1,m-1} + E_{n-1,m+1} - 2E_{n,m} \quad (4.2)$$

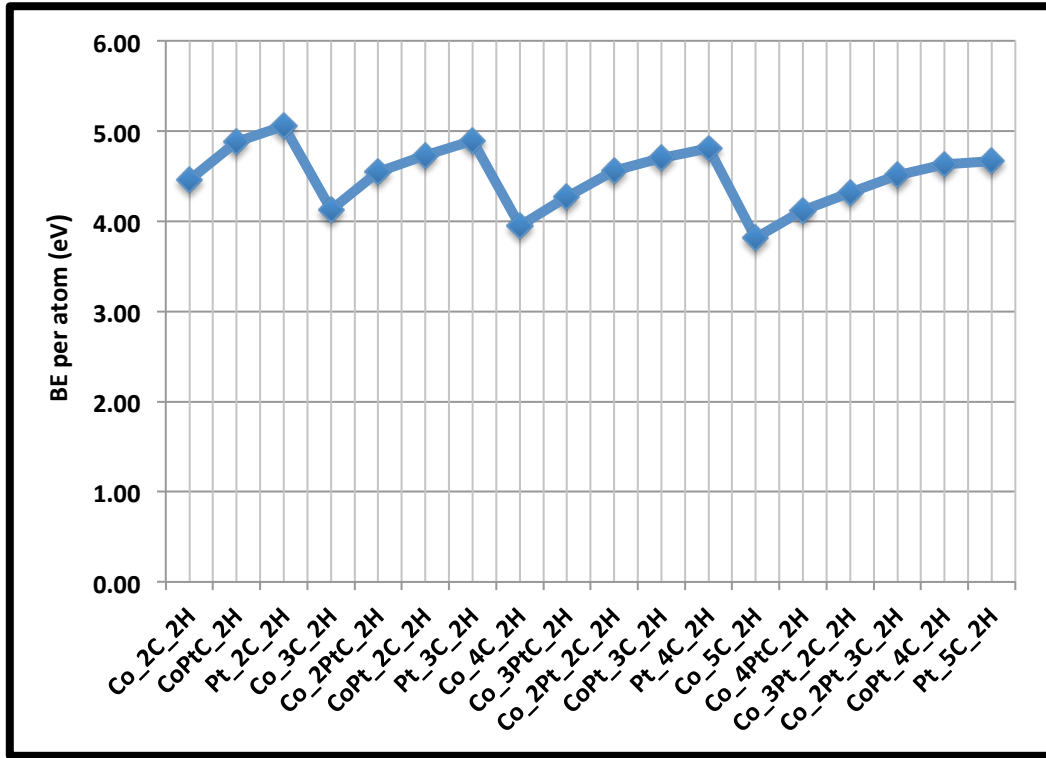


Figure 4.4 The BE per atom of $[Co_nPt_mC_2H]^-$ for $2 \leq n+m \leq 5$

where $E_{n,m}$ is the total energy of the $[Co_nPt_mC_2H]^-$ cluster. The second finite differences in energies of the studied clusters are given in Figure 4.5. Due to the definition of the second finite difference in energies, we examined only 2, 3 and 4 species consisting of 3, 4 and 5 metal atoms respectively. Noticeable peak at the size of Co_nPt_m ($m+n=4$) indicates that the $[Co_2Pt_2C_2H]^-$ cluster is more stable than the neighboring clusters. Anionic Co_3Pt_2 -ethynyl structure can be considered as the least stable structure as it corresponds to a dip in the plot for $n+m=5$ species.

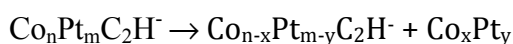
In order to assess the adsorption strength of Co-Pt nanoalloy to anionic C_2H radical, we obtained adsorption energies of anionic ethynyl radical on the bimetallic Co_nPt_m ($2 \leq n+m \leq 5$) clusters and plotted in Figure 4.5. The adsorption energies are given as

$$E_{ads} = E[Co_nPt_m] + E[C_2H^{-1}] - E[Co_nPt_mC_2H^{-1}] \quad (2 \leq n+m \leq 5) \quad (4.3)$$

where $E[*]$ is the total energy of given species in the equation. The adsorption energies reveal a growing tendency with the increasing ratio of Pt/Co for the studied species. The trend has no exception for the species having dimer and tetramer

metallic units. The global peak of the adsorption energies at the cluster $[\text{Pt}_4\text{C}_2\text{H}]^-$ is seen in Figure 4.5 while the adsorption energy of $[\text{Co}_2\text{C}_2\text{H}]^-$ corresponds to a dip in the plot. These two clusters have adsorption energy values of 6.09 eV and 3.59 eV, respectively. Furthermore, for anionic Co_{2-5} -ethynyl clusters, the increase in the size of the cluster leads to an increase in the adsorption energies slightly.

Another sensitive quantity to reflect the relative stability is the dissociation energy E_{dis} . For the anionic $\text{Co}_n\text{Pt}_m\text{C}_2\text{H}^-$ species, the dissociation channels



are investigated within the range of the study and the corresponding dissociation energies are computed respectively:

$$E_{\text{dis}} = E[\text{Co}_{n-x}\text{Pt}_{m-y}\text{C}_2\text{H}^-] + E[\text{Co}_x\text{Pt}_y] - E[\text{Co}_n\text{Pt}_m\text{C}_2\text{H}^-] \quad (4.4)$$

The selected dissociation channels and the corresponding dissociation energies are given in Table 4.2. The most favorable dissociation channels are related to the minimum dissociation energies. From our DFT calculations, when $n+m$ and $x+y$ are odd numbers, clusters prefer to dissociate Co or Pt monomers. This is consistent with experimental results on cationic and anionic metal clusters [207-209]. According to these experiments, small odd numbered clusters in the systems evaporate a neutral monomer. On the other hand, when $n+m$ and $x+y$ are even numbers, the clusters tend to dissociate a CoPt bimetallic molecule.

For pure Pt-ethynyl and Co-ethynyl clusters, as depicted in Table 4.2, the dissociations of Pt and Co dimers are most favorable when the total numbers of Pt and Co atoms are even. From the data given in Table 4.2, it can be seen that the dissociation energy of Pt is larger than that of Co. This is consistent with the trend seen in the BEs. Furthermore, the most favorable reactions are



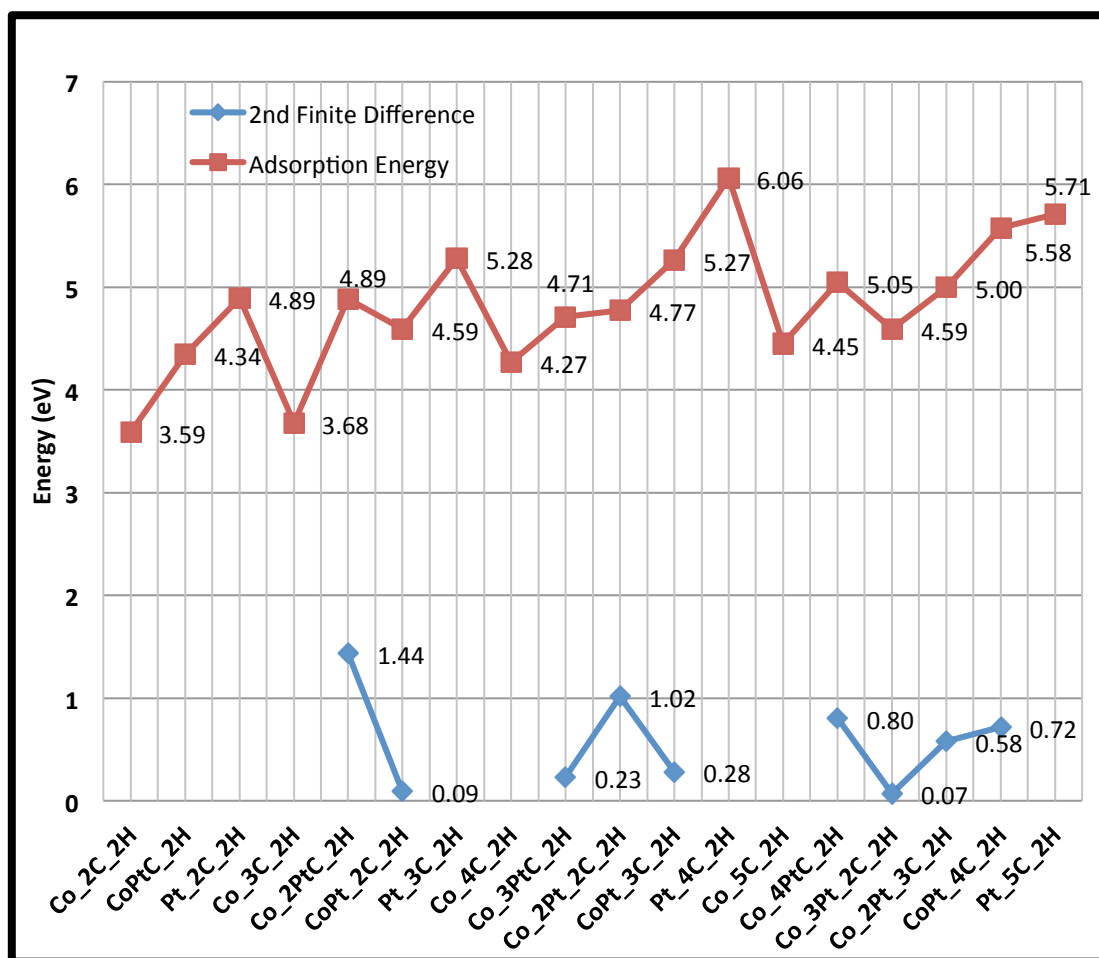
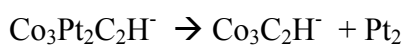
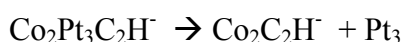


Figure 4.5 The second finite energies and C₂H adsorption energies of [C_nPt_mC₂H]

since the reaction energy for them are the least values in the Table 4.2. On the other hand the least favorable reactions are



since they have the highest reaction energies.

The HOMO energy is related to the ability of the cluster to give an electron, whereas the LUMO energy is an indicator of electron acceptance. The energy gap between HOMO and LUMO reveals the ability of electrons to bounce from HOMO to LUMO and determines a molecule to involve in chemical reactions to some degree, that is, a large HLG has been considered as significant requirement for chemical stability.

The calculated HLGs and lowest and highest vibrational frequencies are presented in the Table 4.1. We have also plotted HLGs and VDEs of $[\text{Co}_n\text{Pt}_m\text{C}_2\text{H}]^-$ species in the Figure 4.6.

$[\text{Co}_3\text{C}_2\text{H}]^-$ has the lowest HLG with the value 0.03 eV in the given study. It was found that the HLG of pure Co_3 is 1.04 eV [197]. By a comparison to the Sebetci's study where the same xc functional and basis functions are used, it can be pointed out that the adsorption of the C_2H radical tends to decrease the energy gap for $[\text{Pt}_{2.5}\text{C}_2\text{H}]^-$, indicating that the species become more conductive while for $[\text{Co}_{2.5}\text{C}_2\text{H}]^-$, it tends to increase the energy gap, indicating that the species become more stable.

According to the Table 4.1, $[\text{Pt}_3\text{C}_2\text{H}]^-$ and $[\text{Pt}_5\text{C}_2\text{H}]^-$ clusters possess high chemical stability due to their large HLGs (1.05 eV and 1.21 eV, respectively) when they are compared to the other species.

VDE is expressed as the energy difference between neutral and ionic clusters at optimized geometry of the neutral clusters. The VDE results we have obtained for $[\text{Co}_{2.5}\text{C}_2\text{H}]^-$ species as well as the corresponding experimental and theoretical results are given in Table 4.1. As seen in Table 4.1, the calculated VDE values in the present study are in an agreement with the previous experimental and theoretical results. The peak in Figure 4.6 is at $[\text{Pt}_4\text{C}_2\text{H}]^-$ with a value of 3.09 eV, while the dip is seen at $[\text{Co}_2\text{C}_2\text{H}]^-$ (1.25 eV). As the VDE increases with the increasing number of Pt atoms in the species with $n+m=4$, it oscillates for $n+m=5$ species with the number of Pt atoms.

Locally stable isomers are distinguished from transition states by vibrational frequency analysis. The lowest and highest vibrational frequencies of all the species studied in the present work are given in Table 4.1.

Table 4.2 The dissociation channels of selected anionic Co_nPt_m -ethynyl clusters

$[\text{Co}_n\text{Pt}_m\text{C}_2\text{H}]^-$	Dissociation Channel	E_{dis} (eV)
$[\text{Co}_3\text{C}_2\text{H}]^-$	$\text{Co}_2\text{C}_2\text{H}^- + \text{Co}$	2.44
$[\text{Co}_2\text{PtC}_2\text{H}]^-$	$\text{Co}_2\text{C}_2\text{H}^- + \text{Pt}$	4.97
$[\text{CoPt}_2\text{C}_2\text{H}]^-$	$\text{CoPtC}_2\text{H}^- + \text{Pt}$	3.96
$[\text{Pt}_3\text{C}_2\text{H}]^-$	$\text{Pt}_2\text{C}_2\text{H}^- + \text{Pt}$	4.07
$[\text{Co}_4\text{C}_2\text{H}]^-$	$\text{Co}_2\text{C}_2\text{H}^- + \text{Co}_2$	2.68
$[\text{Co}_4\text{C}_2\text{H}]^-$	$\text{Co}_3\text{C}_2\text{H}^- + \text{Co}$	2.88
$[\text{Co}_3\text{PtC}_2\text{H}]^-$	$\text{Co}_3\text{C}_2\text{H}^- + \text{Pt}$	5.14
$[\text{Co}_3\text{C}_2\text{H}]^-$	$\text{Co}_2\text{PtC}_2\text{H}^- + \text{Co}$	2.61
$[\text{Co}_2\text{Pt}_2\text{C}_2\text{H}]^-$	$\text{CoPtC}_2\text{H}^- + \text{CoPt}$	3.53
$[\text{Co}_2\text{Pt}_2\text{C}_2\text{H}]^-$	$\text{Pt}_2\text{C}_2\text{H}^- + \text{Co}_2$	3.99
$[\text{Co}_2\text{Pt}_2\text{C}_2\text{H}]^-$	$\text{Co}_2\text{C}_2\text{H}^- + \text{Pt}_2$	5.29
$[\text{CoPt}_4\text{C}_2\text{H}]^-$	$\text{Pt}_3\text{C}_2\text{H}^- + \text{Pt}$	4.29
$[\text{Pt}_4\text{C}_2\text{H}]^-$	$\text{Pt}_2\text{C}_2\text{H}^- + \text{Pt}_2$	4.05
$[\text{Co}_5\text{C}_2\text{H}]^-$	$\text{Co}_4\text{C}_2\text{H}^- + \text{Co}$	2.90
$[\text{Co}_5\text{C}_2\text{H}]^-$	$\text{Co}_3\text{C}_2\text{H}^- + \text{Co}_2$	3.14
$[\text{Co}_5\text{C}_2\text{H}]^-$	$\text{Co}_2\text{C}_2\text{H}^- + \text{Co}_3$	3.24
$[\text{Co}_4\text{C}_2\text{H}]^-$	$\text{Co}_3\text{PtC}_2\text{H}^- + \text{Co}$	3.06
$[\text{Co}_4\text{C}_2\text{H}]^-$	$\text{Co}_2\text{PtC}_2\text{H}^- + \text{Co}_2$	3.03
$[\text{Co}_4\text{PtC}_2\text{H}]^-$	$\text{Co}_3\text{C}_2\text{H}^- + \text{CoPt}$	4.22
$[\text{Co}_4\text{PtC}_2\text{H}]^-$	$\text{CoPtC}_2\text{H}^- + \text{Co}_3$	3.56
$[\text{Co}_3\text{Pt}_2\text{C}_2\text{H}]^-$	$\text{Co}_2\text{Pt}_2\text{C}_2\text{H}^- + \text{Co}$	2.65
$[\text{Co}_3\text{Pt}_2\text{C}_2\text{H}]^-$	$\text{CoPt}_2\text{C}_2\text{H}^- + \text{Co}_2$	3.56
$[\text{Co}_3\text{Pt}_2\text{C}_2\text{H}]^-$	$\text{Co}_2\text{PtC}_2\text{H}^- + \text{CoPt}$	3.31
$[\text{Co}_3\text{Pt}_2\text{C}_2\text{H}]^-$	$\text{Co}_3\text{C}_2\text{H}^- + \text{Pt}_2$	5.50
$[\text{Co}_2\text{Pt}_3\text{C}_2\text{H}]^-$	$\text{Co}_2\text{C}_2\text{H}^- + \text{Pt}_3$	5.81
$[\text{Pt}_5\text{C}_2\text{H}]^-$	$\text{Pt}_4\text{C}_2\text{H}^- + \text{Pt}$	3.67
$[\text{Pt}_5\text{C}_2\text{H}]^-$	$\text{Pt}_3\text{C}_2\text{H}^- + \text{Pt}_2$	3.65
$[\text{Pt}_5\text{C}_2\text{H}]^-$	$\text{Pt}_2\text{C}_2\text{H}^- + \text{Pt}_3$	4.04

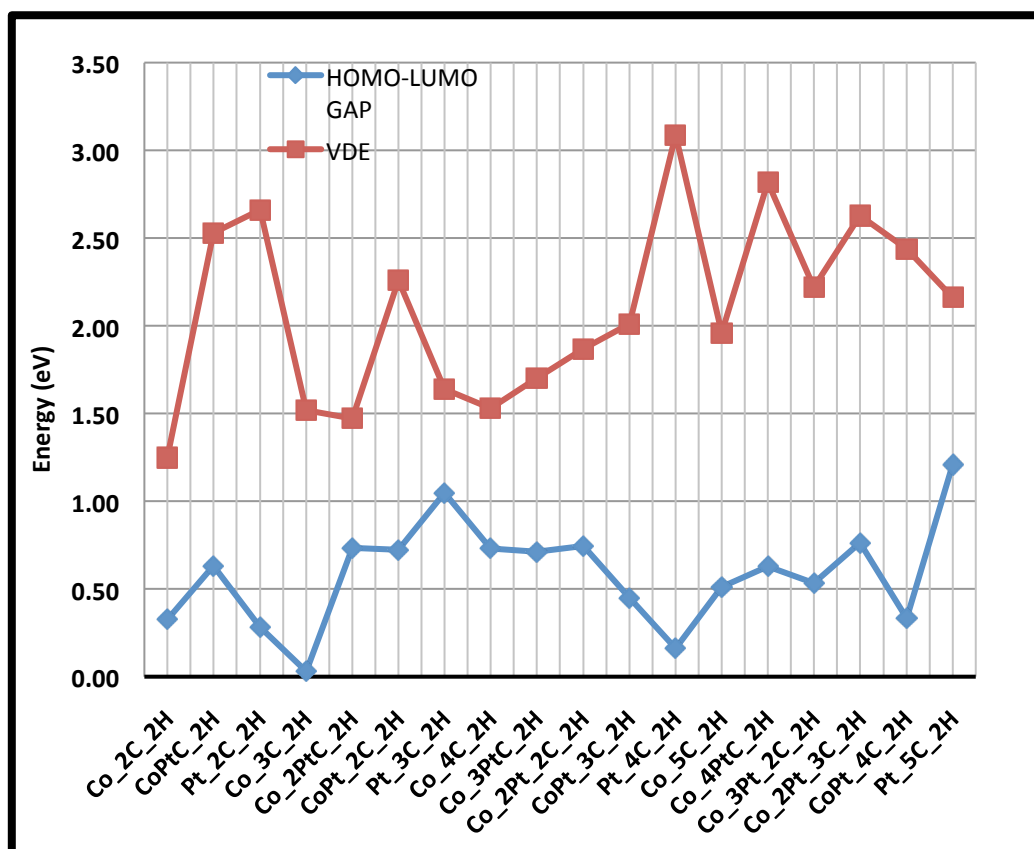


Figure 4.6 The HOMO-LUMO gaps and VDEs of $[\text{Co}_n\text{Pt}_m\text{C}_2\text{H}]^-$

4.3.6 Magnetic Properties

The total spin magnetic moments of low-lying isomers of Co_nPt_m and $[\text{Co}_n\text{Pt}_m\text{C}_2\text{H}]^-$ species within the range of the study are given in Figure 4.7. For the bare and ethynyl clusters, the total spin magnetic moment decreases with doping of Pt atoms in to the species. For more than the half of the studied species, the magnetic moments of lowest energy structure of the anionic ethynyl clusters are close to those of bare Co_nPt_m clusters. The total spin magnetic moments of some certain species are decreased $2 \mu_B$ upon the ethynyl adsorption. That indicates that the magnetic moments of bare clusters are sometimes affected by the adsorption of ethynyl radical. Contrary, for bare Co clusters, according to the Knickelbein, the electronic structures of the cobalt species are affected importantly upon chemical adsorption of benzene molecules, which leads to quench their magnetic moments [210]. This effect can be explained as the interaction between the π electrons of benzene molecules and the d orbitals of Co atoms is very strong due to the formation of the Co-benzene

species as sandwich or rice-ball structures, whereas ethynyl radical reacts with only one or two Co atoms through its terminal carbon atom.

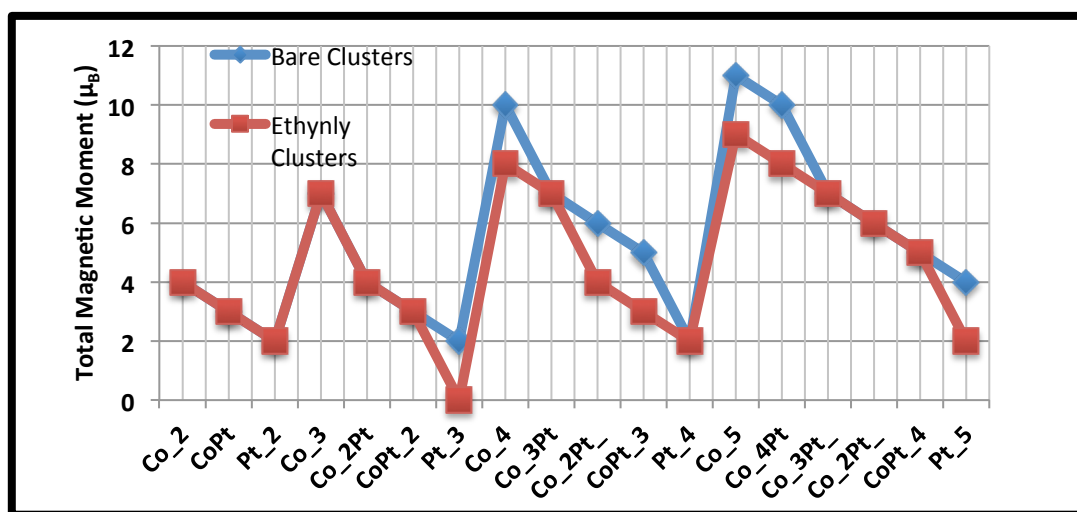


Figure 4.7 Total spin magnetic moments of the ground state, bare Co_nPt_m and anionic Co_nPt_m -ethynly clusters ($2 \leq n+m \leq 5$)

4.4 Conclusion

The DFT study carried out in the present work on the small bimetallic anionic Co_nPt_m -ethynyl clusters indicates that the ground state structures of these nanoparticles are generally three-dimensional structures with low symmetry. As the number of Pt atoms in these systems increases, BE of the clusters increases. In general C_2H^- radical prefers to bind on an atop side for $n+m < 4$, and on a bridge side for the higher sizes with a few exceptions. The species $[\text{Co}_2\text{PtC}_2\text{H}]^-$, $[\text{Co}_2\text{Pt}_2\text{C}_2\text{H}]^-$, $[\text{Co}_4\text{PtC}_2\text{H}]^-$, and $[\text{CoPt}_4\text{C}_2\text{H}]^-$ are found to be more stable than their neighboring sizes since they have relatively high second finite energies. The highest HLGs belong to $[\text{Pt}_3\text{C}_2\text{H}]^-$ and $[\text{Pt}_5\text{C}_2\text{H}]^-$ species which indicates their chemical stability. The most preferred dissociation channel of anionic Co_nPt_m -ethynyl clusters is Co atom ejection. The favorable dissociation channel is independent of cluster size. The calculated magnetic moments of anionic $[\text{Co}_n\text{Pt}_m\text{C}_2\text{H}]^-$ systems indicate that a weak quenching of moments occurs for some of the species after ethynyl adsorption. The lowest and the highest vibrational frequencies are reported to guide further experimental studies.

CHAPTER 5

THE INFLUENCE OF Li_xO LIGANDS ON THE STRUCTURE OF PALLADIUM COBALT CLUSTERS

5.1 Introduction

Thanks to advance in new experimental techniques, scientists and engineers in the field of the material science or engineering can currently synthesize, characterize and design distinct materials with required size and arrangement and this encourages them to study specific structures. Importantly, in the field of catalysis, this motivation has resulted in great advances in order to get better catalysts.

In the chemical industry, the study of nanoalloy catalysts is of high interest. Such materials are noteworthy since one of the metal particles can adjust and/or modify the catalytic properties of the other ones due to the consequences of structural and electronic effects. It is known that in numerous bimetallic nanoalloy particles, a common geometry is the one in which the central part of the structure is mainly occupied by one of the constituents and its surface holds most of the other element. If the active metal in terms of catalytic reaction is the one that separates from the surface, smaller volume of that metal may be required to attain similar results as those obtained by single pure element catalysts. For this reason, it is significant to state that PdCo nanoparticles form ordered patterns at low temperatures and Pd inclines to segregate to the surface in the case of macroscopic samples of PdCo bimetal nanoalloys [64]. Furthermore, PdCo particles have shown improved selectivity over pure Co particles, in Fisher-Tropsch reactions [65-67]. Due to the recent abrupt variations in the prices of hydrocarbons, the artificial production of fuels by converting carbon monoxide and hydrogen is attracting a lot of research in this field.

The mixed metal catalysis to obtain better catalysis than pure metals catalysis is used in different areas. For a direct methanol fuel cell, Serov et al. [211] examined the efficiency of platinum-free palladium-cobalt catalysts in oxygen reduction. They found the dependence of catalytic activity on precursor nature for palladium chloride and palladium nitrate. Another study done by Jung and coworkers [212] is related to the Lithium air batteries. They studied metal-air batteries due to their high energy density but the critical challenges of these technologies involve slow kinetics of the oxygen reduction that is evolution reactions on a cathode. The slow rates of the oxygen reduction reaction (ORR) and the oxygen evolution reaction (OER) of metal-air batteries under development results in charge overpotentials that means large voltage gaps and low round-trip efficiency [213-215]. Hence, for both ORR and OER, lessening the overpotentials by electrocatalysts is of great significance for improving round-trip efficiency and cyclability. The catalysts that have been classically used for ORR and OER are made up of costly metals, such as Pt and Ir [155,216,217]. Their high cost restricts extensive usage in large-scale applications. Vital efforts have been made over the years in the improvement of cost-effective catalysts based on mixed transition metal oxides [218-220]. Among various types of metal oxides, perovskites have recently received a lot of attention due to their high catalytic activity and stability in aqueous alkaline electrolytes [221,222].

There is a number of studies available for metal or mixed transition metal catalysis with Li_xO_y in the field of Li-air batteries. However, to the best our knowledge, there has been no studies reported to date on the interaction of PdCo nanoparticles with Li_2O and LiO compounds. Thus, it is worthy to investigate PdCo Li_xO nanoalloy complexes systematically in order to understand the mechanism and elucidate more details on the formation of such complexes. This study may provide useful information for future experiments concerning the improvement of catalysis of Li-air batteries.

In the present part of the work, we have investigated the structural, electronic and magnetic properties of Pd $_n$ Co $_m$ Li $_x$ O ($2 \leq n+m \leq 4$ and $x=1,2$) bimetallic clusters within the framework of DFT. We present the obtained results and discuss the interaction between PdCo bimetallic clusters and Li $_x$ O in the following sections.

5.2 Computational Details

NWChem 6.0 package [128] has been used to achieve local geometry optimizations, and to determine the total ground state energies and HLGs by DFT calculations. CRENBL [129] basis set and relativistic ECP have been chosen for Pd and Co where the outer most electrons are treated as valence to reduce the number of electrons explicitly considered in the calculations. For Li and O atoms, the split valence 6-311++G** basis set has been employed. The default convergence criteria of the code have been employed during the calculations, which are 1×10^{-6} Hartree for energy and 5×10^{-4} Hartree/ a_0 for energy gradient. The GGA of Becke's exchange functional [130] and Lee-Yang-Parr correlational functional [93] is chosen in the present work. The geometry optimizations without any symmetry constraints in various electronic spin multiplicities were carried out.

5.3 Results and Discussion

5.3.1 Lowest Energy Structures of $\text{Pd}_n\text{Co}_m\text{LiO}$ ($2 \leq n+m \leq 4$)

The most stable structures of $\text{Pd}_n\text{Co}_m\text{LiO}$ ($2 \leq n+m \leq 4$) bimetallic lithium monoxide are presented in Figure 5.1 and the HOMO and LUMO density plots are given in Figure 5.2. In addition, Table 5.1 indicates total spin moments, BEs, Fermi energies and HLGs of the studied clusters. The BEs per atoms of these species is plotted in Figure 5.3. LiO is, see Figure 5.1, adsorbed on the PdCo nanoparticles in a molecular form with oxygen instead of lithium bonding to PdCo nanoparticles for each case studied in the present work. LiO molecule absorbed on PdCo surface on a top or bridge site and prefers to bind Co atom in these structures.

The lowest energy structure of Pd_2LiO has C_s point group symmetry in the quartet magnetic state. The Pd-Pd bond distance of Pd_2LiO is 2.44 Å. The absorption of LiO results in the Pd-O bond distance as 1.90 Å whereas the Li-O bond distance is 1.68 Å. The LiO molecule prefers to be adsorbed on PdCo on the top site of the Co atom (see Figure 5.1b).

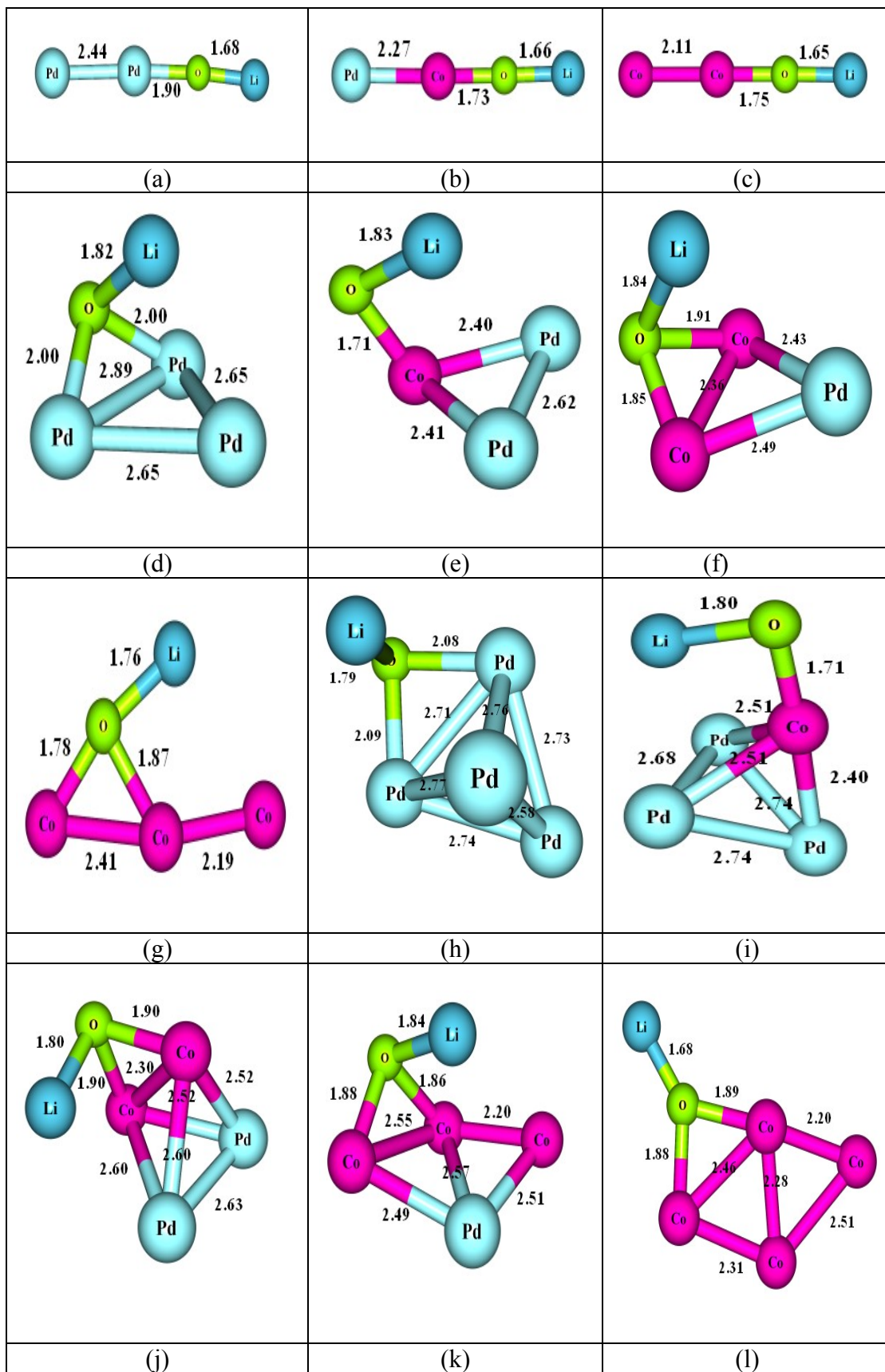


Figure 5.1 The optimized structure of $\text{Pd}_n\text{Co}_m\text{LiO}$ ($2 \leq m+n \leq 4$)

The point group symmetry of the lowest energy structure of PdCoLiO is C_s with a BE of 2.61 eV. The Pd-Co bond distance is 2.27 Å. The bond distance between Li and O in the PdCoLiO nanoparticle is slightly different from that of the Pd₂LiO structure. The replacement of Pd atom with Co leads to a very little stretch in the Co-O bond length where the Co-O bond distance becomes 1.75 Å. The BE of Co₂LiO having 5 μ_B spin moment is 2.65 eV. This value is the highest one among the species with $m+n=2$. For these species, when the ratio of Co/Pd increases, the BE increases.

In the ground state structure of Pd₃LiO (see Figure 5.1d), LiO is adsorbed at the bridge site of the triangularly oriented Pd atoms. When compared with the structure of Pd₂LiO, the Li-O bond length is stretched by 0.14 Å, whereas the Pd-O bond length is elongated as 0.1 Å. The average Pd-Pd bond length of Pd₃LiO is 2.73 Å. The total spin moment of Pd₃LiO is 1 μ_B and the point group symmetry of this structure is C_s . The HLG is calculated as 0.50 eV and its Fermi energy is found to be 3.78 eV. Its BE per atom is 2.36 eV (see Table 5.1).

As one of the Pd atoms replaced with Co, the lowest energy structure of Pd₂CoLiO becomes the structure possessing triangular bimetallic unit including a Co atom at the apex and two Pd atoms at the base. Replacement of the Pd atom with the Co (see Figure 5.1e) has very little effect on Li-O bond length (1.83 Å), which was 1.82 Å in Pd₃LiO. While distances between Pd and Co atoms are 2.40 Å and 2.41 Å in CoPd₂LiO, the Pd-Pd bond distance is longer by 0.18 Å than that of Pd₂LiO nanoparticle. LiO molecule prefers to be adsorbed on the top site of the Co rather than Pd with a 1.71 Å of Co-O bond length. Its BE per atom is 2.64 eV in quintet magnetic state. The HLG of this structure having C_s point group symmetry is 0.73 eV.

As the Co/Pd ratio increases, the triangular unit of the bimetallic part does not change its shape. Thus, PdCo₂LiO nanoparticle has also a triangular unit with increasing BE of 2.65 eV, which is the highest BE for $m+n=3$ species. LiO molecule prefers to bind to two Co atoms in this structure. The Co-O distances are 1.85 and 1.91 Å and the Co-Co distance is 2.36 Å, which is 0.25 Å longer than that of Co₂LiO. Co-Pd bond distances are 2.43 Å and 2.49 Å, which are slightly longer than that of PdCoLiO.

	HOMO	LUMO	HOMO	LUMO	
Pd ₂ LiO					PdCoLiO
Co ₂ LiO					Pd ₃ LiO
Pd ₂ CoLiO					PdCo ₂ LiO
Co ₃ LiO					Pd ₄ LiO
Pd ₃ CoLiO					Pd ₂ Co ₂ LiO
PdCo ₂ LiO					Co ₄ LiO

Figure 5.2 The HOMO and LUMO density plots of Pd_nCo_mLiO (2≤m+n≤4)

Due to the doping of Co atom, the Li-O bond length seems to be affected slightly in this structure. The magnetic moment of PdCo₂LiO is 5 μ_B . The HLG is 0.83 eV, while the Fermi energy of this structure is 3.27 eV.

The BE per atom of Co₃LiO nanoparticle is calculated as 2.53 eV, which is not consistent with the trend that replacement of Pd atom with Co increases the BE. The HLG and the Fermi energy of this species is 0.46 eV and 3.61 eV, respectively. The Fermi energy is 0.17 eV less than that of Pd₃LiO. The magnetic ground state of Co₃LiO is septet. When the LiO molecule is adsorbed on the bridge site as in the case of Co₃LiO, a typical Li-O bond length is 1.76 Å, whereas a typical value of the same bond length for atop adsorptions is 1.83 Å for the species with n+m=3. These values can be compared with Li-O bond length of free LiO molecule, which is calculated as 2.43 Å. This indicates that Li-O bond length is shrunk significantly upon the adsorption of the molecule on the Pd-Co nanoparticles.

The Pd₄LiO structure has tetrahedral unit (see Figure 5.1h) where the average Pd-Pd bond length is 2.72 Å. The LiO is adsorbed on a bridge site of the Pd tetramer, where the Pd-O distances are 2.08 Å and 2.09 Å, which are very close to those of Pd₃LiO, while the Li-O bond length is 1.79 Å. It can be concluded that the addition of a Pd atom to Pd₃LiO leads to expand the length of the triangular unit consisting of Pd atoms that is a face of Pd₄LiO structure. The total magnetic moment of this structure is 3 μ_B with C₁ symmetry. The HLG is 0.03 eV, whereas the Fermi energy is 2.11 eV.

In the lowest energy structure of Pd₃CoLiO, LiO binds to the Co site. The Co-O bond length is 1.71 Å, which is similar to the other atop site absorptions. The addition of a Pd atom to Pd₂CoLiO has little effect on the Li-O bond length. The BE of Pd₃CoLiO is 2.65 eV in quintet magnetic state. The Fermi energy of this structure is 3.59 eV whereas the HLG is 0.50 eV. The magnetic moment of Pd₂Co₂LiO (Figure 5.1j) is 5 μ_B with Fermi energy of 3.36 eV. The HLG is 0.49 eV. The Co-Co bond distance after LiO adsorption is 2.30 Å, which is similar to that of PdCo₂LiO nanoparticle. The LiO molecule is adsorbed on the Co-Co bridge site where Co-O bond length is 1.90 Å, whereas the Li-O bond distance is 1.80 Å.

Table 5.1 The electronic properties of Pd_nCo_mLiO (2≤n+m≤4) structures

Cluster	Symmetry	Spin moment (μ _B)	BE per atom (eV)	Fermi energy (eV)	HOMO-LUMO Gap (eV)
Pd ₂ LiO	C _s	3	2.07	2.05	0.42
PdCoLiO	C _s	4	2.61	2.51	0.05
Co ₂ LiO	C _s	5	2.65	2.81	1.26
Pd ₃ LiO	C _s	1	2.36	3.78	0.50
Pd ₂ CoLiO	C _s	4	2.64	3.65	0.73
PdCo ₂ LiO	C ₁	5	2.65	3.27	0.83
Co ₃ LiO	C ₁	6	2.53	3.61	0.46
Pd ₄ LiO	C ₁	3	2.33	2.11	0.03
Pd ₃ CoLiO	C ₁	4	2.65	3.59	0.50
Pd ₂ Co ₂ LiO	C _s	5	2.68	3.36	0.49
PdCo ₃ LiO	C _s	8	2.61	3.87	0.61
Co ₄ LiO	C ₁	9	2.57	2.83	0.95

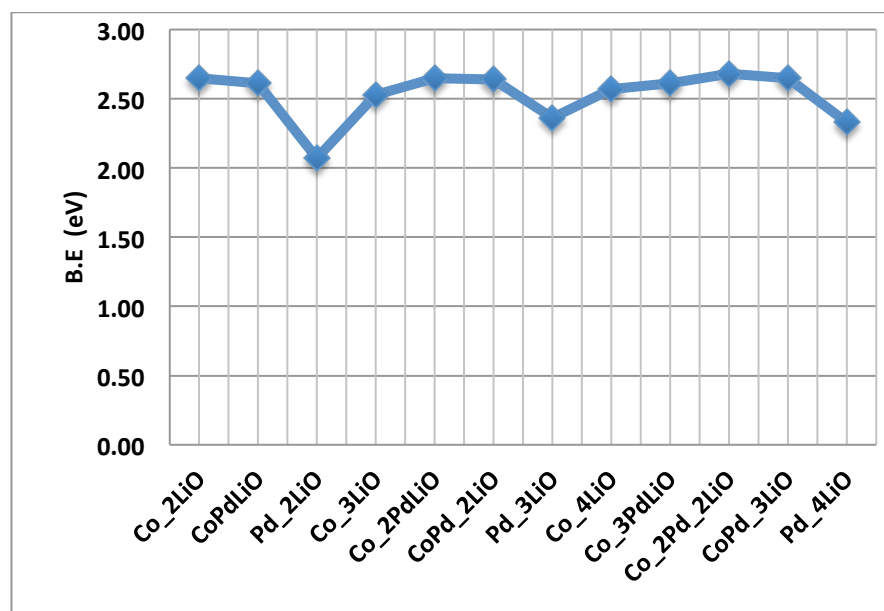


Figure 5.3 The BE per atom of Pd_nCo_mLiO clusters (2≤m+n≤4)

Furthermore, the BE of Pd₂Co₂LiO is 2.68 eV with C_s point group symmetry. The metallic unit of PdCo₃LiO is an out of plane rhombus rather than a tetrahedron. The LiO molecule again prefers to bind on a Co-Co bridge site, where Li-O bond length is 1.84 Å. The HLG of this specie is 0.61 eV, while the Fermi energy is 3.87 eV. This structure has C_s point group symmetry and 2.61 eV BE per atom. The total spin magnetic moment is 8 μ_B. The Co₄LiO nanoparticle (see Figure 5.11) has 0.95 eV HLG, while the Fermi energy is 2.83 eV. The BE of this structure having 9 μ_B is calculated as 2.57 eV. The average Co-Co bond distance is 2.35 Å, whereas Co-O bond distances are 1.88 Å and 1.89 Å, while Li-O bond length is 1.68 Å.

5.3.2 Lowest Energy Structures of Pd_nCo_mLi₂O (2 ≤ n+m ≤ 4)

The most stable structures of Pd_nCo_mLi₂O (2 ≤ n+m ≤ 4) clusters are presented in Figure 5.4 and the HOMO-LUMO density plots are given in Figure 5.5. Table 5.2 indicates the total spin moments, BEs, Fermi energies and HLG of these clusters. The BEs per atoms of these species is plotted in Figure 5.6. Li₂O is, see Figure 5.4a, adsorbed on Pd₂ dimer molecularly at the top site where O is bond to one of the Pd atoms. For PdCo, Li₂O molecule is absorbed on the Co atom. The BE of the lowest energy structure of Pd₂Li₂O is 2.48 eV. This structure has zero magnetic moment. The HLG energy of Pd₂Li₂O cluster having C_s symmetry is 0.77 eV, while its Fermi energy is 1.93 eV. The ground state structure of the PdCoLi₂O is in the quartet magnetic state with C_s symmetry. The Li-O bond length is 1.82 Å in this structure while that bond length in PdCoLiO nanoparticle is 1.66 Å. The addition of the Li atom to LiO molecule at the PdCo cluster leads to expand Co-Pd distance by 0.1 Å. The HLG of the particle is 1.02 eV, whereas the Fermi energy is 1.25 eV. The BE of PdCoLi₂O is 2.66 eV.

The Co-Co bond distance of the Co₂ dimer after Li₂O adsorption became 2.20 Å, which is longer than that of Co₂LiO structure. Furthermore, the Co-O bond length is 1.83 Å, while Li-O bond lengths in this structure (see Figure 5.4c) are 1.69 and 1.78 Å. The HLG energy is 0.73 eV. The BE per atom of this structure, which has 4 μ_B magnetic moment, is 2.56 eV.

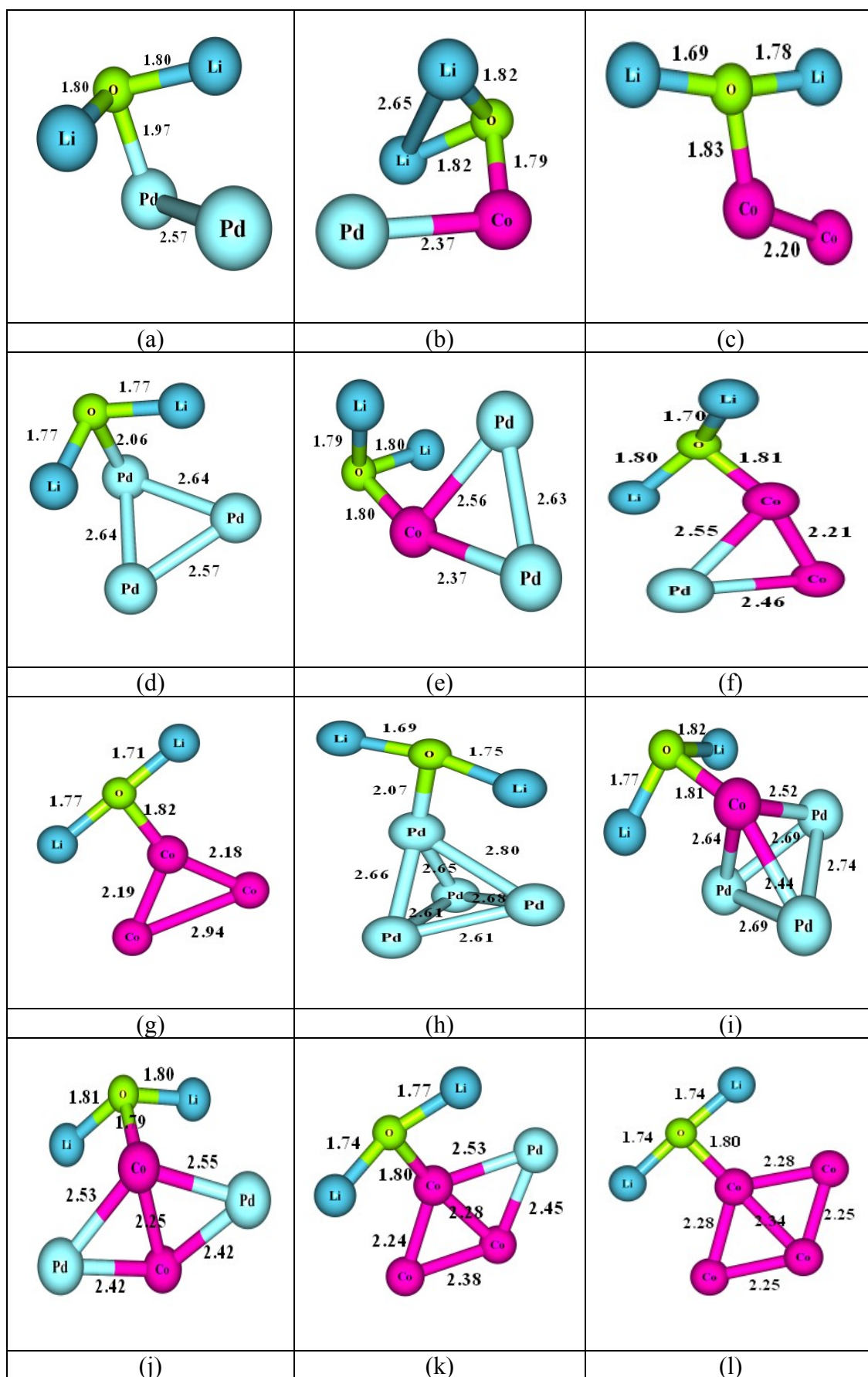


Figure 5.4 The optimized structures of $Pd_nCo_mLi_2O$ clusters ($2 \leq m+n \leq 4$)

	HOMO	LUMO	HOMO	LUMO	
Pd ₃ Li ₂ O					PdCoLi ₅ O
Co ₂ Li ₂ O					Pd ₃ Li ₅ O
Pd ₂ CoLi ₂ O					PdCo ₂ Li ₅ O
Co ₃ Li ₂ O					Pd ₄ Li ₅ O
Pd ₃ CoLi ₂ O					Pd ₅ Co ₂ Li ₅ O
PdCo ₃ Li ₂ O					Co ₄ Li ₅ O

Figure 5.5 The HOMO-LUMO density plots of Pd_nCo_mLi₂O clusters (2 ≤ m+n ≤ 4)

Table 5.2 The electronic properties of Pd_nCo_mLi₂O (2≤n+m≤4) structures

Cluster	Symmetry	Spin moment (μ _B)	BE per atom (eV)	Fermi energy (eV)	HOMO-LUMO Gap (eV)
Pd ₂ Li ₂ O	C _s	0	2.48	1.93	0.77
PdCoLi ₂ O	C _s	3	2.66	1.25	1.02
Co ₂ Li ₂ O	C ₁	4	2.56	1.73	0.73
Pd ₃ Li ₂ O	C ₁	2	2.44	3.97	0.15
Pd ₂ CoLi ₂ O	C ₁	3	2.65	1.04	0.84
PdCo ₂ Li ₂ O	C ₁	4	2.58	2.98	0.46
Co ₃ Li ₂ O	C ₁	7	2.56	2.59	0.89
Pd ₄ Li ₂ O	C ₁	2	2.45	3.10	0.07
Pd ₃ CoLi ₂ O	C ₁	3	2.66	3.18	0.59
Pd ₂ Co ₂ Li ₂ O	C ₁	6	2.69	1.76	0.57
PdCo ₃ Li ₂ O	C ₁	7	2.64	3.01	0.72
Co ₄ Li ₂ O	C _s	8	2.60	2.71	0.66

As Pd doping increases, Pd₃Li₂O has a triangular unit like Pd₃LiO cluster. The magnetic state of this structure is triplet. The BE of the cluster is 0.04 eV less than that of Pd₂Li₂O. The adsorption of Li₂O is again on a top site, which is always the case for the lowest energy structures of Pd_nCo_mLi₂O clusters investigated in the present work. The average Pd-Pd distance is 2.62 Å, while this bond length is larger in Pd₂LiO, which means that the addition of the second Li atom to LiO leads to an elongation of Pd-Pd bond length. Pd-O bond distance is 2.06 Å, which is larger than that of Pd₂LiO. Furthermore, the HLG energy of this structure is 0.15 eV.

As one of the Pd atoms replaces with a Co atom, BE of the lowest energy structure of Pd₂CoLi₂O becomes 2.65 eV, where O binds to the Co atom. The Fermi energy of this structure is 1.04 eV, while the HLG is 0.84 eV. The Co-Pd distances are 2.56 and 2.37 Å and the Co-O bond length is 1.80 Å, which is longer than the Co-O bond length of Pd₂CoLiO. The BE per atom of PdCo₂Li₂O is 2.58 eV. The lowest energy morphology is similar to that of Pd₂CoLi₂O. Li₂O is adsorbed on the Co side as usual. The magnetic state of PdCo₂Li₂O is quintet. The Co-Co bond length of this cluster is 2.21 Å, which is nearly the same as that of Co₂Li₂O cluster. The HLG of Co₃Li₂O is calculated as 0.89 eV, while the Fermi energy is 2.59 eV. 2.56 eV BE of

$\text{Co}_3\text{Li}_2\text{O}$ is 0.02 eV less than that of $\text{PdCo}_2\text{Li}_2\text{O}$. The Co-O bond length is also very similar to that of the previous cluster. Li-O bond lengths are 1.71 Å and 1.77 Å in this case. The lowest energy configurations of Co_3LiO and $\text{Co}_3\text{Li}_2\text{O}$ are highly different.

The ground state structure of $\text{Pd}_4\text{Li}_2\text{O}$ has distorted tetrahedral metallic unit in triplet magnetic state with average Pd-Pd bond distance of 2.72 Å, which is longer than that of the $\text{Pd}_3\text{Li}_2\text{O}$. The BE of this structure is, see Table 5.2, 2.45 eV with Pd-O bond length of 2.07 Å, while Fermi energy is 3.10 eV. The HLG is calculated as 0.07 eV. Placing a Co atom instead of a Pd atom leads to stretch the bonds between Li and O, which are 1.77 Å and 1.82 Å in $\text{Pd}_3\text{CoLi}_2\text{O}$, while they are 1.69 Å and 1.75 Å in $\text{Pd}_4\text{Li}_2\text{O}$. The Co-O bond length in $\text{Pd}_3\text{CoLi}_2\text{O}$ is nearly the same with that of $\text{Pd}_2\text{CoLi}_2\text{O}$. Moreover, the distorted tetrahedral configuration of metallic unit is kept in $\text{Pd}_3\text{CoLi}_2\text{O}$ cluster. The BE per atom for this specie is calculated as 2.66 eV with a Fermi energy of 3.18 eV, while the HLG is calculated as 0.59 eV. The magnetic moment of the structure is found as 3 μ_B . As Co doping increases by keeping fixed the total number of metallic atoms, there is no important change for Li-O and Co-O bond lengths. However, the tetrahedral metallic unit becomes an out of plane rhombus for $\text{Pd}_2\text{Co}_2\text{Li}_2\text{O}$. Li_2O molecule binds to the top site of a Co atom where the Co-O bond length is 1.79 Å, while this bond length in the $\text{Pd}_2\text{Co}_2\text{LiO}$ is 1.90 Å, where adsorption is occurred on the bridge site. Moreover, the average Co-Pd bond distance is 2.48 Å and the Co-Co bond distance is 2.25 Å in this structure (see Figure 5.4j). The HLG is 0.57 eV, while Fermi energy is 1.76 eV. The BE of the structure is 2.69 eV in the quintet magnetic state.

When one of the Pd atoms of $\text{Pd}_2\text{Co}_2\text{Li}_2\text{O}$ is changed with a Co atom, the rhombic morphology does not change. In the ground state structure of $\text{PdCo}_3\text{Li}_2\text{O}$, BE is calculated as 2.64 eV, where Li_2O is adsorbed on the Co side again. The Co-Co bond distances are 2.24 Å and 2.38 Å (see Figure 5.4k) and the Co-Pd bond distances are 2.45 Å and 2.53 Å. The magnetic moment of this structure is 7 μ_B while the Fermi energy is 3.01 eV. The HLG energy of $\text{Pd}_3\text{CoLi}_2\text{O}$ cluster is 0.59 eV.

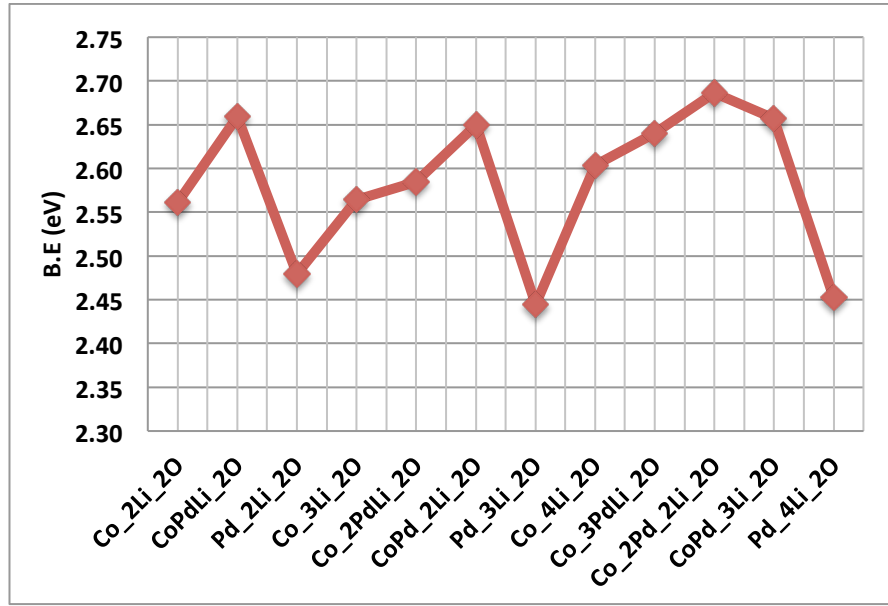


Figure 5.6 The BE per atom of Pd_nCo_mLi₂O clusters (2≤m+n≤4)

The BE per atom of Co₄Li₂O cluster with C_s symmetry is 2.60 eV. Its magnetic state is 8 μ_B. The replacement of the single Pd atom of PdCo₃Li₂O structure by a Co atom has little effect on Li-O bond length. The Co-Co bond distance of 2.28 Å is 0.10 Å longer than the corresponding distances of Co₃Li₂O structure. It can be concluded that the addition of a new Co atom to Co₃Li₂O cluster leads to an expansion in the Co-Co distances. Moreover, the Fermi energy of this structure is 2.71 eV, whereas the HLG is 0.66 eV.

5.3.3 Stability and Electronic Properties

The BEs of the clusters can be used as a measure for their thermodynamic stabilities. Accordingly, to predict the relative stabilities of the Pd_nCo_mLi_xO structures, the BEs per atom are calculated, tabulated in Table 5.1 and Table 5.2 and plotted in Figure 5.3 and Figure 5.6. The BEs per atom have been obtained in the following way:

$$BE = \frac{mE[Co] + nE[Pd] + xE[Li] + E[O]}{n + m + x + 1} \quad \text{for } 2 \leq n+m \leq 4 \quad \text{and } x=1 \text{ or } 2 \quad (5.1)$$

where E[*] is the total energy of Co, Pd, Li and O atoms respectively. While the BEs of the lowest energy structures of Pd_nCo_mLiO vary between 2.07 eV and 2.68 eV,

that of $\text{Pd}_n\text{Co}_m\text{Li}_2\text{O}$ changes from 2.44 eV to 2.69 eV.

For the Pd-Co clusters with LiO, the highest BE belongs to $\text{Pd}_2\text{Co}_2\text{LiO}$, while the lowest one belongs to Pd_2LiO . Similarly, for the Pd-Co clusters with Li_2O , the highest BE belongs to $\text{Pd}_2\text{Co}_2\text{Li}_2\text{O}$, while the lowest one belongs to $\text{Pd}_3\text{Li}_2\text{O}$. Concerning the BEs of all the species studied in the present work, the following conclusions can be drawn: for a given size, the lowest BE is calculated for the species containing no Co atom, while the species having equal or nearly equal number of Pd and Co atoms have the highest BEs.

Since HLG indicates the ability of electrons to bounce from HOMO to LUMO and governs a molecule to involve in chemical reactions to some degree, a large HLG has been considered as significant requirement for chemical stability. Pd_4LiO (0.03 eV) and $\text{Pd}_4\text{Li}_2\text{O}$ (0.07 eV) have the lowest HLGs among the species studied in this work. Thus, one can expect high chemical activities for these two clusters. On the other hand, the highest HLGs belong to Co_2LiO (1.26 eV) and PdCoLi_2O (1.02 eV) for which high chemical stability can be expected.

5.4 Conclusion

The structural, electronic, and magnetic properties of small, neutral, $\text{Pd}_n\text{Co}_m\text{Li}_x\text{O}$ structures where $2 \leq m+n \leq 4$ and $x=1$ or 2 , were studied by using DFT method with BLYP xc-functional. The lowest energy isomers of these systems are obtained. The effect of LiO and Li_2O adsorptions on small Pd-Co bimetallic clusters was examined. It is found that while LiO molecule can be adsorbed at atop or bridge sites of small Pd-Co bimetallic clusters, Li_2O molecule prefers to be adsorbed on atop sites only in the lowest energy structures. We do not observe any hollow site adsorption in any of the studied species. Li_xO ($x=1,2$) molecules like to bind to Co atoms instead of Pd and O atoms construct the binding rather than Li atoms. The morphology of the bare Pd-Co bimetallic clusters generally does not change upon Li_xO adsorptions. The complexes consisting only Pd atoms and Li_xO molecule but not Co have the least

BEs for their sizes. The structures having equal or nearly equal number of Pd and Co atoms possess the highest BEs.

CHAPTER 6

CONCLUSION

The small neutral and/or ionic ligand-passivated metal nanoparticles have been studied in terms of the geometric, electronic, and magnetic properties. The adsorption of a number of organic molecules or metal oxides on Pt, Co, Pd, and their alloy clusters is investigated by means of DFT calculations. Since the method requires heavy quantum mechanical calculations, the High Performance Computing facilities of Zirve University are used to find out the ground state structures, low-lying isomers and to determine electronic and magnetic properties of these structures. Various interaction patterns between the ligands and the metal clusters are examined and screened with extensive structural searches for the low-lying isomers of the ligand-protected complexes. Thus, the optimal adsorption sites are identified and the corresponding electronic and magnetic states are analyzed. Locally stable isomers are distinguished from transition states by vibrational frequency analysis.

$Pt_4(CH)_n$ ($1 \leq n \leq 7$) and $Pt_4(\text{benzene})_2$ metal-organic complexes have been investigated. Our calculations indicate that $Pt_4(CH)_4$ and $Pt_4\text{benzene}$ metal hydrocarbon complexes are the most stable structures among the studied species for CH protected Pt_4 clusters. CH is adsorbed on the tetramer in the molecular form with carbon instead of hydrogen bonding to Pt. The first and second adsorptions of CH ligands occur on the hollow sides of the Pt tetramer. After the size 2, as the number of CH ligands on the Pt tetramer is increased, CH radicals start to form C bonds. This trend continues up to the size 6. The lowest energy configuration of $Pt_4(CH)_6$ becomes a $Pt_4\text{benzene}$ where the ring of 6 C atoms adsorbed on a triangular surface of the Pt tetramer. For $Pt_4(\text{benzene})_2$ structures, the lowest energy structure is obtained as two benzene molecules adsorbed on different bridge sites of the Pt tetramer.

As a second example of ligand protected metal clusters, we examined the effect of anionic ethynyl radical on the CoPt nanoalloys and/or the effect of CoPt nanoalloys on the anionic ethynyl radical extensively, where the total number of Co and Pt atoms is less than or equal to 5. As the number of Pt atoms in $[\text{Co}_n\text{Pt}_m\text{C}_2\text{H}]^-$ systems increases, BE of the clusters increases. In general C_2H^- radical prefers to bind on an atop side for $n+m < 4$, and on a bridge side for the higher sizes with a few exceptions. The species $[\text{Co}_2\text{PtC}_2\text{H}]^-$, $[\text{Co}_2\text{Pt}_2\text{C}_2\text{H}]^-$, $[\text{Co}_4\text{PtC}_2\text{H}]^-$, and $[\text{CoPt}_4\text{C}_2\text{H}]^-$ are found to be more stable than their neighboring sizes since they have relatively high second finite energies. The highest HLGs belong to $[\text{Pt}_3\text{C}_2\text{H}]^-$ and $[\text{Pt}_5\text{C}_2\text{H}]^-$ species which indicates their chemical stability. The most preferred dissociation channel of anionic Co_nPt_m -ethynyl clusters is Co atom ejection. The favorable dissociation channel is independent of cluster size. The calculated magnetic moments of anionic $[\text{Co}_n\text{Pt}_m\text{C}_2\text{H}]^-$ systems indicate that a weak quenching of moments occurs for some of the species after ethynyl adsorption.

In the last part of the thesis, the study of the $\text{Pd}_n\text{Co}_m\text{Li}_x\text{O}$ structures, where $2 \leq m+n \leq 4$ and $x=1$ or 2 , has been carried out with a GGA xc functional. The lowest energy isomers of these systems are obtained. The effect of LiO and Li_2O adsorptions on small Pd-Co bimetallic clusters was examined. It is found that while LiO molecule can be adsorbed at atop or bridge sites of small Pd-Co bimetallic clusters, Li_2O molecule prefers to be adsorbed on atop sites only in the lowest energy structures. We do not observe any hollow site adsorption in any of the studied species of these systems. Li_xO ($x=1,2$) molecules like to bind to Co atoms instead of Pd and O atoms construct the binding rather than Li atoms. The morphology of the bare Pd-Co bimetallic clusters generally does not change upon Li_xO adsorptions. The complexes consisting only Pd atoms and Li_xO molecule but not Co have the least BEs for their sizes. The structures having equal or nearly equal number of Pd and Co atoms possess the highest BEs.

LIST OF REFERENCES

- [1] Yukna, J. (2007). *Computational and Experimental Investigations of the Structural Properties, Electronic Properties, and Applications of Silver, Gold, Mercury Selenide, Silver Sulfide, and Nickel Sulfide Nanoparticles* ProQuest, Southern Illinois University, Carbondale, USA.
- [2] Chan, T.-L. (2005). Theoretical studies of lead on silicon (111) and silicon (100), global search for hydrogen-passivated silicon nanowires, and construction of highly localized quasiautomatic minimal basis orbitals for molybdenum: ProQuest, Iowa State University, Ames, USA.
- [3] Brack, M. (1993). The physics of simple metal clusters: self-consistent jellium model and semiclassical approaches. *Reviews of Modern Physics*, 65(3), 677.
- [4] Raparla, M. (2009). Study of the structural and electronic properties of aluminum nano clusters by DFT, *ETD Collection*, University of Texas, El Paso, USA.
- [5] Johnston, R. L., & CRC Press. (2005). *Atomic and molecular clusters*, London: Taylor & Francis
- [6] Kuppasamy C, M. K. (2009). Mosquitocidal effect of *Andrographis paniculata* against the malaria vector, *Anopheles stephensi* Liston (Diptera: culicidae). *Int j integr Bio* 5(2), 75–81.
- [7] Roopan, S. M., Madhumitha, G., Rahuman, A. A., Kamaraj, C., Bharathi, A., & Surendra, T. (2013). Low-cost and eco-friendly phyto-synthesis of silver nanoparticles using *Cocos nucifera* coir extract and its larvicidal activity. *Industrial Crops and Products*, 43, 631-635.

- [8] Choi, O., Deng, K. K., Kim, N.-J., Ross Jr, L., Surampalli, R. Y., & Hu, Z. (2008). The inhibitory effects of silver nanoparticles, silver ions, and silver chloride colloids on microbial growth. *Water research*, 42(12), 3066-3074.
- [9] Chang, T.-L., Lee, Y.-W., Chen, C.-C., & Ko, F.-H. (2007). Effect of different gold nanoparticle sizes to build an electrical detection DNA between nanogap electrodes. *Microelectronic engineering*, 84(5), 1698-1701.
- [10] Mirkin, C. A., Letsinger, R. L., Mucic, R. C., & Storhoff, J. J. (1996). A DNA-based method for rationally assembling nanoparticles into macroscopic materials. *Nature*, 382(6592), 607-609.
- [11] Cioffi, N., Colaianni, L., Ieva, E., Pilolli, R., Ditaranto, N., Angione, M. D., Sabbatini, L. (2011). Electrosynthesis and characterization of gold nanoparticles for electronic capacitance sensing of pollutants. *Electrochimica Acta*, 56(10), 3713-3720.
- [12] Jiménez-Cadena, G., Riu, J., & Rius, F. X. (2007). Gas sensors based on nanostructured materials. *Analyst*, 132(11), 1083-1099.
- [13] Franke, M. E., Koplín, T. J., & Simon, U. (2006). *Metal and metal oxide nanoparticles in chemiresistors: does the nanoscale matter?*. *Small*, 2(1), 36-50.
- [14] Fabbi, J. C., Langenberg, J. D., Costello, Q. D., Morse, M. D., & Karlsson, L. (2001). Dispersed fluorescence spectroscopy of jet-cooled AgAu and Pt₂. *Journal of Chemical Physics*, 115(16), 7543-7549.
- [15] Gupta, S. K., Nappi, B. M., & Gingerich, K. A. (1981). Mass spectrometric study of the stabilities of the gaseous molecules Pt₂ and PtY. *Inorganic Chemistry*, 20(4), 966-969.
- [16] Taylor, S., Lemire, G. W., Hamrick, Y. M., Fu, Z., & Morse, M. D. (1988). Resonant two-photon ionization spectroscopy of jet-cooled Pt₂. *The Journal of Chemical Physics*, 89(9), 5517-5523.

- [17] Jansson, K., & Scullman, R. (1976). Optical absorption spectra of PtO and Pt₂ in rare-gas matrices. *Journal of Molecular Spectroscopy*, 61(2), 299-312.
- [18] Pontius, N., Bechthold, P. S., Neeb, M., & Eberhardt, W. (2000). Femtosecond multi-photon photoemission of small transition metal cluster anions. *Journal of Electron Spectroscopy and Related Phenomena*, 106(2-3), 107-116.
- [19] Ho, J., Polak, M. L., Ervin, K. M., & Lineberger, W. C. (1993). Photoelectron spectroscopy of nickel group dimers: Ni₂, Pd₂, and Pt₂. *The Journal of Chemical Physics*, 99(11), 8542-8551.
- [20] Airola, M. B., & Morse, M. D. (2002). Rotationally resolved spectroscopy of Pt₂. *Journal of Chemical Physics*, 116(4), 1313-1317.
- [21] Chang, C. M., & Chou, M. Y. (2004). Alternative Low-Symmetry Structure for 13-Atom Metal Clusters. *Physical Review Letters*, 93(13), 133401.
- [22] Watari, N., & Ohnishi, S. (1998). *Physical Review B*, 58(3), 1665-1677.
- [23] Aprà, E., & Fortunelli, A. (2003). Density-functional calculations on platinum nanoclusters: Pt₁₃, Pt₃₈, and Pt₅₅. *Journal of Physical Chemistry A*, 107(16), 2934-2942.
- [24] Wang, L. L., & Johnson, D. D. (2007). Density functional study of structural trends for late-transition-metal 13-atom clusters. *Physical Review B*, 75(23), 235405.
- [25] Longo, R. C., & Gallego, L. J. (2006). Structures of 13-atom clusters of fcc transition metals by ab initio and semiempirical calculations. *Physical Review B*, 74(19), 193409.
- [26] Tian, W. Q., Ge, M., Sahu, B. R., Wang, D., Yamada, T., & Mashiko, S. (2004). Geometrical and electronic structure of the Pt₇ cluster: A density functional study. *Journal of Physical Chemistry A*, 108(17), 3806-3812.

- [27] Aprà, E., & Fortunelli, A. (2000). Density-functional study of Pt₁₃ and Pt₅₅ cuboctahedral clusters. *Journal of Molecular Structure: THEOCHEM*, 501-502, 251-259.
- [28] Yang, S., & Wu, Z. (1997). Effects of shot-peening operation on the high cycle fatigue properties of single crystal superalloy DD3. *Cailiao Gongcheng/Journal of Materials Engineering*(12), 39-41.
- [29] Watari, N., & Ohnishi, S. (1998). Atomic and electronic structures of Pd₁₃ and Pt₁₃ clusters. *Physical Review B - Condensed Matter and Materials Physics*, 58(3), 1665-1677.
- [30] Bhattacharyya, K., & Majumder, C. (2007). Growth pattern and bonding trends in Pt_n (n=2-13) clusters: Theoretical investigation based on first principle calculations. *Chemical Physics Letters*, 446(4-6), 374-379.
- [31] Xiao, L., & Wang, L. (2004). Structures of platinum clusters: Planar or spherical. *Journal of Physical Chemistry A*, 108(41), 8605-8614.
- [32] Nie, A., Wu, J., Zhou, C., Yao, S., Luo, C., Forrey, R. C., & Cheng, H. (2007). Structural evolution of subnano platinum clusters. *International Journal of Quantum Chemistry*, 107(1), 219-224.
- [33] Fortunelli, A. (1999). Density functional calculations on small platinum clusters: Pt_n^q (n=1-4, q=0, ±1). *Journal of Molecular Structure: THEOCHEM*, 493, 233-240.
- [34] Varga, S., Fricke, B., Nakamatsu, H., Mukoyama, T., Anton, J., Geschke, D., Baştuğ, T. (2000). Four-component relativistic density functional calculations of heavy diatomic molecules. *Journal of Chemical Physics*, 112(8), 3499-3506.
- [35] Wang, X., & Tian, D. (2009). *Computational Materials Science*, 46(1), 239-244.

- [36] Doye, J. P. K., & Wales, D. J. (1998). Global minima for transition metal clusters described by Sutton-Chen potentials. *New Journal of Chemistry*, 22(7), 733-744.
- [37] Uppenbrink, J., & Wales, D. J. (1992). Structure and energetics of model metal clusters. *The Journal of Chemical Physics*, 96(11), 8520-8534.
- [38] Sebetci, A., & Güvenç, Z. B. (2004). Global minima for free Pt_N clusters (N=22-56): A comparison between the searches with a molecular dynamics approach and a basin-hopping algorithm. *European Physical Journal D*, 30(1), 71-79.
- [39] Sachdev, A., Masel, R. I., & Adams, J. B. (1992). An investigation of the shape of small platinum clusters using the embedded atom method. *Catalysis Letters*, 15(1-2), 57-64.
- [40] Sebetci, A., & Güvenç, Z. B. (2003). Energetics and structures of small clusters: Pt_N, N = 2-21. *Surface Science*, 525(1-3), 66-84.
- [41] Sachdev, A., Masel, R. I., & Adams, J. B. (1993). An embedded atom method study of the equilibrium shapes of small platinum and palladium clusters. *Zeitschrift für Physik D Atoms, Molecules and Clusters*, 26(1), 310-312.
- [42] Douglass, D. C., Cox, A. J., Bucher, J. P., & Bloomfield, L. A. (1993). Magnetic properties of free cobalt and gadolinium clusters. *Physical Review B*, 47(19), 12874-12889.
- [43] Gerion, D., Hirt, A., Billas, I. M. L., Châtelain, A., & De Heer, W. A. (2000). Experimental specific heat of iron, cobalt, and nickel clusters studied in a molecular beam. *Physical Review B - Condensed Matter and Materials Physics*, 62(11), 7491-7501.
- [44] Billas, I. M. L., Châtelain, A., & De Heer, W. A. (1997). Magnetism of Fe, Co and Ni clusters in molecular beams. *Journal of Magnetism and Magnetic Materials*, 168(1-2), 64-84.

- [45] Dong, C. D., & Gong, X. G. (2008). Magnetism enhanced layer-like structure of small cobalt clusters. *Physical Review B*, 78(2), 020409.
- [46] Lü, J., Xu, X. H., & Wu, H. S. (2008). Structure and magnetism of $(\text{CoCr})_n$ ($n=1-5$) alloy clusters. *Wuli Huaxue Xuebao/ Acta Physico - Chimica Sinica*, 24(7), 1252-1256.
- [47] Xu, X., Yin, S., Moro, R., & de Heer, W. A. (2005). Magnetic Moments and Adiabatic Magnetization of Free Cobalt Clusters. *Physical Review Letters*, 95(23), 237209.
- [48] Ganguly, S., Kabir, M., Datta, S., Sanyal, B., & Mookerjee, A. (2008). Magnetism in small bimetallic Mn-Co clusters. *Physical Review B*, 78(1), 014402.
- [49] Pellarin, M., Baguenard, B., Vialle, J. L., Lermé, J., Broyer, M., Miller, J., & Perez, A. (1994). Evidence for icosahedral atomic shell structure in nickel and cobalt clusters. Comparison with iron clusters. *Chemical Physics Letters*, 217(4), 349-356.
- [50] Parks, E. K., Klots, T. D., Winter, B. J., & Riley, S. J. (1993). Reactions of cobalt clusters with water and ammonia: Implications for cluster structure. *The Journal of Chemical Physics*, 99(8), 5831-5839.
- [51] Parks, E. K., Winter, B. J., Klots, T. D., & Riley, S. J. (1992). Evidence for polyicosahedral structure in ammoniated iron, cobalt, and nickel clusters. *The Journal of Chemical Physics*, 96(11), 8267-8274.
- [52] Yoshida, H., Terasaki, A., Kobayashi, K., Tsukada, M., & Kondow, T. (1995). Spin-polarized electronic structure of cobalt cluster anions studied by photoelectron spectroscopy. *The Journal of Chemical Physics*, 102(15), 5960-5965.
- [53] Kittel, C. (1996). *Introduction to Solid State Physics* (Vol. 7). New York: John Wiley & Sons.

- [54] Valden, M., Aaltonen, J., Kuusisto, E., Pessa, M., & Barnes, C. (1994). Molecular beam studies of CO oxidation and CO-NO reactions on a supported Pd catalyst. *Surface Science*, 307, 193-198.
- [55] Che, M., & Bennett, C. O. (1989). of Supported Metals. *Advances in Catalysis*, 36, 55.
- [56] Zakumbaeva, G., Toktabaeva, N., Kubasheva, A. Z., & Efremenko, I. (1994). Effect of palladium dispersity on the selective hydrogenation of acetylene in ethane-ethylene fraction. *Neftekhimiia*, 34(3), 258-267.
- [57] Douglass, D. C., Bucher, J. P., & Bloomfield, L. A. (1992). Magnetic studies of free nonferromagnetic clusters. *Physical Review B*, 45(11), 6341-6344.
- [58] Cox, A. J., Louderback, J. G., & Bloomfield, L. A. (1993). Experimental observation of magnetism in rhodium clusters. *Physical Review Letters*, 71(6), 923-926.
- [59] Douglass, D. C., Bucher, J. P., & Bloomfield, L. A. (1992). Magic numbers in the magnetic properties of gadolinium clusters. *Physical Review Letters*, 68(11), 1774-1777.
- [60] Cox, A. J., Louderback, J. G., Apsel, S. E., & Bloomfield, L. A. (1994). *Physical Review B*, 49(17), 12295-12298.
- [61] Taniyama, T., Ohta, E., & Sato, T. (1997). Observation of 4d ferromagnetism in free-standing Pd fine particles. *EPL (Europhysics Letters)*, 38(3), 195.
- [62] Ganteför, G., & Eberhardt, W. (1996). *Physical Review Letters*, 76(26), 4975-4978.
- [63] Kalita, B., & Deka, R. C. (2007). Stability of small Pd_n (n=1–7) clusters on the basis of structural and electronic properties: A density functional approach. *The Journal of Chemical Physics*, 127(24).
- [64] Cantera-López, H., Montejano-Carrizales, J. M., Aguilera-Granja, F., & Morán-López, J. L. (2010). Theoretical study of bimetallic magnetic

nanostructures: $\text{Co}_n\text{Pd}_{N-n}$, $n=0,1,\dots,N$, $N=3,5,7,13$. *The European Physical Journal D*, 57(1), 61-69.

- [65] Bischoff, S., Weigt, A., Fujimoto, K., & Lücke, B. (1995). The role of promoter metals in the hydrocarbonylation of methanol over active carbon supported cobalt catalysts. *Journal of Molecular Catalysis A: Chemical*, 95(3), 259-268.
- [66] Heemeier, M., Carlsson, A. F., Naschitzki, M., Schmal, M., Bäumer, M., & Freund, H. J. (2002). Preparation and characterization of a model bimetallic catalyst: Co–Pd nanoparticles supported on Al_2O_3 . *Angewandte Chemie International Edition*, 41(21), 4073-4076.
- [67] Noronha, F. B., Schmal, M., Nicot, C., Moraweck, B., & Frety, R. (1997). Characterization of graphite-supported palladium–cobalt catalysts by temperature-programmed reduction and magnetic measurements. *Journal of Catalysis*, 168(1), 42-50.
- [68] Ariake, J., Chiba, T., Watanabe, S., Honda, N., & Ouchi, K. (2005). Magnetic and structural properties of Co-Pt perpendicular recording media with large magnetic anisotropy. *Journal of Magnetism and Magnetic Materials*, 287(SPEC. ISS.), 229-233; Harp, G.R., Weller, D., Rabedeau, T.A., Farrow, R.F.C., Toney, M.F., (1993) *Phys. Rev. Lett.*, 71, p. 2493
- [69] Stamenkovic, V. R., Mun, B. S., Arenz, M., Mayrhofer, K. J. J., Lucas, C. A., Wang, G., Markovic, N. M. (2007). Trends in electrocatalysis on extended and nanoscale Pt-bimetallic alloy surfaces. *Nat Mater*, 6(3), 241-247.
- [70] Wieckowski, A., Savinova, E. R., & Vayenas, C. G. (2003). *Catalysis and electrocatalysis at nanoparticle surfaces*: CRC Press.
- [71] Kinoshita, K. (1992). *Electrochemical oxygen technology* (Vol. 30): John Wiley & Sons.
- [72] Toda, T., Igarashi, H., Uchida, H., & Watanabe, M. (1999). Enhancement of the electroreduction of oxygen on Pt alloys with Fe, Ni, and Co. *Journal of The Electrochemical Society*, 146(10), 3750-3756.

- [73] Bing, Y., Liu, H., Zhang, L., Ghosh, D., & Zhang, J. (2010). Nanostructured Pt-alloy electrocatalysts for PEM fuel cell oxygen reduction reaction. *Chemical Society Reviews*, 39(6), 2184-2202.
- [74] Zhou, D. An Introduction of Density Functional Theory and its Application. Yayın evi, yayın yılı ???
- [75] Koch, W., Holthausen, M. C., & Holthausen, M. C. (2001). *A chemist's guide to density functional theory* (Vol. 2): Wiley-Vch Weinheim.
- [76] Szabo, A., & Ostlund, N. S. (2012). *Modern quantum chemistry: introduction to advanced electronic structure theory*: Courier Dover Publications.
- [77] Harrison, N. (2003). An introduction to density functional theory. *NATO SCIENCE SERIES SUB SERIES III COMPUTER AND SYSTEMS SCIENCES*, 187, 45-70.
- [78] Hammond, B., Lester Jr, W., Reynolds, P., Andre, J., Delhalle, J., & Bredas, J. (1994). World Scientific Lecture and Course Notes in Chemistry.
- [79] Coleman, J. (1981). *Calculation of the first- and second-order density matrices, in, The Force Concept in Chemistry* (B. M. Deb ed.). New York: Van Nostrand Reinhold.
- [80] Smith, R. E. a. V. H. (1987). *Density matrices and Density Functionals*. Reidel, Dordrecht.
- [81] Hohenberg, P., & Kohn, W. (1964). Inhomogeneous electron gas. *Physical review*, 136(3B), B864.
- [82] Levy, M., & Perdew, J. P. (1985). The constrained search formulation of density functional theory *Density Functional Methods in Physics* (pp. 11-30): Springer.
- [83] Foley, M., & Madden, P. A. (1996). Further orbital-free kinetic-energy functionals for ab initio molecular dynamics. *Physical Review B*, 53(16), 10589.

- [84] W. Kohn and L. J. Sham. (1965). Becke 3 Perdew-Wang 86 (B3P86). *Phys. Rev*, 140, 1133.
- [85] Yildirim, H. (2010). *Structural, electronic, vibrational and thermodynamical properties of surfaces and nanoparticles*. University of Central Florida Orlando, Florida.
- [86] Kohanoff, J., & Gidopoulos, N. (2003). *Handbook of Molecular Physics and Quantum Chemistry*, vol: Chichester: John Wiley & Sons, Ltd.
- [87] Perdew, J. P., & Zunger, A. (1981). Self-interaction correction to density-functional approximations for many-electron systems. *Physical Review B*, 23(10), 5048.
- [88] Ceperley, D. M., & Alder, B. (1980). Ground state of the electron gas by a stochastic method. *Physical Review Letters*, 45(7), 566.
- [89] Perdew, J. P., Burke, K., & Wang, Y. (1996). Generalized gradient approximation for the exchange-correlation hole of a many-electron system. *Physical Review B*, 54(23), 16533.
- [90] Perdew, J. P., Chevary, J., Vosko, S., Jackson, K. A., Pederson, M. R., Singh, D., & Fiolhais, C. (1993). Erratum: Atoms, molecules, solids, and surfaces: Applications of the generalized gradient approximation for exchange and correlation. *Physical Review B*, 48(7), 4978.
- [91] Perdew, J. P., Chevary, J., Vosko, S., Jackson, K. A., Pederson, M. R., Singh, D., & Fiolhais, C. (1992). Atoms, molecules, solids, and surfaces: Applications of the generalized gradient approximation for exchange and correlation. *Physical Review B*, 46(11), 6671.
- [92] Perdew, J. P., Burke, K., & Ernzerhof, M. (1996). Generalized gradient approximation made simple. *Physical Review Letters*, 77(18), 3865.
- [93] Lee, C., Yang, W., & Parr, R. G. (1988). Development of the Colle-Salvetti correlation-energy formula into a functional of the electron density. *Physical Review B*, 37(2), 785.

- [94] Neumann, R., & Handy, N. C. (1997). Higher-order gradient corrections for exchange-correlation functionals. *Chemical Physics Letters*, 266(1), 16-22.
- [95] Tschinke, V., & Ziegler, T. (1989). On the shape of spherically averaged Fermi-hole correlation functions in density functional theory. 1. Atomic systems. *Canadian Journal of Chemistry*, 67(3), 460-472.
- [96] Kurth, S., Perdew, J. P., & Blaha, P. (1999). Molecular and solid-state tests of density functional approximations: LSD, GGAs, and meta-GGAs. *International Journal of Quantum Chemistry*, 75(4-5), 889-909.
- [97] Pines, D., & Nozieres, P. (1990). *The theory of quantum liquids*: Addison-Wesley.
- [98] Becke, A. D. (1993). Density-functional thermochemistry. III. The role of exact exchange. *The Journal of Chemical Physics*, 98(7), 5648-5652.
- [99] Perdew, J. P., & Wang, Y. (1992). Pair-distribution function and its coupling-constant average for the spin-polarized electron gas. *Physical Review B*, 46(20), 12947.
- [100] Adamo, C., Ernzerhof, M., & Scuseria, G. E. (2000). The meta-GGA functional: Thermochemistry with a kinetic energy density dependent exchange-correlation functional. *The Journal of Chemical Physics*, 112(6), 2643-2649.
- [101] Shylesh, S., Schünemann, V., & Thiel, W. R. (2010). Magnetically Separable Nanocatalysts: Bridges between Homogeneous and Heterogeneous Catalysis. *Angewandte Chemie International Edition*, 49(20), 3428-3459.
- [102] Robinson, I., Zacchini, S., Tung, L. D., Maenosono, S., & Thanh, N. T. K. (2009). Synthesis and Characterization of Magnetic Nanoalloys from Bimetallic Carbonyl Clusters. *Chemistry of Materials*, 21(13), 3021-3026.
- [103] Baletto, F., & Ferrando, R. (2005). Structural properties of nanoclusters: Energetic, thermodynamic, and kinetic effects. *Reviews of Modern Physics*, 77(1), 371-423.

- [104] Goel, S., Velizhanin, K. A., Piryatinski, A., Tretiak, S., & Ivanov, S. A. (2010). DFT Study of Ligand Binding to Small Gold Clusters. *The Journal of Physical Chemistry Letters*, 1(6), 927-931.
- [105] Yang, J., Tschamber, V., Habermacher, D., Garin, F., & Gilot, P. (2008). Effect of sintering on the catalytic activity of a Pt based catalyst for CO oxidation: Experiments and modeling. *Applied Catalysis B: Environmental*, 83(3-4), 229-239.
- [106] Ertl, G., Prigge, D., Schloegl, R., & Weiss, M. (1983). Surface characterization of ammonia synthesis catalysts. *Journal of Catalysis*, 79(2), 359-377.
- [107] Götz, M., & Wendt, H. (1998). Binary and ternary anode catalyst formulations including the elements W, Sn and Mo for PEMFCs operated on methanol or reformat gas. *Electrochimica Acta*, 43(24), 3637-3644.
- [108] Bönnemann, H., & Brijoux, W. (1996). Chapter 7 - Surfactant-Stabilized Nanosized Colloidal Metals and Alloys as Catalyst Precursors. In W. R. Moser (Ed.), *Advanced Catalysts and Nanostructured Materials* (pp. 165-196). San Diego: Academic Press.
- [109] Schmidt, T. J., Noeske, M., Gasteiger, H. A., Behm, R. J., Britz, P., Brijoux, W., & Bönnemann, H. (1997). Electrocatalytic Activity of PtRu Alloy Colloids for CO and CO/H₂ Electrooxidation: Stripping Voltammetry and Rotating Disk Measurements. *Langmuir*, 13(10), 2591-2595.
- [110] Barcaro, G., & Fortunelli, A. (2009). Structural and electronic properties of small platinum metallorganic complexes. *Theoretical Chemistry Accounts*, 123(3-4), 317-325.
- [111] Temkin, O. N., Zeigarnik, A. V., & Bonchev, D. (1996). *Chemical reaction networks: a graph-theoretical approach*: CRC Press.
- [112] Cornils, B., & Herrmann, W. A. (1996). *Applied homogeneous catalysis with organometallic compounds* (Vol. 2): VCH Weinheim etc.

- [113] Schmidt, T., Noeske, M., Gasteiger, H. A., Behm, R., Britz, P., & Bönnemann, H. (1998). PtRu alloy colloids as precursors for fuel cell catalysts a combined XPS, AFM, HRTEM, and RDE study. *Journal of The Electrochemical Society*, 145(3), 925-931.
- [114] Toshima, N., & Yonezawa, T. (1998). Bimetallic nanoparticles-novel materials for chemical and physical applications. *New Journal of Chemistry*, 22(11), 1179-1201.
- [115] Aiken Iii, J. D., & Finke, R. G. (1999). A review of modern transition-metal nanoclusters: their synthesis, characterization, and applications in catalysis. *Journal of Molecular Catalysis A: Chemical*, 145(1-2), 1-44.
- [116] LEISNER, T., ROSCHE, C., WOLF, S., GRANZER, F., & WÖSTE, L. (1996). THE CATALYTIC ROLE OF SMALL COINAGE-METAL CLUSTERS IN PHOTOGRAPHY. *Surface Review and Letters*, 03(01), 1105-1108.
- [117] Faraday, M. (1857). The Bakerian Lecture: Experimental Relations of Gold (and Other Metals) to Light. *Philosophical Transactions of the Royal Society of London*, 147, 145-181.
- [118] Jia, C.-J., & Schuth, F. (2011). Colloidal metal nanoparticles as a component of designed catalyst. *Physical Chemistry Chemical Physics*, 13(7), 2457-2487.
- [119] Haensel, V., & Bloch, H. S. (1964). Duofunctional platinum catalysts in the petroleum industry. *Platinum Metals Review*, 8(1), 2-8.
- [120] Lewis, L. N., & Lewis, N. (1986). Platinum-catalyzed hydrosilylation - colloid formation as the essential step. *Journal of the American Chemical Society*, 108(23), 7228-7231.
- [121] Bradley, J. S. (1994). *Clusters and Colloids* (i. G. Schmid Ed.). Weinheim: VCH.

- [122] Blackborow, J. R., & Young, D. (1979). *Metal vapour synthesis in organometallic chemistry* (Vol. 179): Springer-Verlag New York, NY).
- [123] Mittendorfer, F., Thomazeau, C., Raybaud, P., & Toulhoat, H. (2003). Adsorption of Unsaturated Hydrocarbons on Pd(111) and Pt(111): A DFT Study. *The Journal of Physical Chemistry B*, 107(44), 12287-12295.
- [124] Zaera, F. (1991). Reversibility of C1 hydrogenation-dehydrogenation reactions on platinum surfaces under vacuum. *Langmuir*, 7(10), 1998-1999.
- [125] Wang, X., & Andrews, L. (2004). Infrared Spectra and Density Functional Calculations for Three Pt-C₂H₂ Reaction Product Isomers: PtCCH₂, HPtCCH, and Pt- η -2-(C₂H₂). *The Journal of Physical Chemistry A*, 108(22), 4838-4845.
- [126] Granatier, J., Dubecký, M. s., Lazar, P., Otyepka, M., & Hobza, P. (2013). Spin-Crossing in an Organometallic Pt-Benzene Complex. *Journal of Chemical Theory and Computation*, 9(3), 1461-1468.
- [127] Majumdar, D., Roszak, S., & Balasubramanian, K. (2001). Interaction of benzene (Bz) with Pt and Pt₂: A theoretical study on Bz-Pt₂, Bz₂-Pt, Bz₂-Pt₂, and Bz₃-Pt₂ clusters. *The Journal of Chemical Physics*, 114(23), 10300-10310.
- [128] Valiev, M., Bylaska, E. J., Govind, N., Kowalski, K., Straatsma, T. P., Van Dam, H. J., Windus, T. L. (2010). NWChem: a comprehensive and scalable open-source solution for large scale molecular simulations. *Computer Physics Communications*, 181(9), 1477-1489.
- [129] Hurley, M. M., Pacios, L. F., Christiansen, P. A., Ross, R. B., & Ermler, W. C. (1986). Abinitio relativistic effective potentials with spin-orbit operators. II. K through Kr. *The Journal of Chemical Physics*, 84(12), 6840-6853.
- [130] Becke, A. D. (1988). Density-functional exchange-energy approximation with correct asymptotic behavior. *Physical Review A*, 38(6), 3098-3100.

- [131] Vosko, S., Wilk, L., & Nusair, M. (1980). Accurate spin-dependent electron liquid correlation energies for local spin density calculations: a critical analysis. *Canadian Journal of Physics*, 58(8), 1200-1211.
- [132] Sebetci, A. (2009). Does spin-orbit coupling effect favor planar structures for small platinum clusters? *Phys. Chem. Chem. Phys.*, 11(6), 921-925.
- [133] Sebetci, A. (2006). A density functional study of bare and hydrogenated platinum clusters. *Chemical physics*, 331(1), 9-18.
- [134] Li, J., Li, X., Zhai, H.-J., & Wang, L.-S. (2003). Au₂₀: A tetrahedral cluster. *Science*, 299(5608), 864-867.
- [135] Parr, R. G., & Pearson, R. G. (1983). Absolute hardness: companion parameter to absolute electronegativity. *Journal of the American Chemical Society*, 105(26), 7512-7516.
- [136] Heredia, C., Ferraresi-Curotto, V., & López, M. (2012). *Computational Materials Science*, 53(1), 18-24.
- [137] Tournus, F., Blanc, N., Tamion, A., Ohresser, P., Perez, A., & Dupuis, V. (2008). XMCD study of CoPt nanoparticles embedded in MgO and amorphous carbon matrices. *Journal of Electron Spectroscopy and Related Phenomena*, 166-167(1-3 C), 84-88.
- [138] Tournus, F., Tamion, A., Blanc, N., Hannour, A., Bardotti, L., Prével, B., Dupuis, V. (2008). *Physical Review B*, 77(14), 144411.
- [139] Gruner, M. E., Rollmann, G., Entel, P., & Farle, M. (2008). Multiply Twinned Morphologies of FePt and CoPt Nanoparticles. *Physical Review Letters*, 100(8), 087203.
- [140] An, B. H., Wu, J. H., Liu, H. L., Ko, S. P., Ju, J. S., & Kim, Y. K. (2008). CoPt nanoparticles by a modified polyol process. *Colloids and Surfaces A: Physicochemical and Engineering Aspects*, 313-314, 250-253.
- [141] Rossi, G., Ferrando, R., & Mottet, C. (2008). Structure and chemical ordering in CoPt nanoalloys. *Faraday Discussions*, 138(0), 193-210.

- [142] Moskovkin, P., & Hou, M. (2007). Metropolis Monte Carlo predictions of free Co-Pt nanoclusters. *Journal of Alloys and Compounds*, 434-435(SPEC. ISS.), 550-554.
- [143] J.H. Kim, J. K., N. Oh, Y-H. Kim, C.K. Kim, C.S. Yoon, S. Jin. (2007). Monolayer CoPt magnetic nanoparticle array using multiple thin film depositions. *Applied Physics Letters*, 90, 023117.
- [144] Alloyeau, D., Ricolleau, C., Mottet, C., Oikawa, T., Langlois, C., Le Bouar, Y., . . . Loiseau, A. (2009). Size and shape effects on the order-disorder phase transition in CoPt nanoparticles. *Nat Mater*, 8(12), 940-946.
- [145] Dave, M. N., Wears, M. L., Michael, J., & Desmond, C. (2007). Fabrication and characterization of nano-particulate PtCo media for ultra-high density perpendicular magnetic recording. *Nanotechnology*, 18(20), 205301.
- [146] Favre, L., Dupuis, V., Bernstein, E., Mélinon, P., Pérez, A., Stanescu, S., Hodeau, J. L. (2006). *Physical Review B*, 74(1), 014439.
- [147] Hannour, A., Bardotti, L., Prével, B., Bernstein, E., Mélinon, P., Perez, A., Maily, D. (2005). 2D arrays of CoPt nanocluster assemblies. *Surface Science*, 594(1-3), 1-11.
- [148] Rohart, S., Raufast, C., Favre, L., Bernstein, E., Bonet, E., & Dupuis, V. (2006). Magnetic anisotropy of $\text{Co}_x\text{Pt}_{1-x}$ clusters embedded in a matrix: Influences of the cluster chemical composition and the matrix nature. *Physical Review B*, 74(10), 104408.
- [149] Seto, T., Koga, K., Akinaga, H., Takano, F., Orii, T., & Hirasawa, M. (2006). Laser ablation synthesis of monodispersed magnetic alloy nanoparticles. *Journal of Nanoparticle Research*, 8(3-4), 371-378.
- [150] Tzitzios, V., Niarchos, D., Gjoka, M., Boukos, N., & Petridis, D. (2005). Synthesis and Characterization of 3D CoPt Nanostructures. *Journal of the American Chemical Society*, 127(40), 13756-13757.

- [151] Mizuno, M., Sasaki, Y., Inoue, M., Chinnasamy, C. N., Jeyadevan, B., Hasegawa, D., Hisano, S. (2005). Structural and magnetic properties of monolayer film of CoPt nanoparticles synthesized by polyol process. *Journal of Applied Physics*, 97(10),.
- [152] Castaldi, L., Giannakopoulos, K., Travlos, A., Niarchos, D., Boukari, S., & Beaurepaire, E. (2005). CoPt nanoparticles deposited by electron beam evaporation. *Journal of Magnetism and Magnetic Materials*, 290-291 PART I, 544-546.
- [153] Vassilios, T., Dimitrios, N., Gjoka, M., Fidler, J., & Dimitrios, P. (2005). Synthesis of CoPt nanoparticles by a modified polyol method: characterization and magnetic properties. *Nanotechnology*, 16(2), 287.
- [154] Jiao-Ming Qiu, Y.-H. X., Jack, H. Judy, Jian-Ping, Wang, J. P. (2005). Nanocluster deposition for high density magnetic recording tape media *Journal of Applied Physics*, 97(10), 10P704.
- [155] Wang, Y., & Yang, H. (2005). Synthesis of CoPt Nanorods in Ionic Liquids. *Journal of the American Chemical Society*, 127(15), 5316-5317.
- [156] Sun, X., Jia, Z. Y., Huang, Y. H., Harrell, J. W., Nikles, D. E., Sun, K., & Wang, L. M. (2004). Synthesis and magnetic properties of CoPt nanoparticles. *Journal of Applied Physics*, 95(11), 6747-6749.
- [157] Chinnasamy, C. N., Jeyadevan, B., Shinoda, K., & Tohji, K. (2003). Polyol-process-derived CoPt nanoparticles: Structural and magnetic properties. *Journal of Applied Physics*, 93(10), 7583-7585.
- [158] Wang, H. R., Huang, C. X., Jiang, H., Li, J. J., Xu, J. L., Zhu, G. Y., Li, G. S. (2004). Direct proinflammatory effect of C-reactive protein on human monocytes isolated from patients with acute coronary syndrome and statins intervention. *Chinese Pharmacological Bulletin*, 20(11), 1279-1283.
- [159] Yu, M., Liu, Y., & Sellmyer, D. J. (2000). Nanostructure and magnetic properties of composite CoPt:C films for extremely high-density recording. *Journal of Applied Physics*, 87(9), 6959-6961.

- [160] Sui, Y., Yue, L., Skomski, R., Li, X. Z., Zhou, J., & Sellmyer, D. J. (2003). CoPt hard magnetic nanoparticle films synthesized by high temperature chemical reduction. *Journal of Applied Physics*, *93*(10 2), 7571-7573.
- [161] Xu, Y., Sun, Z. G., Qiang, Y., & Sellmyer, D. J. (2003). Preparation and magnetic properties of CoPt and CoPt:Ag nanocluster films. *Journal of Magnetism and Magnetic Materials*, *266*(1-2), 164-170.
- [162] Yu, A. C. C., Mizuno, M., Sasaki, Y., Kondo, H., & Hiraga, K. (2002). Structural characteristics and magnetic properties of chemically synthesized CoPt nanoparticles. *Applied Physics Letters*, *81*(20), 3768-3770.
- [163] Shevchenko, E. V., Talapin, D. V., Rogach, A. L., Kornowski, A., Haase, M., & Weller, H. (2002). Colloidal Synthesis and Self-Assembly of CoPt₃ Nanocrystals. *Journal of the American Chemical Society*, *124*(38), 11480-11485.
- [164] Ely, T. O., Pan, C., Amiens, C., Chaudret, B., Dassenoy, F., Lecante, P., Broto, J. M. (2000). Nanoscale Bimetallic Co_xPt_{1-x} Particles Dispersed in Poly(vinylpyrrolidone): Synthesis from Organometallic Precursors and Characterization. *The Journal of Physical Chemistry B*, *104*(4), 695-702.
- [165] Zhang, Z., Blom, D. A., Gai, Z., Thompson, J. R., Shen, J., & Dai, S. (2003). High-Yield Solvothermal Formation of Magnetic CoPt Alloy Nanowires. *Journal of the American Chemical Society*, *125*(25), 7528-7529.
- [166] Sellmyer, D. J., Yu, M., & Kirby, R. D. (1999). Nanostructured magnetic films for extremely high density recording. *Nanostructured Materials*, *12*(5), 1021-1026.
- [167] Blundell, S., & Thouless, D. (2003). Magnetism in condensed matter. *American Journal of Physics*, *71*(1), 94-95.
- [168] Sebetci, A. (2012). Density functional study of small cobalt–platinum nanoalloy clusters. *Journal of Magnetism and Magnetic Materials*, *324*(4), 588-594.

- [169] Huang, W.-F., Zhang, Q., Zhang, D.-F., Zhou, J., Si, C., Guo, L., Wu, Z.-Y. (2013). Investigation of structural and magnetic properties of CoPt/CoAu bimetallic nanochains by x-ray absorption spectroscopy. *The Journal of Physical Chemistry C*, 117(13), 6872-6879.
- [170] Kiefer, J. H., & Von Drasek, W. A. (1990). The mechanism of the homogeneous pyrolysis of acetylene. *International journal of chemical kinetics*, 22(7), 747-786.
- [171] Boullart, W., Devriendt, K., Borms, R., & Peeters, J. (1996). Identification of the sequence $\text{CH} (2\pi)^+ \text{C}_2\text{H}_2 \rightarrow \text{C}_3\text{H}_2^+ + \text{H}$ (and $\text{C}_3\text{H}^+ + \text{H}_2$) followed by $\text{C}_3\text{H}_2^+ + \text{O} \rightarrow \text{C}_2\text{H}^+ + \text{HCO}$ (or $\text{H}^+ + \text{CO}$) as C_2H source in $\text{C}_2\text{H}_2/\text{O}/\text{H}$ atomic flames. *The Journal of Physical Chemistry*, 100(3), 998-1007.
- [172] Kiefer, J., Sidhu, S., Kern, R., Xie, K., Chen, H., & Harding, L. (1992). The homogeneous pyrolysis of acetylene II: the high temperature radical chain mechanism. *Combustion science and technology*, 82(1-6), 101-130.
- [173] Dutrey, A., Guilloteau, S., & Guelin, M. (1997). Chemistry of protosolar-like nebulae: The molecular content of the DM Tau and GG Tau disks. *Astron. Astrophys*, 317, L55-L58.
- [174] Wootten, A., Bozyan, E., Garrett, D., Loren, R., & Snell, R. (1980). Detection of C/H in cold dark clouds. *Astrophys. J.:(United States)*, 239(3).
- [175] Olofsson, A., Persson, C. M., Koning, N., Bergman, P., Bernath, P., Black, J. H., Hjalmarsen, A. (2009). A spectral line survey of Orion KL in the bands 486-492 and 541-577 GHz with the Odin satellite I. The observational data. *arXiv preprint arXiv:0910.1825*.
- [176] Tucker, K., Kutner, M., & Thaddeus, P. (1974). The ethynyl radical C_2H a new interstellar molecule: Goddard Institute for Space Studies, New York.
- [177] Lucas, R., & Liszt, H. (2000). Comparative chemistry of diffuse clouds. I. C_2H and C_3H_2 . *Astronomy and Astrophysics*, 358, 1069-1076.

- [178] Zhou, J., Garand, E., & Neumark, D. M. (2007). Vibronic structure in C₂H and C₂D from anion slow electron velocity-map imaging spectroscopy. *The Journal of Chemical Physics*, 127(11), 114313.
- [179] Shepherd, R. A., & Graham, W. R. M. (1987). FTIR study of D and ¹³C substituted C₂H in solid argon. *The Journal of Chemical Physics*, 86(5), 2600-2605.
- [180] Hsu, Y. C., Shiu, Y. J., & Lin, C. M. (1995). *The Journal of Chemical Physics*, 103(14), 5919-5930.
- [181] Wu, Y.-J., & Cheng, B.-M. (2008). Infrared absorption spectra of ethynyl radicals isolated in solid Ne: Identification of the fundamental C–H stretching mode. *Chemical Physics Letters*, 461(1), 53-57.
- [182] Ervin, K. M. L., W. C. (1991). *J. Phys. Chem*, 95, 1167.
- [183] Anderson, M., & Ziurys, L. (1995). Laboratory detection and millimeter spectrum of the MgCCH radical. *The Astrophysical Journal*, 439, L25-L28.
- [184] Nuccio, B. P., Apponi, A. J., & Ziurys, L. M. (1995). The millimeter-wave spectrum of SrCCH(X²Σ⁺): chemical trends in metal monoacetylide species. *Chemical Physics Letters*, 247(3), 283-288.
- [185] Anderson, M., & Ziurys, L. (1995). The millimeter/submillimeter rotational spectrum of CaCCH. *The Astrophysical Journal*, 444, L57-L60.
- [186] Bopegedera, A. M. R. P., Brazier, C. R., & Bernath, P. F. (1988). *Journal of Molecular Spectroscopy*, 129(2), 268-275.
- [187] Brewster, M. A., Apponi, A. J., Xin, J., & Ziurys, L. M. (1999). Millimeter-wave spectroscopy of vibrationally-excited NaCCH and MgCCH: the ν_5 bending mode. *Chemical Physics Letters*, 310(5–6), 411-422.
- [188] Brugh, D. J., DaBell, R. S., & Morse, M. D. (2004). Vibronic spectroscopy of unsaturated transition metal complexes: CrC₂H, CrCH₃, and NiCH₃. *Journal of Chemical Physics*, 121(24), 12379-12385.

- [189] Loock, H.-P., Bércecs, A., Simard, B., & Linton, C. (1997). *The Journal of Chemical Physics*, 107(8), 2720-2727.
- [190] Fan, J., & Wang, L.-S. (1994). A Study of FeC₂ and FeC₂H by Anion Photoelectron Spectroscopy. *The Journal of Physical Chemistry*, 98(46), 11814-11817.
- [191] Moravec, V. D., Klopčič, S. A., & Jarrold, C. C. (1999). Anion photoelectron spectroscopy of small tin clusters. *The Journal of Chemical Physics*, 110(11), 5079-5088.
- [192] Li, D.-Z., Song, M.-Z., Xu, Q.-H., & Zhang, S.-G. (2012). Theoretical Investigation on the Interaction of C₂H Radical with Small Gold Clusters Au_nO⁻ (n=1-4). *Journal of Cluster Science*, 23(2), 481-489.
- [193] Yuan, J., Xu, H.-G., Zhang, Z.-G., Feng, Y., & Zheng, W. (2010). Adsorption of C₂H radical on cobalt clusters: anion photoelectron spectroscopy and density functional calculations. *The Journal of Physical Chemistry A*, 115(2), 182-186.
- [194] Dean, J. A. (1999). Properties of atoms, radicals, and bonds. *Lange's Handbook of Chemistry*, 4.
- [195] Zhou, H., Tamura, H., Takami, S., Kubo, M., Belosludov, R., Zhanpeisov, N., & Miyamoto, A. (2000). Periodic density functional study on adsorption properties of organic molecules on clean Al (111) surface. *Applied Surface Science*, 158(1-2), 38-42.
- [196] Sebetci, A. (2008). Cobalt clusters and their anions. *Chemical physics*, 354(1-3), 196-201.
- [197] Ma, Q. M., Xie, Z., Wang, J., Liu, Y., & Li, Y. C. (2006). Structures, stabilities and magnetic properties of small Co clusters. *Physics Letters, Section A: General, Atomic and Solid State Physics*, 358(4), 289-296.

- [198] Castro, M., Jamorski, C., & Salahub, D. R. (1997). Structure, bonding, and magnetism of small Fe_n , Co_n , and Ni_n clusters, $n \leq 5$. *Chemical Physics Letters*, 271(1-3), 133-142.
- [199] Datta, S., Kabir, M., Ganguly, S., Sanyal, B., Saha-Dasgupta, T., & Mookerjee, A. (2007). Structure, bonding, and magnetism of cobalt clusters from first-principles calculations. *Physical Review B*, 76(1), 014429.
- [200] Jamorski, C., Martinez, A., Castro, M., & Salahub, D. R. (1997). Structure and properties of cobalt clusters up to the tetramer: A density-functional study. *Physical Review B - Condensed Matter and Materials Physics*, 55(16), 10905-10921.
- [201] Yoshida, H., Terasaki, A., Kobayashi, K., Tsukada, M., & Kondow, T. (1995). Spin-polarized electronic structure of cobalt cluster anions studied by photoelectron spectroscopy. *The Journal of Chemical Physics*, 102(15), 5960-5965.
- [202] Aslan, M., Öztürk, Z., & Sebetci, A. (2014). The Influence of Unsaturated Hydrocarbon Ligands on the Stabilization of Platinum Tetramer. *Journal of Cluster Science*, 25(5), 1187-1201.
- [203] Fan, H.-J., Liu, C.-W., & Liao, M.-S. (1997). Geometry, electronic structure and magnetism of small Co_n ($n=2-8$) clusters. *Chemical Physics Letters*, 273(5-6), 353-359.
- [204] Ma, Q.-M., Xie, Z., Wang, J., Liu, Y., & Li, Y.-C. (2006). Structures, stabilities and magnetic properties of small Co clusters. *Physics Letters A*, 358(4), 289-296.
- [205] Rodríguez-López, J. L., Aguilera-Granja, F., Michaelian, K., & Vega, A. (2003). Structure and magnetism of cobalt clusters. *Physical Review B*, 67(17), 174413.
- [206] Pereiro, M., Man'kovsky, S., Baldomir, D., Iglesias, M., Mlynarski, P., Valladares, M., Arias, J. E. (2001). Model potential nonlocal density

- functional calculations of small cobalt clusters, $\text{Co}_n, n \leq 5$. *Computational Materials Science*, 22(1–2), 118-122.
- [207] Hansen, K., Andersen, J. U., Forster, J. S., & Hvelplund, P. (2001). Formation and fragmentation of negative metal clusters. *Physical Review A*, 63(2), 023201.
- [208] Spasov, V. A., Lee, T. H., & Ervin, K. M. (2000). Threshold collision-induced dissociation of anionic copper clusters and copper cluster monocarbonyls. *Journal of Chemical Physics*, 112(4), 1713-1720.
- [209] Vogel, M., Hansen, K., Herlert, A., & Schweikhard, L. (2001). Energy dependence of the decay pathways of optically excited small gold clusters. *Applied Physics B: Lasers and Optics*, 73(4), 411-416.
- [210] Knickelbein, M. B. (2006). Magnetic moments of bare and benzene-capped cobalt clusters. *The Journal of Chemical Physics*, 125(4).
- [211] Serov, A., Nedoseykina, T., Shvachko, O., & Kwak, C. (2010). Effect of precursor nature on the performance of palladium–cobalt electrocatalysts for direct methanol fuel cells. *Journal of Power Sources*, 195(1), 175-180.
- [212] Jung, K.-N., Jung, J.-H., Im, W. B., Yoon, S., Shin, K.-H., & Lee, J.-W. (2013). Doped Lanthanum Nickelates with a Layered Perovskite Structure as Bifunctional Cathode Catalysts for Rechargeable Metal–Air Batteries. *ACS applied materials & interfaces*, 5(20), 9902-9907.
- [213] Cheng, F., & Chen, J. (2012). Metal-air batteries: from oxygen reduction electrochemistry to cathode catalysts. *Chemical Society Reviews*, 41(6), 2172-2192.
- [214] Girishkumar, G., McCloskey, B., Luntz, A. C., Swanson, S., & Wilcke, W. (2010). Lithium–Air Battery: Promise and Challenges. *The Journal of Physical Chemistry Letters*, 1(14), 2193-2203.

- [215] Neburchilov, V., Wang, H., Martin, J. J., & Qu, W. (2010). A review on air cathodes for zinc–air fuel cells. *Journal of Power Sources*, 195(5), 1271-1291.
- [216] Lee, Y., Suntivich, J., May, K. J., Perry, E. E., & Shao-Horn, Y. (2012). Synthesis and Activities of Rutile IrO₂ and RuO₂ Nanoparticles for Oxygen Evolution in Acid and Alkaline Solutions. *The Journal of Physical Chemistry Letters*, 3(3), 399-404.
- [217] Wang, C., Daimon, H., Lee, Y., Kim, J., & Sun, S. (2007). Synthesis of Monodisperse Pt Nanocubes and Their Enhanced Catalysis for Oxygen Reduction. *Journal of the American Chemical Society*, 129(22), 6974-6975.
- [218] Oh, S. H., Black, R., Pomerantseva, E., Lee, J.-H., & Nazar, L. F. (2012). Synthesis of a metallic mesoporous pyrochlore as a catalyst for lithium–O₂ batteries. *Nat Chem*, 4(12), 1004-1010.
- [219] Hardin, W. G., Slanac, D. A., Wang, X., Dai, S., Johnston, K. P., & Stevenson, K. J. (2013). Highly Active, Nonprecious Metal Perovskite Electrocatalysts for Bifunctional Metal–Air Battery Electrodes. *The Journal of Physical Chemistry Letters*, 4(8), 1254-1259.
- [220] Cui, B., Lin, H., Li, J.-B., Li, X., Yang, J., & Tao, J. (2008). Core–Ring Structured NiCo₂O₄ Nanoplatelets: Synthesis, Characterization, and Electrocatalytic Applications. *Advanced Functional Materials*, 18(9), 1440-1447.
- [221] Takeguchi, T., Yamanaka, T., Takahashi, H., Watanabe, H., Kuroki, T., Nakanishi, H., Ueda, W. (2013). Layered Perovskite Oxide: A Reversible Air Electrode for Oxygen Evolution/Reduction in Rechargeable Metal-Air Batteries. *Journal of the American Chemical Society*, 135(30), 11125-11130.
- [222] Jin, C., Cao, X., Zhang, L., Zhang, C., & Yang, R. (2013). Preparation and electrochemical properties of urchin-like La_{0.8}Sr_{0.2}MnO₃ perovskite oxide as a bifunctional catalyst for oxygen reduction and oxygen evolution reaction. *Journal of Power Sources*, 241(0), 225-230.

VITA

Personal Information:

Name and Surname: Mikail Aslan

Natioality: Turkish

Birth place and date: Gaziantep 30.11.1984

Marial status: Single

Phone number: +905557393085

Email: mikailsln@gmail.com.tr

Education:

- Ph.D. Physics Engineering, University of G.antep (Turkey): 2010-2014
Thesis Title: The Electronic Structure of Ligand Passivated Metal Nanoclusters
M.S. Physics Education, Middle East Technical University (Turkey): 2010.
- B.S. Physics Education, Middle East Technical University (Turkey): 2010.
GPA: 3.06/4 (second of the department)
Senior Project-I: Quantum Dot Laser
- Gaziantep Anotolian High School: 2003
GPA: 4.76/5.00

Experiences:

- Researcher, Dept of Engineering and Natural Sciences, Birmingham University, UK: 2014
Adviser: Prof. Roy L. Johnston.
Group: Roy Johnston Research Groups

- Research Assistant, Dept. of Electrical and Electronics Engineering, Zirve University: 2010-2014
- Teacher, AÇI Private Teaching Institution, Ankara: 2009-2010
- Student, First Degree Class, UGUR Private Teaching Institution, Gaziantep: 2003-2004

Research Interests:

Modeling and Simulation in Materials Science and Engineering, Computational Nanoscience and Nanotechnology, Computational Quantum Chemistry, Density Functional Theory, Parallel and High Performance Computing, Atomic and Molecular Clusters, Electromagnetic Theory and Numerical Methods

Publications :

- M. Aslan and G. Apaydin, "The b-spline finite element based parabolic wave propagation inside a parallel plate waveguide," International Journal of RF and Microwave Computer-Aided Engineering, vol. 23, no. 4, pp. 488-493, Jul. 2013.
- Aslan, M., Öztürk, Z., & Sebetci, A. (2014). The Influence of Unsaturated Hydrocarbon Ligands on the Stabilization of Platinum Tetramer. Journal of Cluster Science, 1-15.

Conference Proceedings and Presentations:

- M.Aslan, A.Sebetci and Z.Öztürk “The influence of ligands on the stabilization of pure and bimetallic clusters “, Cost Action Conference, 19-21 November 2012, Antalya.
- M.Aslan “The effect of organic hydrocarbon on tetramer platinum” Turkish Physical Society 29th International Physics Congress, 5-8 Eylül 2012, Bodrum

- M. Aslan and G. Apaydin, "The b-spline finite element based parabolic wave propagation inside a parallel plate waveguide," 12th Mediterranean Microwave Symposium, 2-5 September 2012, Istanbul.

Programming Skills:

Nwchem, Quantum Espresso, Matlab, C++, Proteous, Root, Birmingham Genetic Algorithm Program and VASP

The Given Courses and Labs:

Physics 1, Physics 2, Circuit 1, Circuit 2, Digital Design, Electromagnetic Field Theory, Electromagnetic Waves and Electromechanical Energy Conversion 2.

Languages:

English (Fluent)

ÜDS: 80

Awards:

- TUBITAK 2214-A Abroad Scholarship for Doctoral Research.
- The Usage Scholarship of Birmingham University, Bluebear, High Power Computer System (HPC), UK (continue).
- The Usage Scholarship of Warrick University, Minerva, High Power Computer System (HPC), UK (continue)
- The Usage Scholarship of Archer National, High Power Computer System (HPC), UK (continue).
- Full Scholarship from UGUR Private Teaching Institution

Interests:

Martial Arts, Football, Swimming, Check, Travelling and Reading